

Fall 2021

Polymeric Sorbents for Solid-Phase Extraction (SPE) Of Polar Analytes And Carbon Dioxide Capture

Ishwor Karki

Follow this and additional works at: <https://scholarcommons.sc.edu/etd>



Part of the [Chemistry Commons](#)

Recommended Citation

Karki, I.(2021). *Polymeric Sorbents for Solid-Phase Extraction (SPE) Of Polar Analytes And Carbon Dioxide Capture*. (Doctoral dissertation). Retrieved from <https://scholarcommons.sc.edu/etd/6731>

This Open Access Dissertation is brought to you by Scholar Commons. It has been accepted for inclusion in Theses and Dissertations by an authorized administrator of Scholar Commons. For more information, please contact digres@mailbox.sc.edu.

POLYMERIC SORBENTS FOR SOLID-PHASE EXTRACTION (SPE) OF POLAR ANALYTES AND
CARBON DIOXIDE CAPTURE

by

Ishwor Karki

Bachelor of Science
Tribhuvan University of Nepal, 2011

Masters of Science
Tribhuvan University of Nepal, 2013

Submitted in Partial Fulfillment of the Requirements

For the Degree of Doctor of Philosophy in

Chemistry

College of Arts and Sciences

University of South Carolina

2021

Accepted by:

Ken D. Shimizu, Major Professor

Linda S. Shimizu, Committee Member

Sophya Garashchuk, Committee Member

Bo Cai, Committee Member

Tracey L. Weldon, Interim Vice Provost and Dean of the Graduate School

© Copyright by Ishwor Karki, 2021
All Rights Reserved.

DEDICATION

To my family.

ACKNOWLEDGEMENTS

First and most importantly I would like to acknowledge my advisor Prof. Dr. Ken D. Shimizu for his continuous guidance, support, and advice throughout the five years in graduate school. It would be impossible for me to achieve my goal without your help and encouragement. It will be hard for me to forget the way you guided and motivated me at the beginning of my Ph.D. program. I feel blessed to have you as my advisor who shaped and made me capable of getting a Ph.D.

Next, I would like to thank my Ph.D. committee members: Prof. Dr. Linda S. Shimizu, Prof. Dr. Sophya Garashchuk, and Prof. Dr. Bo Cai. I would like to thank them for their suggestions, advice, and direction in my research plan and research proposal.

I would like to thank the Department of Chemistry and Biochemistry, for giving me this great opportunity in my life. Jennifer C. Merkel has always been very supportive and helpful from the day I started my application to UofSC.

I would like to thank all my group members Joe, Erik, Chris, Alex, Daniel, Binzhou, Hao, and especially Ping who was like a senior brother to me. I am truly amazed by the way he treats his colleagues. I will always remember my late-night stay in the lab with Ping, helping and guiding my research tirelessly, without any hesitation. I was very lucky to have Ping as my senior lab member.

I would also like to thank my parents, sister, and brother for always supporting and encouraging me to achieve highly and make them proud. Finally, it's time for them to be proud. Lastly, I would like to thank Surendra, Atit, Arun, Ritu, Paras, Rajendra, Narayan,

Gyanendra, Arjun, Arya, Nima, Tika, Bharat, Hem, Laxman, Rabins, and Bishal for their encouragement. Special thanks to Jayanti.

ABSTRACT

The main topics of this dissertation are: 1) the study of hydrophilic-lipophilic balance (HLB) polymer monoliths for solid-phase extraction (SPE) applications, 2) molecularly imprinted polymers (MIPs) for capturing the CO₂ gas and 3) the application of symmetry-adapted perturbation theory (SAPT) calculations to examine the origins of non-covalent interactions.

HLB polymers are popular sorbent materials in separation science. The Divinylbenzene-*co*-N-vinylpyrrolidone (DVB-*co*-NVP) polymer is one of the most widely used general-purpose HLB polymers. Despite the popularity of HLB polymer stationary phases, the studies of the adsorption properties of DVB-*co*-NVP have only been reported over a narrow range of monomer ratios. Thus a series of DVB-*co*-NVP polymers that span a wide range of NVP monomer ratios from 0 mol% to 60 mol% were prepared to study the absorption properties. The DVB-*co*-NVP polymer series were capable of extracting different analytes from aqueous samples successfully, hence the polymeric series were tested for extraction properties for an array of real-world SPE analytes from human urine samples.

The strategy to develop MIPs with higher capacities and adsorption efficiencies for CO₂ is also discussed in this dissertation. MIPs having higher specific surface areas can have optimized CO₂ adsorption. A functional monomer, 4-vinylbenzyl amidine was synthesized and crosslinked with divinylbenzene crosslinker and tested for its CO₂

adsorption property. The application of symmetry-adapted perturbation theory (SAPT) calculations is also detailed in this dissertation. SAPT is a type of energy decomposition analysis that calculates the total intermolecular interaction energies as a sum of component fundamental interactions. These include a practical tutorial on how to perform the calculations and examples of the application of SAPT studies to examine the non-covalent interactions in molecular balances and molecular rotors.

TABLE OF CONTENTS

DEDICATION	iii
ACKNOWLEDGEMENTS.....	iv
ABSTRACT	vi
LIST OF TABLES	xi
LIST OF FIGURES	xii
LIST OF SCHEMES.....	xv
LIST OF ABBREVIATIONS	xvi
CHAPTER 1 INTRODUCTION TO HYDROPHILIC–LYPOPHILIC BALANCE COPOLYMERS, MOLECULARLY IMPRINTED POLYMERS, AND COMPUTATIONAL METHODOLOGIES.....	1
1.1 ABSTRACT.....	2
1.2 DEVELOPMENT OF SOLID-PHASE EXTRACTION (SPE) SORBENTS	2
1.3 TYPES OF SPE SORBENTS.....	4
1.4 METHODS OF SYNTHESIZING HYDROPHILIC POLYMERIC SORBENTS	7
1.5 MOLECULARLY IMPRINTED POLYMERS (MIPs) FOR CO ₂ CAPTURE.....	10
1.6 COMPUTATIONAL STUDIES.....	10
1.7 REFERENCES	15
CHAPTER 2 ABSORPTION PROPERTIES OF MONOLITH POLY (DIVINYLBENZENE- <i>CO</i> - <i>N</i> - VINYLPIRROLIDONE) OVER A WIDE RANGE OF MONOMER RATIOS	20
2.1 ABSTRACT.....	21
2.2 INTRODUCTION	21
2.3 EXPERIMENTAL SECTION.....	25

2.4 RESULTS AND DISCUSSION	28
2.5 CONCLUSIONS.....	39
2.6 SUPPLEMENTAL INFORMATION	40
2.7 REFERENCES	41
CHAPTER 3 SOLID-PHASE EXTRACTION OF REGULATED ANALYTES WITH DIFFERENT LOG P VALUES FORM HUMAN URINE SAMPLE BY POLY (DIVINYL- <i>co</i> - <i>N</i> - VINYLPIRROLIDONE) WITH WIDE RANGE OF MONOMER RATIOS	45
3.1 ABSTRACT.....	46
3.2 INTRODUCTION	46
3.3 EXPERIMENTAL SECTION.....	48
3.4 RESULTS AND DISCUSSION.....	49
3.5 CONCLUSIONS.....	56
3.6 REFERENCES	56
CHAPTER 4 MOLECULARLY IMPRINTED POLYMERS (MIPs) FOR CO ₂ CAPTURE	58
4.1 ABSTRACT.....	59
4.2 INTRODUCTION	59
4.3 EXPERIMENTAL SECTION	62
4.4 CONCLUSIONS.....	70
4.5 REFERENCES	70
CHAPTER 5 A TUTORIAL ON PERFORMING SAPT AND I-SAPT CALCULATIONS.....	73
5.1 ABSTRACT.....	74
5.2 INTRODUCTION	74
5.3 CONCLUSIONS.....	86
5.4 SUPPLEMENTAL INFORMATION.....	86

5.5 REFERENCES	88
APPENDIX A COPYRIGHT CLEARANCE.....	90

LIST OF TABLES

Table 1.1 Properties of commercial polymeric sorbents	6
Table 1.2 Classification of DFT Methods.....	12
Table 1.3 Basis sets by different groups	14
Table 2.1 Specific surface area measurement of representative monolith (DVB- <i>co</i> -NVP) polymers calculated from BET nitrogen adsorption isotherms.....	36
Table 3.1 Recovery percentages of different analytes for series of DVB- <i>co</i> -NVP monolith polymer series.....	50
Table 5.1 XYZ coordinates of optimized phenol rotor TS that will be used for an I-SAPT calculation in Psi4.....	78
Table 5.2 I-SAPT Psi4 input file for the norbornene-PhOH hydrogen bonding rotor for the I-SAPT0 calculation between the phenol(OH) fragment and the imide C=O fragment	80
Table 5.3 SAPT decomposed energies for the OH•••O=C interaction in the norbornene-PhOH rotor TS.....	82
Table 5.4 Calculated decomposed SAPT0 energies for different rotors	83
Table 5.5 XYZ coordinates of the TS structures of the norbornene-PhOH and the norbornene-PHOCH ₃ rotors.....	87

LIST OF FIGURES

Figure 1.1 Example of the application of SPE sorbents in DPX pipet tips	3
Figure 1.2 Structure of polar monomers to make hydrophilic polymeric sorbents	6
Figure 1.3 Schematic of suspension polymerization process	8
Figure 1.4 Schematic of monolith polymerization	9
Figure 2.1 (top) DVB- <i>co</i> -NVP polymer synthesis by free radical polymerization and (bottom) analytes used to test the adsorption properties from most polar (adenosine) to least polar (<i>p</i> -toluidine).....	23
Figure 2.2 The percent yields of monolith and suspension DVB- <i>co</i> -NVP polymers versus the NVP mol% feed ratio. The yields were measured based on polymer weights before sieving	28
Figure 2.3 Optical microscope images comparing the size and shape of the representative monolith (left) and suspension (right) DVB- <i>co</i> -NVP polymers formed using 30:70 NVP/DVB mol/mol feed ratios	29
Figure 2.4 SEM images of the monolith (left) and suspension (right) polymers prepared with 30 mol% NVP feed ratios.	30
Figure 2.5 Plot of the NVP incorporation mol percentages (mol%) for monolith (black circles) and suspension (red triangles) polymers versus the NVP monomer feed percentages (mol%) used in the polymerization reaction mixtures. The green line represents an ideal NVP incorporation efficiency where the NVP incorporation percentages equal the feed percentages. The non-zero values for the 0 mol% NVP feed ratio polymers are due to the presence of nitrogen from the AIBN initiator. The error bars were smaller than the data points	30
Figure 2.6 (left) Monolith polymers with 0 mol% NVP feed percentages having poor wettability floating on top of the aqueous solution after shaking (right) and monolith polymer with 30 mol% NVP feed percentages having good wettability and falling to the bottom of the aqueous solution.....	32
Figure 2.7 Comparison of the weight of caffeine bound from aqueous solution by DVB- <i>co</i> -NVP monolith and suspension polymers with similar NVP	

incorporation percentages (27 mol% and 25 mol%). The data points were collected via batch binding studies of 5 mL of 0.16 mM caffeine solutions using 10, 20, 30, 40, and 50 mg of polymers.....	33
Figure 2.8 The percent yields of monolith and suspension DVB- <i>co</i> -NVP polymers versus the NVP mol% feed ratio. The yields were measured based on polymer weights before sieving.....	35
Figure 2.9 Single point binding capacities of the monolith DVB- <i>co</i> -NVP polymers with varying NVP feed ratios (0 – 60 mol%) for p-toluidine, caffeine, and adenosine. The batch binding conditions were: 0.5 mM p-toluidine with 10 mg polymer, 0.16 mM caffeine with 20 mg polymer, and 0.1 mM adenosine with 40 mg polymer in 5 mL of solvent.....	37
Figure 2.10 Time-dependent binding curve for 5 mL of 0.16mM caffeine solution to 20 mg DVB- <i>co</i> -NVP polymer prepared with 50% NVP.....	41
Figure 3.1 Binding capacities of monolith DVB- <i>co</i> -NVP polymers with varying NVP feed ratios (0 – 60 mol%) for amitriptyline, cyclobenzaprine, and nortriptyline showing similar binding patterns.....	51
Figure 3.2 Examples of structurally similar analytes a) amitriptyline, b) cyclobenzaprine, and c) nortriptyline	52
Figure 3.3 Binding capacities of monolith DVB- <i>co</i> -NVP polymers with varying NVP feed ratios (0 – 60 mol%) for methylphenidate, 6-mam, MDMA, and tramadol showing similar binding patterns.....	52
Figure 3.4 Structure of analytes a) MDMA, b) 6-MAM, c) tramadol, and d) methylphenidate.....	53
Figure 3.5 Structure of analytes a) oxymorphone (log P = 0.83), b) methamphetamine (log P = 2.07) , and c) fentanyl (log P = 4.05).....	53
Figure 3.6 Binding capacities of monolith DVB- <i>co</i> -NVP polymers with varying NVP feed ratios (0 – 60 mol%) for oxymorphone, fentanyl, and methamphetamine.....	54
Figure 3.7 Principal component analysis plot for different analytes in response to binding patterns.....	55
Figure 4.1 Schematic representation of molecular imprinting process to make MIPs.....	60
Figure 4.2 (left) DBU in methanol before bubbling CO ₂ (right) [DBUH ⁺][HCO ₃ ⁻] formed after bubbling in CO ₂ for 10 minutes.....	63

Figure 4.3 IR spectrum of DBU in methanol before and after CO ₂ bubbling	63
Figure 4.4 ¹ H NMR spectra of vinylbenzyl amine monomer	65
Figure 4.5 ¹ H NMR spectra of vinylbenzyl amidine monomer	66
Figure 4.6 IR spectrum of DVB- <i>co</i> -VBA polymer made with 10 mol% VBA.....	67
Figure 4.7 IR spectrum of DVB- <i>co</i> -VBA polymer made with 15 mol% VBA.....	68
Figure 4.8 IR spectrum of DVB only polymer	68
Figure 4.9 IR absorption for DVB- <i>co</i> -VBA polymer soaked in solvents and CO ₂ bubbled (red spectrum soaked in methanol, blue spectrum soaked in dichloromethane)	69
Figure 4.10 IR absorption for DVB- <i>co</i> -VBA polymer soaked in chloroform and CO ₂ bubbled.....	69
Figure 5.1 Optimized transition state (TS) structure of phenol rotor with labels turned on	78
Figure 5.2 Commands in anaconda terminal for activating Psi4 environment and job submission	81
Figure 5.3 Transition state structure of norbornene-PhOH (HB), norbornene- PhOH (nHB), and norbornene-PhOCH ₃ rotors with the interacting fragments highlighted in blue	83
Figure 5.4 I-SAPT decomposed energies for the intramolecular interaction for different rotors calculated with jun-cc-pVDZ basis set	83
Figure 5.5 Correlation of total SAPT energies (SAPT E _{total}) and experimental (ΔG [‡]) rotational barriers for norbornene-PhOH, norbornene-PhOCH ₃ , norbornene-PhNH ₂ , norbornene-PhN(CH ₃) ₂ , and norbornene- PhNHCOCF ₃ rotors	84

LIST OF SCHEMES

Scheme 4.1 a) reaction of ethanolamine (EA) with carbon dioxide to form a stable carbamic acid salt b) chemisorption polymers based on polyamine materials	61
Scheme 4.2 Reaction of CO ₂ with DBU in methanol solvent to form [DBUH ⁺][HCO ₃ ⁻]	62
Scheme 4.3 Synthesis route of 4-vinylbenzyl amidine monomer.....	64

LIST OF ABBREVIATIONS

6-MAM	6-acetylmorphine
BSSE	Basis set superposition error
DBU	1, 8-diazabicyclo[5.4.0]undec-7-ene
DFT	Density Functional Theory
DVB	Divinylbenzene
EA	Ethanolamine
GS	Ground State
HLB	Hydrophilic-lipophilic balance
LLE	Liquid-liquid extraction
MDMA	Methylenedioxymethamphetamine
MIP	Molecularly imprinted polymer
NCI	Non-covalent interactions
NVP	N-vinylpyrrolidone
SAPT	Symmetry Adapted Perturbation Theory
SPE	Solid-phase extraction
TS	Transition State

CHAPTER 1

INTRODUCTION TO HYDROPHILIC-LIPOPILIC BALANCE COPOLYMERS, MOLECULARLY IMPRINTED POLYMERS, AND COMPUTATIONAL METHODOLOGIES

1.1 Abstract

This chapter provides an introduction to hydrophilic-lipophilic balance (HLB) copolymers, molecularly imprinted polymers (MIPs), and quantum mechanical SAPT calculations, which are the subjects of study in Chapters 2-5. Hydrophilic-lipophilic balance copolymers are polymeric sorbents that have hydrophilic and hydrophobic properties and the capability to extract polar and non-polar analytes from aqueous and non-aqueous samples. HLB polymers are in high demand in the separation science field and are widely used as the solid-phase extraction materials. HLB polymers are generally composed of a hydrophobic cross-linker monomer and the hydrophilic functional monomer. Molecularly imprinted polymer (MIP) for capturing the CO₂ gas is discussed in the fourth chapter. The fifth chapter is a tutorial on the computational tools and techniques that will help new users to become familiar with computational skills and successfully perform the symmetry-adapted perturbative theory (SAPT) calculation. SAPT is a perturbation theory based quantum calculation method that decomposes the total interaction energy into its physically meaningful components: electrostatics, exchange, induction, and dispersion.

1.2 Development of Solid-Phase Extraction (SPE) sorbents

Chapters 2 and 3 describe the preparation and study of new polymeric stationary phases for solid-phase extraction (SPE). This section will provide a brief introduction and background on SPEs. SPEs have become a popular method for sample preparation in the field of separation science.¹ SPE is commonly used in the purification and concentration of analytes from complex matrices such as environmental and biological samples.^{2,3} SPE is usually preferred over the liquid-liquid extraction (LLE) method for small samples or when processing a large number of samples. Important advantages of SPE over LLE are

lower amounts of organic solvent consumption and fewer solvent handling steps. These minimize the loss of analyte in extraction/concentration processes, making SPE faster and more cost-effective. SPEs work by partitioning the analytes from a mobile liquid phase into a solid phase.

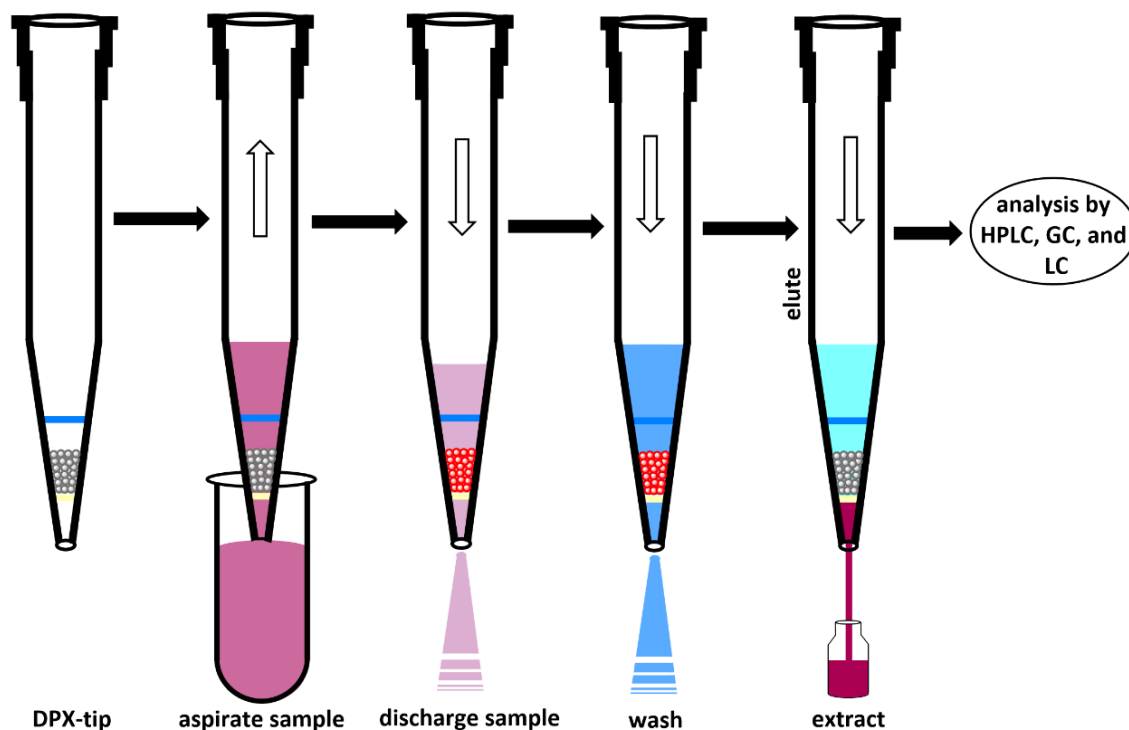


Figure 1.1 Example of the application of SPE sorbents in DPX pipet tips.

An example of SPE use for sample preparation is shown in Figure 1.1 using a DPX pipet tip filled with a SPE sorbent. The DPX tip has a frit at the bottom and a barrier at the top to prevent the loss of sorbent. First, a solution containing the analytical sample is drawn into the tip to allow the absorption of the analytes onto the SPE sorbent. Second, the analyte solution in the tip is discharged, leaving the SPE sorbent with bound analytes. Third, the sorbent is washed with water to remove interferences like salts and other polar interferences. Finally, the analyte is eluted from sorbents with a very small amount (microliters) of an organic solvent such as methanol or acetonitrile. The partially purified

and concentrated sample can then be directly analyzed using standard analytical techniques like HPLC, LC, or GC.

SPE processes are easily automated and are generally faster than LLE methods. SPE can also be easily integrated with common analytical techniques like HPLC, GC, and LC. The selection of the sorbent is a key factor for optimal extraction efficiencies, capacities, and purities.^{4,5} SPE sorbents contain functional groups that can form interactions with the analytes of interest while having low affinities for the matrix. Hence this has led to the continuous development of new sorbent materials that can fulfill the demand for higher extraction efficiencies.⁶⁻⁸

1.3 Types of SPE sorbents

SPE sorbents can be categorized into silica-based, carbon-based, or porous polymer-based materials. The most common sorbents are functionalized silica, which can yield reverse-phase or normal-phase sorbents. The reverse-phase silica sorbents are functionalized with octadecyl (C₁₈), octacyl (C₈), ethyl (C₂), phenyl (Ph), or cyclohexyl (CH) groups. Normal-phase silica sorbents are commonly functionalized with cyanopropyl (CN), aminopropyl (NH₂), or diol functional groups (HO—CH—CH₂—OH).¹ Reverse-phase silica sorbents interact with the analytes mainly by hydrophobic interactions. However, there are several drawbacks to silica-based sorbents including low recovery rates of polar analytes, instability at extreme pHs, and reactivity of the silanol group.^{1,3}

The drawbacks of carbon-based sorbents are low specific surface areas and excessive or even irreversible retention. Advantages include better absorption capacities

and improved chemical and thermal resistance.^{5,9} Some of these disadvantages can be overcome with the porous polymeric sorbents.

Porous polymeric sorbents have attractive properties such as higher specific surface areas, greater stability throughout the pH range, better analyte desorption properties, and also easier to tune properties by changing the structure. Accordingly, porous polymeric sorbents are the most popular type of SPE sorbents and are used in food safety, water contamination and purity, and regulated drug testing analyses.¹⁰⁻¹⁶ The most commonly used reverse-phase polymeric sorbent is styrene-divinylbenzene (St-DVB) which is a macroporous hydrophobic sorbent with moderate specific surface areas up to 800 m²g⁻¹.² A disadvantage of these reverse-phase sorbents is the need to prewet the sorbents prior to the extraction of polar analytes from the aqueous samples. This increases the consumption of organic solvents and adds an extra step to the extraction process. To address these limitations, second-generation polymeric sorbent materials such as hydrophilic-lipophilic balance (HLB) polymers⁶ were developed from a combination of hydrophobic and hydrophilic monomers. The hydrophilic properties of HLB sorbents eliminate the need for the pre-wetting step. Thus, HLB sorbents have the ability to extract polar and non-polar analytes directly from aqueous and non-aqueous samples. Examples of the commonly used macroporous reverse-phase polymeric sorbents and second-generation hydrophilic polymeric sorbents are listed in Table 1.1.¹

Hydrophilic sorbents materials can also be made by post-modification of reverse-phase sorbents such as St-DVB. Whereas, HLB hydrophilic polymeric sorbents are generally prepared by copolymerizing a hydrophobic cross-linking monomer with a hydrophilic monomer containing polar functional groups like cyano, amide, and esters

groups (Figure 1.2).^{1,2,17-19} The polar moieties of HLB sorbents interact with polar functional groups in the analytes and the hydrophobic surfaces interact with the hydrophobic and aromatic functional groups. HLB polymers are also compatible with aqueous and organic solvents.

Table 1.1 Properties of commercial polymeric sorbents.¹

	Sorbents	material	supplier	surface area (m ² /g)
Macroporous	Amberlite XAD-1	St-DVB	Rohm & Hass	100
	Amberlite XAD-1	St-DVB	Rohm & Hass	300
	Amberlite XAD-1	St-DVB	Rohm & Hass	≥750
	PLRP-S-10	St-DVB	Polymer Laboratories	500
	PLRP-S-30	St-DVB	Polymer Laboratories	375
Hydrophilic	Amberlite XAD-1	MA-DVB	Rohm & Hass	450
	Amberlite XAD-1	MA-DVB	Rohm & Hass	310
	Oasis HLB	NVP-DVB	Waters	830
	Porapak RDX	NVP-DVB	Waters	n.d.
	Absolut Nexus	MA-DVB	Varian	575
	Discovery DPA-6S	Polyamide	Supelco	n.d.

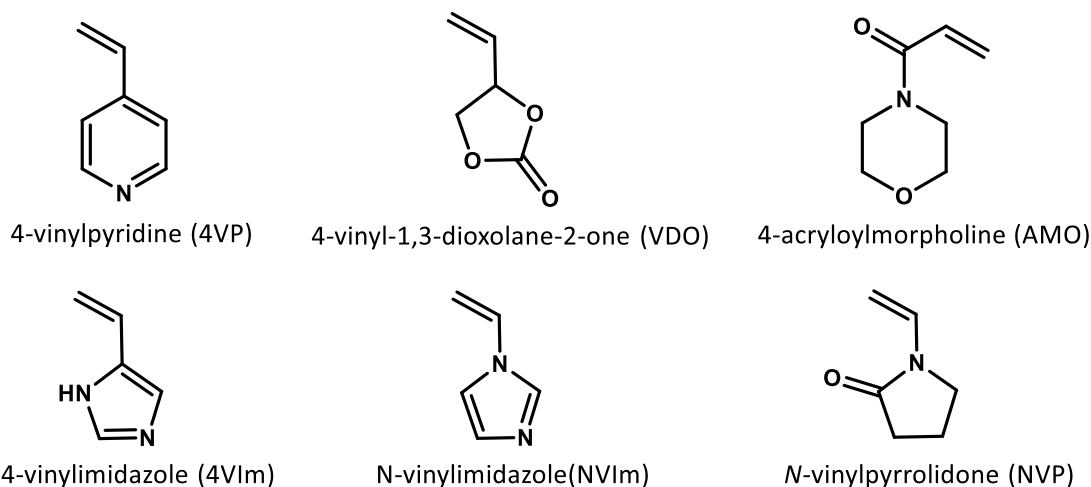


Figure 1.2 Structure of polar monomers to make hydrophilic polymeric sorbents.

Most polymeric SPE sorbents are spherical beads formed by suspension polymerization. While suspension polymerization is well-suited for making hydrophobic reverse-phase polymeric sorbents, suspension polymerization has limitations when synthesizing highly polar or hydrophilic polymeric sorbents. Hence, in Chapters 2 and 3, we discuss and develop possible alternate polymerization methods for preparing hydrophilic, HLB polymeric sorbents.

1.4 Methods of synthesizing hydrophilic polymeric sorbents.

1.4.1 Suspension polymerization

Suspension polymerization was developed by Hoffman and Delburch in 1909.²⁰ It is the most common free radical polymerization technique to synthesize polymeric SPE sorbents in the form of spherical beads of sizes ranging from 5-1000 μm . Suspension polymerization is a biphasic polymerization with spherical organic droplets within a continuous aqueous phase. The polymerization takes place in the organic droplets as the initiator and monomers are more soluble in the organic phase while the aqueous phase serves as a heat transfer medium. The organic droplets are formed with the help of a stabilizer additive. Typically the volume ratio of organic to the aqueous phase is kept within 0.1 - 0.5.^{21,20} The reaction mixture is stirred vigorously to form an emulsion, which is then heated at a suitable temperature to allow the initiator to form free radicals and initiate the polymerization reaction. Uniform spherical polymer beads are formed after the completion of the suspension polymerization which can be collected by suction filtration. A schematic is shown in Figure 1.3.

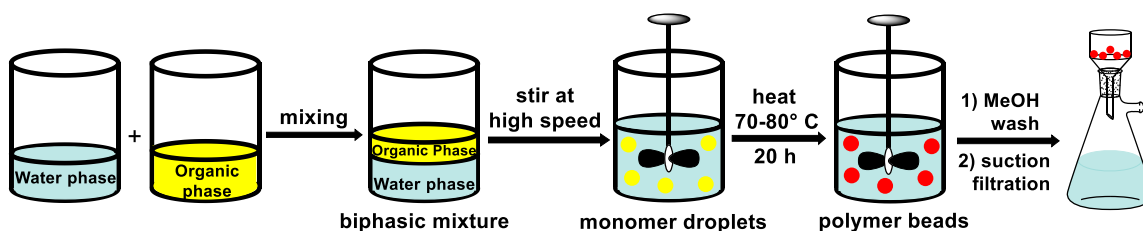


Figure 1.3 Schematic of the suspension polymerization process.

The suspension polymerizations containing more polar or hydrophilic monomers are more challenging due to the possibility of the polar monomers partitioning into the aqueous layer. This reduces the incorporation percentage and efficiency of the polar monomer in the polymer beads and often inhibits the formation of stable emulsions with uniform spherical droplets.

1.4.2 Monolith polymerization

Porous polymer monoliths are an alternative polymer morphology for sorbents used in SPE and chromatographic stationary phases.^{22–24} Use of polymer monolith stationary phases started in the late 1980s and early 1990s.^{25–27} Porous polymer monoliths can be used as formed or can be ground into small particles for use as SPE sorbents. The monolith polymerization process has fewer variables than suspension polymerization and does not rely on the formation of a meta-stable emulsion. Hence, they are easier and have higher success rates, with improved monomer incorporation efficiencies and yields. Polymer particles prepared by grinding polymer monoliths have heterogeneous shapes and sizes. However, for SPE applications homogeneous adsorption kinetic are not as important. Monolithic SPE sorbents are well suited to SPE applications.^{23,24,28–35} Also another advantage of monolith polymerizations is the monophasic reaction mixture. Hence, the loss

of polar monomers into an aqueous phase is not a concern. Thus, monolith polymerizations can be used to make sorbents with highly polar or hydrophilic monomers.

Due to these attractive characteristics, the monolith polymerization methods were employed in Chapters 2 and 3 as the primary method for preparing hydrophilic SPE sorbents. A simple schematic of the monolith polymerization process is shown in Figure 1.4 below. Monophasic reaction mixtures were made by mixing the crosslinking monomers, functional monomers, and initiators in the organic solvent. The reaction mixture was then heated at a suitable temperature to allow the initiator to form free radicals and initiate the polymerization reactions. Next, the monolith formed was ground with mortar and pestle to yield small polymer particles. The ground particles are washed with organic solvent and collected by suction filtration.

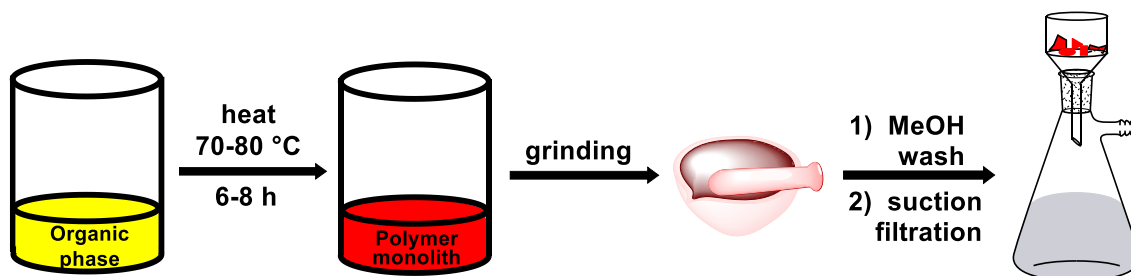


Figure 1.4 Schematic of monolith polymerization.

In Chapter 2, we investigate the extraction properties of HLB monolith polymer SPEs. The monolithic SPE sorbents were tested against real-world analytes. For the initial studies, batch binding studies were used to assess the absorption efficiencies of the monolith polymer particles. In Chapter 3, the real-world analytical applications of the polymers were tested by their extraction efficiency of different regulated drugs from human urine samples in collaboration with the DPX lab and then measured by LC-MS.

1.5 Molecularly imprinted polymers (MIPs) for CO₂ capture

The fourth chapter of this dissertation describes the synthetic strategy for preparing MIPs that have higher capacities and adsorption efficiencies for CO₂ capture. MIPs are inexpensive and easy to prepare synthetic polymers that have tailored molecular recognition properties. The strategy to develop and optimize the CO₂ absorption capacities of MIPs by increasing the surface area of MIPs is described in this chapter.

1.6 Computational Studies

The fifth chapter of this dissertation provides a tutorial for future group members interested in the application of computational techniques for the study and understanding of non-covalent interactions. A commonly used perturbation theory method, symmetry adapted perturbation theory (SAPT)³⁶ is introduced, and examples are provided of different systems. This quantum chemical calculation has assisted in making predictions about experimental measurements and in understanding the underlying forces behind non-covalent interactions.^{37,38}

1.6.1 Techniques

To introduce the topic of quantum mechanical calculations, general methods of molecular computational analysis will be discussed in this section. These include: (1) conformer distribution, (2) energy profile, (3) ground state (GS), and transition state (TS) geometry optimization. These techniques are required prior to applying SAPT analyses.

1.6.2 Optimization methods

In computational chemistry, there are a range of quantum mechanical methods that can be used to calculate the energy of a ground state or a transition state. Depending upon

the needed degree of accuracy and the time available for the calculation, an appropriate method of calculation can be selected. The methods in order of increasing calculation time and accuracy are: molecular mechanics (MM), semi-empirical (SE), Hartree-Fock (HF), density functional theory (DFT), and correlated wavefunctions (CW). The DFT method is the most commonly used method for molecular energy calculation as this method usually provides the best balance of accuracy and computational cost.

Molecular mechanics is often used in the conformational analysis because it is the fastest method. However, molecular mechanics is an empirical method based on classical mechanics and thus is very limited in providing quantum mechanical information. Therefore, this method is often used to generate initial structures but rarely to calculate the final GS or TS geometries and energies. MMFF and SYBYL are the two molecular mechanic force fields available in Spartan'18.

Semi-empirical methods are hybrid methods which combine *ab initio* methods and empirical parameters. The Empirical parameters are used to simplify and speed up *ab initio* quantum chemical calculations. Some semi-empirical methods are able to reproduce the interaction energies computed by higher and costlier methods like density functional theory.³⁹ Examples of semi-empirical methods in Spartan'18 are AM1, RM1, PM3, PM6, and MNDO. One application of semi-empirical methods is to generate molecular orbital (HOMO and LUMO) quickly for large systems.

Hartree-Fock (HF) method, also called a self-consistent field (SCF) theory, uses the mean field theory for electrons. This *ab initio* method approximates the Schrodinger equation using a single Slater determinant and can be used to solve the optimized single electron wavefunction under the condition that the dynamics of this single electron is

influenced by the nucleus and potential of surrounding electrons.⁴⁰ Therefore, HF disregards electron correlation,⁴¹ which is the basis for polarization and dispersion-based phenomenon. HF calculations are often less accurate and more costly than density functional theory calculations.

Density functional theory (DFT) is an *ab initio* method which explicitly introduces an empirical correlation parameter (electron correlation parameter). DFT methods are generally faster and more accurate than HF as long as range electron exchange is not needed. Spartan'18 offers a wide selection of DFT methods listed in Table 1.2. Due to their improved accuracy and lower cost, DFT methods are the most widely used methods. In our studies, we commonly used B3LYP, B3LYP-D3, M06-2X, and ω B97X-D.

Table 1.2 Classification of DFT methods.

DFT methods	Functionals
Generalized Gradient Approximation (GGA)	B86PW91, BLYP, BPW91, B97-D2, SOGGA11, PBE-D3, VV10
Global Hybrid Generalized Gradient Approximation (GH-GGA)	B3LYP, B3LYP-D3, EDF2, B97-3, B3PW91, SOGGA11-X
Range Separated Hybrid Generalized Gradient Approximation (RSH-GGA)	ω B97X-D, ω B97X-V, ω B97X, CAM-B3LYP, N12-SX, LC-VV10
Meta Generalized Gradient Approximation (mGGA)	B97M-V, M06-L, BMK, M11-L, TPSS-D3
Global Hybrid meta Generalized Gradient Approximation (GH-GGA)	M06-2X, M06, M08-HX, M08-SO, MPW1B95
Range Separated Hybrid meta Generalized Gradient Approximation (RSH-GGA)	M11, ω B97M-V, MN12-SX
Double Hybrid meta Gradient Approximation (DH-RSH-mGGA)	ω B97M(2)

Correlated wavefunction (CW) methods include electron correlation functions and are the most accurate. DFT methods use the electron density for energy approximation rather than the wave function and include all-electron correlation hence exhibiting over-correlation and are less accurate than CW methods. DFT methods incorporate correlation limited to the present-day functionals and ignore long-range electron correlation like dispersion interactions. CW methods available in Spartan'18 are MP2, RI-MP2, MP3, MP4, QCISD, QCISD(T), CCSD, CCSD(T), electronic G3, electronic G4, electronic G3(MP2), and electronic G4(MP2). Correlation-based methods are more accurate but also significantly more expensive than the other methods and thus, they are generally only applied for single-point energy calculations.

Quantum mechanical calculations generally employ a calculation method and a basis set.⁴² Only molecular mechanics and semi-empirical methods do not require basis sets. A basis set refers to the set of (nonorthogonal) particle functions used to build the molecular orbitals. Basis sets differ in types and number of atomic orbitals (s, p, d, f), treatment of polarization and the diffuse functions added. Basis sets developed by different groups are listed in Table 1.3.⁴²

Basis sets are classified by the number of functions that describe the valence atomic orbitals: single zeta (SZ), double zeta (DZ), triple zeta (TZ). A single zeta basis set has only 1 s-function for first row elements (H and He), but has 2 s-functions (1s and 2s) and 1 set of p-functions (2p_x, 2p_y, and 2p_z) hence a total of 2 basis functions for s-block elements, and 5 basis functions for p-block elements. Commonly used single zeta basis sets are STO-2G, STO-3G, and STO-6G. Likewise, double zeta basis sets have two basis functions for each atomic orbital. For example, C- atom has 4 s-functions (1s, 1s', 2s and 2s') and 6 p-

functions ($2p_x$, $2p_y$, $2p_z$, $2p_x'$, $2p_y'$ and $2p_z'$) so a total of 10 functions. Commonly used double zeta basis sets are 6-31G*, cc-pVDZ, and def2-SVPD.

Table 1.3 Basis sets by different groups.

Developers	Basis set name	Basis set type available in Spartan'18
Pople and coworkers	Pople-style $k-lmnG$	6-31G**, 6-311G**, 6-311+G(2d,p), 6-31+G**, 6-311G(2d,p), 6-311+G(3df,2p)
Ahlrichs and coworkers	Ahlrichs SVP, TZP, QZP basis sets	def-SV(P), def2-TZVP, def2-QZVP, def2-SVPD, def2-TZVPPD, def2-QZVPPD
Jorge and coworkers	XZP basis sets	n.a.
Koga and coworkers	Sapporo basis sets	n.a.
Roos and coworkers	ANO basis sets	n.a.
Dunning and Peterson and coworkers	cc-pVXZ basis sets	cc-pVDZ, cc-pVTZ, cc-pVQZ, aug-cc-pVDZ, aug-cc-pVTZ, aug-cc-pVQZ
Petersson and coworkers	$nZaP$ basis sets	n.a.
Jensen and coworkers	pc- n basis sets	n.a.

In general, more complex basis sets will yield more accurate energies and geometries, but the cost increases exponentially with complexity. Thus the selection of a suitable method and proper basis set is quite important. Prospective low energy conformers can be identified using faster methods such as molecular mechanics and then optimized at higher levels of theory. Finally, quantitative analysis calculations like symmetry-adapted perturbation theory (SAPT) can be performed on the optimized structures.^{43,44} SAPT can calculate and partition the intramolecular or intermolecular interaction energy into fundamental electrostatics, exchange, induction, dispersion, and charge-transfer (using

SAPT/cDFT) components. NBO (Natural bond orbital) analysis can calculate the orbital interactions for intramolecular or intermolecular interactions.^{45,46} The quantitative analysis were performed on either Q-Chem or Psi4.^{47,48}

1.7 References

- (1) Fontanals, N.; Marcé, R. M.; Borrull, F. New Hydrophilic Materials for Solid-Phase Extraction. *TrAC, Trends Anal. Chem.* **2005**, *24* (5), 394–406. <https://doi.org/10.1016/j.trac.2005.01.012>.
- (2) Fontanals, N.; Marcé, R. M.; Borrull, F. New Materials in Sorptive Extraction Techniques for Polar Compounds. *J. Chromatogr. A* **2007**, *1152* (1–2), 14–31. <https://doi.org/10.1016/j.chroma.2006.11.077>.
- (3) Poole, C. F. New Trends in Solid-Phase Extraction. *TrAC, Trends Anal. Chem.* **2003**, *22* (6), 362–373. [https://doi.org/10.1016/S0165-9936\(03\)00605-8](https://doi.org/10.1016/S0165-9936(03)00605-8).
- (4) Dean, J. R. *Extraction Methods for Environmental Analysis*; John Wiley: Chichester; New York, 1998.
- (5) Masqué, N.; Marcé, R. M.; Borrull, F. New Polymeric and Other Types of Sorbents for Solid-Phase Extraction of Polar Organic Micropollutants from Environmental Water. *TrAC, Trends Anal. Chem.* **1998**, *17* (6), 384–394. [https://doi.org/10.1016/S0165-9936\(98\)00019-3](https://doi.org/10.1016/S0165-9936(98)00019-3).
- (6) Dias, N. C.; Poole, C. F. Mechanistic Study of the Sorption Properties of Oasis® HLB and Its Use in Solid-Phase Extraction. *Chromatographia* **2002**, *56* (5–6), 269–275.
- (7) Weigel, S.; Kallenborn, R.; Hühnerfuss, H. Simultaneous Solid-Phase Extraction of Acidic, Neutral and Basic Pharmaceuticals from Aqueous Samples at Ambient (Neutral) PH and Their Determination by Gas Chromatography–Mass Spectrometry. *J. Chromatogr. A* **2004**, *1023* (2), 183–195. <https://doi.org/10.1016/j.chroma.2003.10.036>.
- (8) Xiao, J.; Wang, J.; Fan, H.; Zhou, Q.; Liu, X. Recent Advances of Adsorbents in Solid Phase Extraction for Environmental Samples. *Int. J. Environ. Anal. Chem.* **2016**, *96* (5), 407–435. <https://doi.org/10.1080/03067319.2016.1150459>.
- (9) Barceló, D. *Environmental Analysis: Techniques, Applications, and Quality Assurance*; Elsevier: Amsterdam, The Netherlands, 1993.
- (10) Zhang, Y.; Li, G.; Wu, D.; Li, X.; Yu, Y.; Luo, P.; Chen, J.; Dai, C.; Wu, Y. Recent Advances in Emerging Nanomaterials Based Food Sample Pretreatment Methods for Food Safety Screening. *TrAC, Trends Anal. Chem.* **2019**, *121*, 115669. <https://doi.org/10.1016/j.trac.2019.115669>.
- (11) Ansari, S. Application of Magnetic Molecularly Imprinted Polymer as a Versatile and Highly Selective Tool in Food and Environmental Analysis: Recent Developments and Trends. *TrAC, Trends Anal. Chem.* **2017**, *90*, 89–106. <https://doi.org/10.1016/j.trac.2017.03.001>.

- (12) Socas-Rodríguez, B.; González-Sálamo, J.; Hernández-Borges, J.; Rodríguez-Delgado, M. Á. Recent Applications of Nanomaterials in Food Safety. *TrAC, Trends Anal. Chem.* **2017**, *96*, 172–200. <https://doi.org/10.1016/j.trac.2017.07.002>.
- (13) Jiang, H.-L.; Li, N.; Cui, L.; Wang, X.; Zhao, R.-S. Recent Application of Magnetic Solid Phase Extraction for Food Safety Analysis. *TrAC, Trends Anal. Chem.* **2019**, *120*, 115632. <https://doi.org/10.1016/j.trac.2019.115632>.
- (14) Richardson, S. D.; Kimura, S. Y. Water Analysis: Emerging Contaminants and Current Issues. *Anal. Chem.* **2020**, *92* (1), 473–505. <https://doi.org/10.1021/acs.analchem.9b05269>.
- (15) Richardson, S.; Ternes, T.; Van, D. Water Analysis: Emerging Contaminants and Current Issues. *Anal. Chem.* **2018**, *90*, 546–582. <https://doi.org/10.1021/acs.analchem.7b04577>.
- (16) Boonjob, W.; Sklenářová, H.; Lara, F. J.; García-Campaña, A. M.; Solich, P. Retention and Selectivity of Basic Drugs on Solid-Phase Extraction Sorbents: Application to Direct Determination of β -Blockers in Urine. *Anal. Bioanal. Chem.* **2014**, *406* (17), 4207–4215. <https://doi.org/10.1007/s00216-014-7753-4>.
- (17) Murakami, H.; Aoyanagi, T.; Miki, Y.; Tomita, H.; Esaka, Y.; Inoue, Y.; Teshima, N. Effects of Hydrophilic Monomers on Sorptive Properties of Divinylbenzene-Based Reversed Phase Sorbents. *Talanta* **2018**, *185*, 427–432. <https://doi.org/10.1016/j.talanta.2018.03.093>.
- (18) Murakami, H.; Tomita, H.; Aoyanagi, T.; Sugita, T.; Miki, Y.; Esaka, Y.; Inoue, Y.; Teshima, N. Effects of Pendant-like Hydrophilic Monomers on the Adsorption Properties of Reversed-Phase-Type Sorbents for Solid-Phase Extraction. *Anal. Chim. Acta* **2019**, *1075*, 106–111. <https://doi.org/10.1016/j.aca.2019.05.019>.
- (19) Trochimczuk, A. W.; Streat, M.; Kolarz, B. N. Highly Polar Polymeric Sorbents: Characterization and Sorptive Properties towards Phenol and Its Derivatives. *React. Funct. Polym.* **2001**, *46* (3), 259–271. [https://doi.org/10.1016/S1381-5148\(00\)00056-0](https://doi.org/10.1016/S1381-5148(00)00056-0).
- (20) Chaudhary, V.; Sharma, S. Suspension Polymerization Technique: Parameters Affecting Polymer Properties and Application in Oxidation Reactions. *J. Polym. Res.* **2019**, *26* (5), 102. <https://doi.org/10.1007/s10965-019-1767-8>.
- (21) Arshady, R. Suspension, Emulsion, and Dispersion Polymerization: A Methodological Survey. *Colloid Polym. Sci.* **1992**, *270* (8), 717–732. <https://doi.org/10.1007/BF00776142>.
- (22) Xie, S.; Svec, F.; Fréchet, J. M. J. Porous Polymer Monoliths: Preparation of Sorbent Materials with High-Surface Areas and Controlled Surface Chemistry for High-Throughput, Online, Solid-Phase Extraction of Polar Organic Compounds. *Chem. Mater.* **1998**, *10* (12), 4072–4078. <https://doi.org/10.1021/cm9804867>.
- (23) Svec, F. Porous Polymer Monoliths: Amazingly Wide Variety of Techniques Enabling Their Preparation. *J. Chromatogr. A* **2010**, *1217* (6), 902–924. <https://doi.org/10.1016/j.chroma.2009.09.073>.
- (24) Svec, F. Less Common Applications of Monoliths: Preconcentration and Solid-Phase Extraction. *J. Chromatogr. B* **2006**, *841* (1), 52–64. <https://doi.org/10.1016/j.jchromb.2006.03.055>.

- (25) Svec, Frantisek.; Frechet, J. M. J. Continuous Rods of Macroporous Polymer as High-Performance Liquid Chromatography Separation Media. *Anal. Chem.* **1992**, *64* (7), 820–822. <https://doi.org/10.1021/ac00031a022>.
- (26) Wang, Q. Ching.; Svec, Frantisek.; Frechet, J. M. J. Macroporous Polymeric Stationary-Phase Rod as Continuous Separation Medium for Reversed-Phase Chromatography. *Anal. Chem.* **1993**, *65* (17), 2243–2248. <https://doi.org/10.1021/ac00065a013>.
- (27) Wang, Q. C.; Švec, F.; Fréchet, J. M. J. Reversed-Phase Chromatography of Small Molecules and Peptides on a Continuous Rod of Macroporous Poly (Styrene-Co-Divinylbenzene). *J. Chromatogr. A* **1994**, *669* (1), 230–235. [https://doi.org/10.1016/0021-9673\(94\)80352-8](https://doi.org/10.1016/0021-9673(94)80352-8).
- (28) Svec, F.; Fréchet, J. M. J. Molded Rigid Monolithic Porous Polymers: An Inexpensive, Efficient, and Versatile Alternative to Beads for the Design of Materials for Numerous Applications. *Ind. Eng. Chem. Res.* **1999**, *38* (1), 34–48. <https://doi.org/10.1021/ie970598s>.
- (29) Potter, O. G.; Hilder, E. F. Porous Polymer Monoliths for Extraction: Diverse Applications and Platforms. *J. Sep. Sci.* **2008**, *31* (11), 1881–1906. <https://doi.org/10.1002/jssc.200800116>.
- (30) Saunders, K. C.; Ghanem, A.; Boon Hon, W.; Hilder, E. F.; Haddad, P. R. Separation and Sample Pre-Treatment in Bioanalysis Using Monolithic Phases: A Review. *Anal. Chim. Acta* **2009**, *652* (1), 22–31. <https://doi.org/10.1016/j.aca.2009.05.043>.
- (31) Namera, A.; Nakamoto, A.; Saito, T.; Miyazaki, S. Monolith as a New Sample Preparation Material: Recent Devices and Applications. *J. Sep. Sci.* **2011**, *34* (8), 901–924. <https://doi.org/10.1002/jssc.201000795>.
- (32) Arrua, R. D.; Causon, T. J.; Hilder, E. F. Recent Developments and Future Possibilities for Polymer Monoliths in Separation Science. *The Analyst* **2012**, *137* (22), 5179. <https://doi.org/10.1039/c2an35804b>.
- (33) Arrua, R. D.; Talebi, M.; Causon, T. J.; Hilder, E. F. Review of Recent Advances in the Preparation of Organic Polymer Monoliths for Liquid Chromatography of Large Molecules. *Anal. Chim. Acta* **2012**, *738*, 1–12. <https://doi.org/10.1016/j.aca.2012.05.052>.
- (34) Hong, T.; Yang, X.; Xu, Y.; Ji, Y. Recent Advances in the Preparation and Application of Monolithic Capillary Columns in Separation Science. *Anal. Chim. Acta* **2016**, *931*, 1–24. <https://doi.org/10.1016/j.aca.2016.05.013>.
- (35) Masini, J. C.; Svec, F. Porous Monoliths for On-Line Sample Preparation: A Review. *Anal. Chim. Acta* **2017**, *964*, 24–44. <https://doi.org/10.1016/j.aca.2017.02.002>.
- (36) Patkowski, K. Recent Developments in Symmetry-Adapted Perturbation Theory. *Wiley Interdiscip. Rev.: Comput. Mol. Sci.* **2020**, *10* (3), e1452. <https://doi.org/10.1002/wcms.1452>.
- (37) Szalewicz, K.; Jeziorski, B. Symmetry-Adapted Double-Perturbation Analysis of Intramolecular Correlation Effects in Weak Intermolecular Interactions. *Mol. Phys.* **1979**, *38* (1), 191–208. <https://doi.org/10.1080/00268977900101601>.
- (38) Dunning, T. H. A Road Map for the Calculation of Molecular Binding Energies. *J. Phys. Chem. A* **2000**, *104* (40), 9062–9080. <https://doi.org/10.1021/jp001507z>.

- (39) Yilmazer, N. D.; Korth, M. Comparison of Molecular Mechanics, Semi-Empirical Quantum Mechanical, and Density Functional Theory Methods for Scoring Protein-Ligand Interactions. *J. Phys. Chem. B* **2013**, *117* (27), 8075–8084. <https://doi.org/10.1021/jp402719k>.
- (40) Shikano, Y.; Watanabe, H. C.; Nakanishi, K. M.; Ohnishi, Y. Post-Hartree–Fock Method in Quantum Chemistry for Quantum Computer. *Eur. Phys. J. Spec. Top.* **2021**, *230* (4), 1037–1051. <https://doi.org/10.1140/epjs/s11734-021-00087-z>.
- (41) Slater, J. C. The Self Consistent Field and the Structure of Atoms. *Phys. Rev.* 1928, *32*, 339–347. <https://doi.org/10.1103/PhysRev.32.339>.
- (42) Jensen, F. Atomic Orbital Basis Sets. *Wiley Interdiscip. Rev.: Comput. Mol. Sci.* **2013**, *3* (3), 273–295. <https://doi.org/10.1002/wcms.1123>.
- (43) Domagała, M.; Matczak, P.; Palusiak, M. Halogen Bond, Hydrogen Bond and N···C Interaction – On Interrelation among These Three Noncovalent Interactions. *Comput. Theor. Chem.* **2012**, *998*, 26–33. <https://doi.org/10.1016/j.comptc.2012.05.012>.
- (44) C. Vik, E.; Li, P.; M. Maier, J.; O. Madukwe, D.; A. Rassolov, V.; J. Pellechia, P.; Masson, E.; D. Shimizu, K. Large Transition State Stabilization from a Weak Hydrogen Bond. *Chem. Sci.* **2020**, *11* (28), 7487–7494. <https://doi.org/10.1039/D0SC02806A>.
- (45) Grabowski, S. J. Non-Covalent Interactions – QTAIM and NBO Analysis. *J. Mol. Model* **2013**, *19* (11), 4713–4721. <https://doi.org/10.1007/s00894-012-1463-7>.
- (46) Vik, E. C.; Li, P.; Pellechia, P. J.; Shimizu, K. D. Transition-State Stabilization by N→ π^* Interactions Measured Using Molecular Rotors. *J. Am. Chem. Soc.* **2019**, *141* (42), 16579–16583. <https://doi.org/10.1021/jacs.9b08542>.
- (47) Shao, Y.; Gan, Z.; Epifanovsky, E.; Gilbert, A. T. B.; Wormit, M.; Kussmann, J.; Lange, A. W.; Behn, A.; Deng, J.; Feng, X.; Ghosh, D.; Goldey, M.; Horn, P. R.; Jacobson, L. D.; Kaliman, I.; Khaliullin, R. Z.; Kuś, T.; Landau, A.; Liu, J.; Proynov, E. I.; Rhee, Y. M.; Richard, R. M.; Rohrdanz, M. A.; Steele, R. P.; Sundstrom, E. J.; Woodcock, H. L.; Zimmerman, P. M.; Zuev, D.; Albrecht, B.; Alguire, E.; Austin, B.; Beran, G. J. O.; Bernard, Y. A.; Berquist, E.; Brandhorst, K.; Bravaya, K. B.; Brown, S. T.; Casanova, D.; Chang, C.-M.; Chen, Y.; Chien, S. H.; Closser, K. D.; Crittenden, D. L.; Diedenhofen, M.; DiStasio, R. A.; Do, H.; Dutoi, A. D.; Edgar, R. G.; Fatehi, S.; Fusti-Molnar, L.; Ghysels, A.; Golubeva-Zadorozhnaya, A.; Gomes, J.; Hanson-Heine, M. W. D.; Harbach, P. H. P.; Hauser, A. W.; Hohenstein, E. G.; Holden, Z. C.; Jagau, T.-C.; Ji, H.; Kaduk, B.; Khistyayev, K.; Kim, J.; Kim, J.; King, R. A.; Klunzinger, P.; Kosenkov, D.; Kowalczyk, T.; Krauter, C. M.; Lao, K. U.; Laurent, A. D.; Lawler, K. V.; Levchenko, S. V.; Lin, C. Y.; Liu, F.; Livshits, E.; Lochan, R. C.; Luenser, A.; Manohar, P.; Manzer, S. F.; Mao, S.-P.; Mardirossian, N.; Marenich, A. V.; Maurer, S. A.; Mayhall, N. J.; Neuscamman, E.; Oana, C. M.; Olivares-Amaya, R.; O’Neill, D. P.; Parkhill, J. A.; Perrine, T. M.; Peverati, R.; Prociuk, A.; Rehn, D. R.; Rosta, E.; Russ, N. J.; Sharada, S. M.; Sharma, S.; Small, D. W.; Sodt, A.; Stein, T.; Stück, D.; Su, Y.-C.; Thom, A. J. W.; Tsuchimochi, T.; Vanovschi, V.; Vogt, L.; Vydrov, O.; Wang, T.; Watson, M. A.; Wenzel, J.; White, A.; Williams, C. F.; Yang, J.; Yeganeh, S.; Yost, S. R.; You, Z.-Q.; Zhang, I. Y.; Zhang, X.; Zhao, Y.; Brooks, B. R.; Chan, G. K. L.; Chipman, D. M.; Cramer, C. J.; Goddard, W. A.; Gordon, M. S.; Hehre, W. J.; Klamt, A.; Schaefer, H. F.; Schmidt,

- M. W.; Sherrill, C. D.; Truhlar, D. G.; Warshel, A.; Xu, X.; Aspuru-Guzik, A.; Baer, R.; Bell, A. T.; Besley, N. A.; Chai, J.-D.; Dreuw, A.; Dunietz, B. D.; Furlani, T. R.; Gwaltney, S. R.; Hsu, C.-P.; Jung, Y.; Kong, J.; Lambrecht, D. S.; Liang, W.; Ochsenfeld, C.; Rassolov, V. A.; Slipchenko, L. V.; Subotnik, J. E.; Van Voorhis, T.; Herbert, J. M.; Krylov, A. I.; Gill, P. M. W.; Head-Gordon, M. Advances in Molecular Quantum Chemistry Contained in the Q-Chem 4 Program Package. *Mol. Phys.* **2015**, *113* (2), 184–215. <https://doi.org/10.1080/00268976.2014.952696>.
- (48) Smith, D. G. A.; Burns, L. A.; Simmonett, A. C.; Parrish, R. M.; Schieber, M. C.; Galvelis, R.; Kraus, P.; Kruse, H.; Di Remigio, R.; Alenaizan, A.; James, A. M.; Lehtola, S.; Misiewicz, J. P.; Scheurer, M.; Shaw, R. A.; Schriber, J. B.; Xie, Y.; Glick, Z. L.; Sirianni, D. A.; O'Brien, J. S.; Waldrop, J. M.; Kumar, A.; Hohenstein, E. G.; Pritchard, B. P.; Brooks, B. R.; Schaefer, H. F.; Sokolov, A. Yu.; Patkowski, K.; DePrince, A. E.; Bozkaya, U.; King, R. A.; Evangelista, F. A.; Turney, J. M.; Crawford, T. D.; Sherrill, C. D. P si4 1.4: Open-Source Software for High-Throughput Quantum Chemistry. *J. Chem. Phys.* **2020**, *152* (18), 184108. <https://doi.org/10.1063/5.0006002>.

CHAPTER 2

ABSORPTION PROPERTIES OF MONOLITH POLY (DIVINYLBENZENE-*CO-N*- VINYLPIRROLIDONE) OVER A WIDE RANGE OF MONOMER RATIOS

Karki, I.; Li, P.; Vik, E. C.; Manzewitsch, A.; Divirgilio, E.; Brewer, W. E.; Shimizu, K. D. Absorption Properties of Monolithic Poly (Divinylbenzene-*co-N*-Vinylpyrrolidone) over a Wide Range of Monomer Ratios. *Reactive and Functional Polymers* **2021**, *163*, 104888.

2.1 Abstract

The hydrophilic-lipophilic balance (HLB) polymers are able to directly extract polar and non-polar analytes from the aqueous samples, making them very popular for analytical separation and SPE applications. However, the commonly used suspension polymerization method for preparing HLB polymers is only able to efficiently prepare HLB polymers with low or medium mol percentages of the hydrophilic monomer due to the hydrophilic monomer partitioning into the aqueous phase at higher concentrations. Thus, in this study a series of HLB polymers based on divinylbenzene (DVB) (lipophilic) and N-vinylpyrrolidone (NVP) (hydrophilic) of widely varying hydrophilicities were prepared by the more robust monolith polymerization method. The monolith polymerization enabled the preparation of co(DVB-NVP) from low to high NVP percentages (0 mol% to 55 mol% NVP). The comparative adsorption and separation properties of the series of DVB-co-NVP were assessed using three analytes of varying polarity: adenosine ($\log P = -1.5$), caffeine ($\log P = -0.07$), and *p*-toluidine ($\log P = 1.39$). Interestingly, the highest binding capacity for binding polar analytes was observed for the monolith polymer prepared with the intermediate 70:30 feed ratio of DVB/NVP, due to an optimal balance of surface area and hydrophilicity. Whereas, for the separation of the non-polar analytes such as *p*-toluidine from polar analytes like caffeine or adenosine, the hydrophobic polymers containing the lower percentages of the polar monomer (20 mol% NVP) were superior.

2.2 Introduction

Tuning polymer properties by changing the ratio of co-monomers is an important strategy for optimizing and tailoring polymer properties in many applications.¹ However,

this approach has limitations when studying polymers that contain co-monomers with very different polarities and solubilities. An example are hydrophilic-lipophilic balance (HLB) polymers, which have become popular in separation sciences due to their ability to extract both non-polar and polar analytes directly from aqueous samples.²⁻⁶ The hydrophobic crosslinking monomer creates a rigid framework with a high internal surface area while the hydrophilic monomer enhances interactions with polar analytes and enhances water wettability.^{3,6-9} Poly(divinylbenzene-*co*-*N*-vinylpyrrolidone) (DVB-*co*-NVP) is an example of an HLB polymer (Figure 2.1) where divinylbenzene (DVB) is the lipophilic crosslinking monomer and *N*-vinylpyrrolidone (NVP) is the hydrophilic monomer. HLB polymers are commonly prepared for analytical applications via suspension polymerization, which yields uniform spherical beads. However, the synthesis of HLB polymers with higher hydrophilic monomer ratios (>30 mol%) presents a challenge when using standard biphasic suspension polymerization conditions.¹⁰⁻¹² The hydrophilic monomer can partition from the organic phase (where the polymer beads are formed) to the surrounding aqueous phase.¹³ The depletion of the hydrophilic monomer from the organic phase becomes increasingly problematic at higher hydrophilic monomer feed percentages (>30 mol%), leading to poor incorporation efficiencies and lower polymer yields.

The goal of this study was to prepare and study the absorption properties of DVB-*co*-NVP polymers that span a wide range of NVP monomer ratios from 0 mol% to 60 mol% using monolith polymerizations.¹²⁻¹⁵ Monolith polymerizations are monophasic, which eliminates the possibility of monomers partitioning into other phases. Therefore, the monomer incorporation ratios more closely match the feed ratios even at high NVP mol%.

We were particularly interested in whether HLB polymers with high hydrophilic monomer ratios, that could not be easily achieved by suspension polymerization, would have unique or superior adsorption and separation properties in comparison to HLB polymers with moderate or low hydrophilic monomer ratios. Therefore, the specific aims were to: 1) prepare a series of DVB-*co*-NVP polymers by monolith polymerization that span a wider range of NVP monomer ratios than can be achieved by suspension polymerization, 2) establish that the monolith and suspension polymers with similar monomer incorporation ratios have similar adsorption properties, and 3) compare the adsorption properties of HLB monolith polymers with low, medium, and high percentages of NVP.

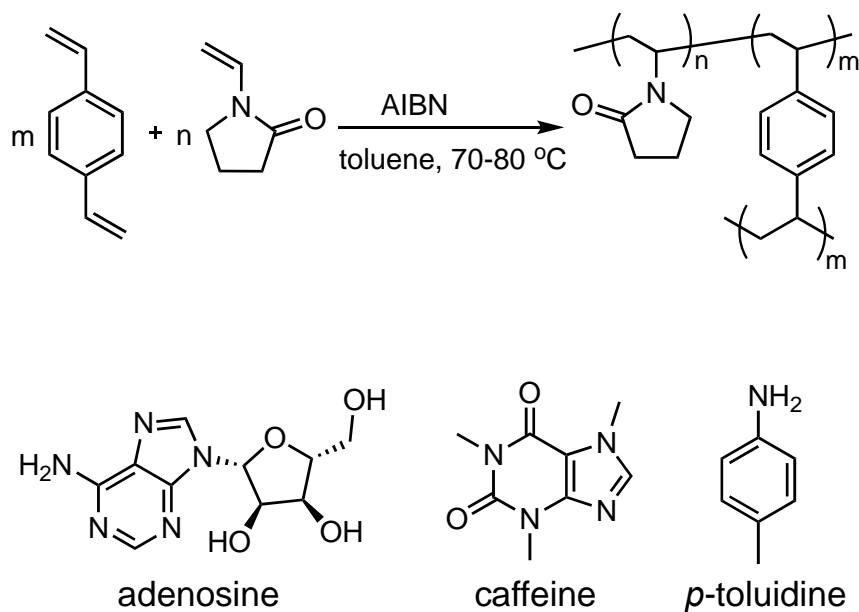


Figure 2.1 (top) DVB-*co*-NVP polymer synthesis by free radical polymerization and (bottom) analytes used to test the adsorption properties from most polar (adenosine) to least polar (*p*-toluidine).

The HLB system selected for study was poly(divinylbenzene-*co*-N-vinylpyrrolidone) (Figure 2.1). DVB-*co*-NVP is one of the most widely used general-purpose HLB polymer stationary phases for chromatography and SPE applications and is

the constituent polymer in the Waters Corporation Oasis HLB product line.¹⁶ A key attribute of (DVB-*co*-NVP) is the ability of the polymer matrix to be solvated by water due to the polar amide functional group in NVP. This wettability enables the direct extraction of analytes from aqueous media.^{2,5,9,17} Despite the popularity of Waters Oasis stationary phases, the studies of the adsorption properties of DVB-*co*-NVP have only been reported over a narrow range of monomer ratios, most likely due to the difficulties in synthesizing copolymers with higher NVP ratios via suspension polymerization. Most studies used commercially available Waters Oasis DVB-*co*-NVP,⁷ which we measured to have 28 mol% of NVP (*vide infra*). The few studies that varied the monomer ratios of DVB-*co*-NVP were conducted at lower to moderate ratios of NVP (5 mol% to 30 mol%).^{9,18}

Using monolith polymerization, we were able to efficiently prepare DVB-*co*-NVP with low to moderate (0 to 30 mol%) and high (30 to 55 mol%) NVP mole percentages. In contrast to suspension polymers, the monomer ratios of the monolith DVB-*co*-NVP more closely matched the initial monomer feed percentages specially.^{10,13,19} The monolith polymerizations were easier to carry out, had higher yields, and provided greater control over the co-monomer percentages than suspension polymerizations. The monolith polymers had similar surface area, wettability, and adsorption properties as suspension polymers with analogous NVP mole percentages. The adsorption properties of the monolith DVB-*co*-NVP polymers were compared using analytes of low (*p*-toluidine), medium (caffeine), and high polarities (adenosine) (Figure 2.1).

2.3 Experimental section

2.3.1 Reagents and Instrumentation

DVB (80% purity, Sigma-Aldrich) stabilized with 1000 ppm *p-tert*-butylcatechol was made stabilizer-free by passing through activated alumina. NVP (99.9%, Tokyo Chemical Industry) stabilized with *N,N'*-di-*sec*-butyl-*p*-phenylenediamine, was used as purchased. The free radical initiator, 2,2'-azobis(isobutyronitrile) (98%, Sigma-Aldrich) and the suspension stabilizer, (hydroxypropyl)methylcellulose (Sigma-Aldrich), were used as purchased. The analytes, adenosine (99%), caffeine (99%), and *p*-toluidine (99%), were purchased from Sigma-Aldrich and Acros Organics.

A UV-vis spectrophotometer (Jasco V-730) was used for the absorbance measurements in the batch binding studies. Elemental analyses of the polymers were performed by Midwest Microlab. The mol percentages of NVP in the polymers were calculated based on the elemental analysis of the nitrogen percentages from the NVP monomers based on an ideal DVB-*co*-NVP polymer that did not contain any radical initiator. The specific surface areas of the polymers were measured by Particle Testing Authority, on a Micromeritics Tristar II Plus, model 3030. The surface area measurements were performed using the low-temperature nitrogen adsorption method at 77 K, which was preceded by degassing the samples at 140 °C for 2 hours. Specific surface areas of the samples were calculated by the Brunauer-Emmett-Teller (BET) method in the range of the relative pressures 0.05 to 0.3 p/p_0 .

2.3.2 Synthesis of DVB-co-NVP polymers

Monolith DVB-co-NVP polymers were prepared by free radical polymerization. Polymers were prepared with 0:100, 20:80, 30:70, 40:60, 50:50, 60:40 NVP/DVB mol/mol feed ratios using toluene as porogen. An example of a monolith polymerization procedure is provided below for the preparation of DVB-co-NVP with a 30 mol% NVP feed ratio. Divinylbenzene (1.04 mL, 7.31 mmol), *N*-vinylpyrrolidone (0.336 mL, 3.14 mmol), and 3 mol% AIBN (0.052 g, 0.316 mmol) were dissolved in 2 mL toluene in a 2 dram vial. The mixture was sonicated and then degassed under nitrogen for 5 min. The vials were sealed and heated at 70 °C for 8 hours. The resulting monoliths were ground into small particles using a mortar and pestle. The ground polymer was washed three times with 5 mL of methanol, which was decanted to remove the smallest particles. The remaining particles were washed using Soxhlet extraction with water for 24 hours. The washed polymer particles were dried under vacuum and then mechanically sieved to isolate the 75 to 125 μm fraction.

DVB-co-NVP polymer beads were synthesized by free radical suspension polymerization in toluene/water solutions stabilized with (hydroxypropyl)methylcellulose. Suspension polymerizations were conducted over a similar range of monomer feed ratios as the monolith polymerizations. Suspension polymers were prepared with 0:100, 20:80, 30:70, 40:60, 50:50, and 60:40 NVP/DVB mol/mol feed ratios. An example of the suspension polymerization procedure is provided for the polymer with a 30 mol% NVP feed ratio. DVB (22.177 mL, 155.69 mmol), NVP (7.135 mL, 66.76 mmol), and 1 mol% AIBN (2.25 mmol) were added to a heterogeneous mixture of 27.8 mL toluene and 100 mL water containing (hydroxypropyl)methylcellulose

stabilizer (0.5 g). The mixture was sealed into a reaction vessel, which was stirred using an overhead stirrer at 800 rpm for 30 minutes while nitrogen was continuously bubbled into the mixture. The suspension mixture was then heated for 20 h at 70 °C while stirring at 800 rpm. After cooling the solution, the beads were separated by suction filtration, washed by Soxhlet extraction with water for 24 hours, and dried under vacuum. The polymer beads were mechanically sieved to separate the particles between 75 and 125 μm .

2.3.3 Batch binding measurements

The binding isotherms for the monolith and suspension polymers were measured by shaking varying weights of polymer with aqueous solutions of the individual analytes. Three analytes with different polarities were used: adenosine ($\log P = -1.5$), caffeine ($\log P = -0.07$) and *p*-toluidine ($\log P = 1.39$). Specific weights of polymer (10, 20, 30, 40, or 50 mg) were added to 5 mL aqueous solutions of 0.1 mM adenosine, 0.16 mM caffeine, or 0.5 mM *p*-toluidine. The mixtures were mechanically shaken for 30 min and then filtered through a 0.2-micron polyether-sulfone filter. The concentration of the analyte remaining in the filtrate was measured using a UV-vis spectrophotometer. The difference in the absorbance at a specific wavelength (260 nm, 271.5 nm, and 233 nm for adenosine, caffeine, and *p*-toluidine) of the stock and filtrate solutions provided the concentration of the free analyte in solution. The concentration of analyte bound to the polymers was calculated based on the mass balance between the stock solution and the unbound free analyte in solution. The binding isotherms were best fit by the Freundlich isotherm.^{20–23}

2.4 Results and discussion

2.4.1 Comparison of the feed ratios and actual mol% of monomers in DVB-*co*-NVP

The first goal was to synthesize a series of DVB-*co*-NVP sorbents via monolith polymerization that systematically varied the NVP mol percentages. Polymers were prepared using feed ratios of 0:100, 20:80, 30:70, 40:60, 50:50, and 60:40 NVP/DVB mol/mol ratios. The yields (85-93%) of the monolith polymerizations were consistently high even with feed percentages above 30 mol% NVP (Figure 2.2).

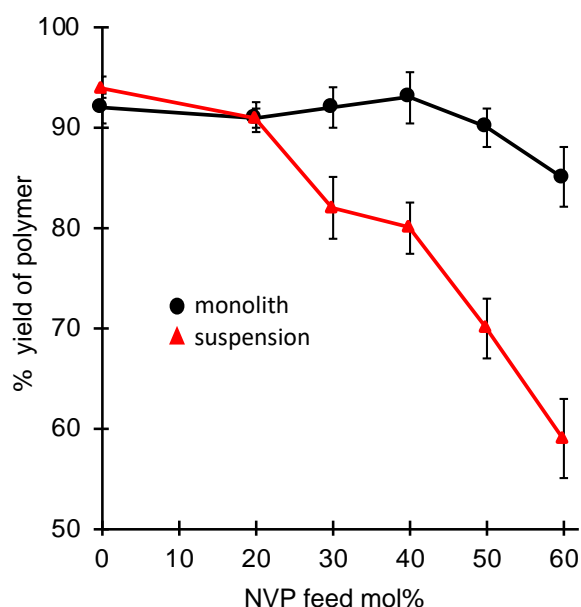


Figure 2.2 The percent yields of monolith and suspension DVB-*co*-NVP polymers versus the NVP mol% feed ratio. The yields were measured based on polymer weights before sieving.

One disadvantage of monolith polymerizations in preparing sorbents is the shape and size heterogeneity of the polymer particles. Typically, the polymer monoliths are mechanically ground into particles of irregular size and shape, which can be problematic in chromatographic applications. However, for solid-phase extraction (SPE), homogeneous adsorption kinetics are not as important, and thus SPE is more tolerant of sorbents with

irregular shaped particles.^{14,15,24-31} We were also able to mitigate the size heterogeneity of the monolith particles by sieving and collecting particles within specific size ranges (75 to 125 μm). The sieved particles (Figure 2.3) provided more consistent adsorption results and yielded materials with comparable adsorption properties to the more uniform and spherical suspension polymers. The polymers prepared by the monolith and suspension polymers appeared to have similar morphologies. The SEM images (Figure 2.4) of the monolith and suspension polymers prepared with 30 mol% NVP feed ratios had similar morphology and roughness, and were consistent with previous studies of DVB-based crosslinked monoliths formed in toluene.³²

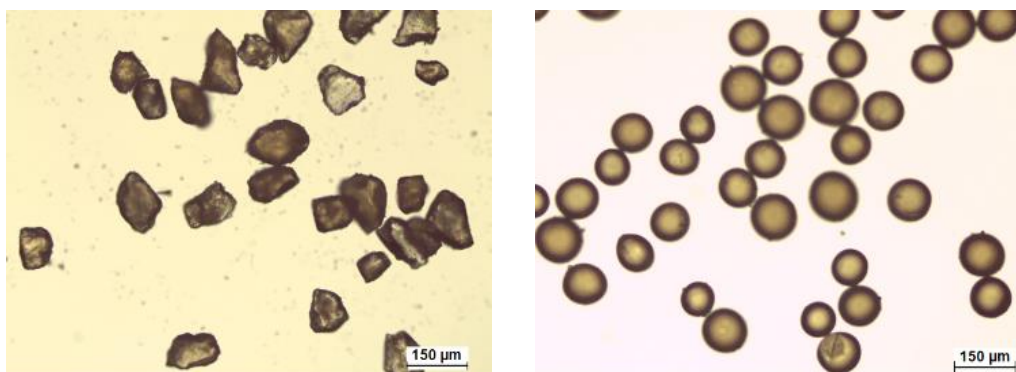


Figure 2.3 Optical microscope images comparing the size and shape of the representative monolith (left) and suspension (right) DVB-*co*-NVP polymers formed using 30:70 NVP/DVB mol/mol feed ratios.

In addition to higher yields, the monolith polymerizations provided excellent control over the incorporation efficiencies of the hydrophilic NVP monomer. The NVP mol-percentages in the monolith polymers closely matched the original feed ratios even at high NVP feed ratios (Figure 2.5). For example, the monolith polymer prepared with a 60 mol% NVP feed ratio (60:40 mol/mol NVP/DVB) contained 55% NVP. The NVP mol% of the polymers were calculated from the measured weight percent of nitrogen from the

elemental analyses. Only the NVP monomer contains a nitrogen atom; thus nitrogen weight percentages were linearly correlated with NVP mol percentages in the polymers.

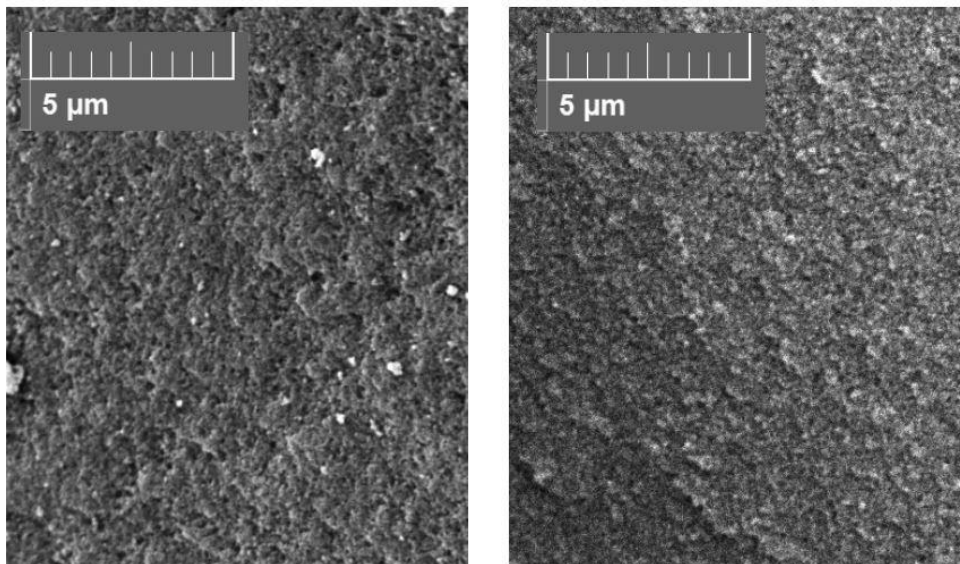


Figure 2.4 SEM images of monolith (left) and suspension (right) polymers prepared with 30 mol% NVP feed ratios.

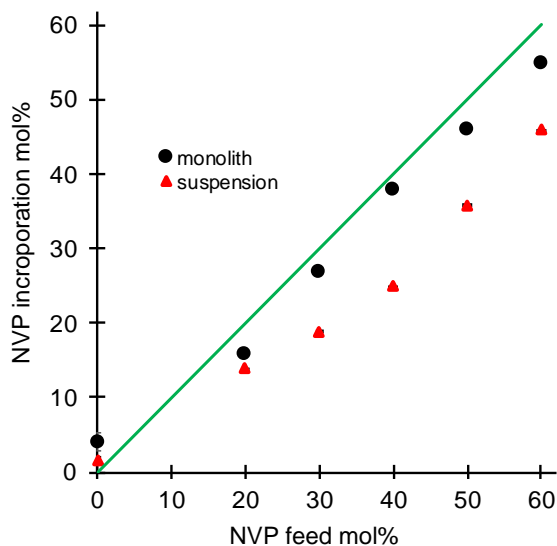


Figure 2.5 Plot of the NVP incorporation mol percentages (mol%) for monolith (black circles) and suspension (red triangles) polymers versus the NVP monomer feed percentages (mol%) used in the polymerization reaction mixtures. The green line represents an ideal NVP incorporation efficiency where the NVP incorporation percentages equal the feed percentages. The non-zero values for the 0 mol% NVP feed ratio polymers are due to the presence of nitrogen from the AIBN initiator. The error bars were smaller than the data points.

By comparison, the yields and NVP incorporation percentages were lower for the suspension polymers. Like the monolith polymers, the suspension polymers had high yields (> 90%) for the polymers with low NVP feed percentages (0 to 20 mol%) (Figure 2.2). However, the yields of the suspension polymerizations decreased rapidly when the NVP feed percentages were higher than 20 mol%. For example, the yield of the 60 mol% NVP feed ratio suspension polymer was only 59%. The modest yields were only possible after careful optimization of stirring speed and stabilizer, (hydroxypropyl)methylcellulose, concentrations for each NVP feed ratios. The suspensions polymerization mixtures formed with higher NVP percentages were unstable due to the polar NVP monomer disrupting the formation of the organic-phase droplets in the polymerization mixture.^{10,12,13,15} The partitioning of the NVP into the aqueous phase was evident from the low NVP incorporation efficiencies, especially for suspension polymers with higher NVP feed percentages (Figure 2.5). For example, the 60 mol% NVP feed ratio suspension polymer had an NVP incorporation of only 46 mol%. Thus, the monolith polymerizations provided higher yields and better control over the NVP ratios at higher NVP mol-percentages in comparison to the suspension polymerizations.

Next, the absorption properties of the monolith and suspension polymers were compared to see if the monolith polymers could serve as reasonable models for the suspension polymers. DVB-*co*-NVP polymers prepared via monolith and suspension polymerizations showed similar wettability and adsorption properties. Therefore, analyses of the monolith polymerizations provide insight into the factors that modulate the adsorption and separation properties of both suspension and monolith DVB-*co*-NVP polymers. Comparative wettability studies were carried out by shaking the polymers in

water (Figure 2.6). Wettability is a key attribute of the HLB polymers allowing faster binding kinetics and the direct extraction of polar analytes from aqueous samples.^{33,34} Polymers which were wettable would sink to the bottom due to the ability of water and analytes to wet the interior surfaces of the polymers. Polymers which were not wettable would float on top. For both monolith and suspension polymers, the polymers with <20% NVP feed percentages were not wettable; whereas monolith polymers with 30% or greater NVP feed percentages were readily wettable.



Figure 2.6 (left) Monolith polymers with 0 mol% NVP feed percentages having poor wettability floating on top of the aqueous solution after shaking (right) and monolith polymer with 30 mol% NVP feed percentages having good wettability and falling to the bottom of the aqueous solution.

The adsorption properties of the monolith and suspension DVB-*co*-NVP polymers were also very similar when comparing polymers with similar NVP incorporation ratios. For example, monolith polymers with a 30 mol% NVP feed percentages and suspension polymers with a 40 mol% NVP feed percentages had similar NVP incorporation

percentages of 27 mol% and 25 mol%, respectively. The adsorption properties of the monolith and suspension polymers were measured for a series of different weights of polymer (10 - 50 mg), which were equilibrated with 5 mL aqueous solutions of 0.1 mM caffeine (Figure 2.7). The amount of caffeine bound to the polymers was measured from the difference in concentration of the solution before and after equilibration. The monolith and suspension polymers had nearly identical binding percentages over a range of polymer concentrations. The correlation plot was linear ($R^2 = 0.99$) with a slope that was close to unity (slope 1.08). This confirmed that the monolith polymer had very similar binding properties to a suspension polymer with similar DVB-*co*-NVP ratios but with the added benefit of being easier to synthesize and with better control over the NVP incorporation percentages.

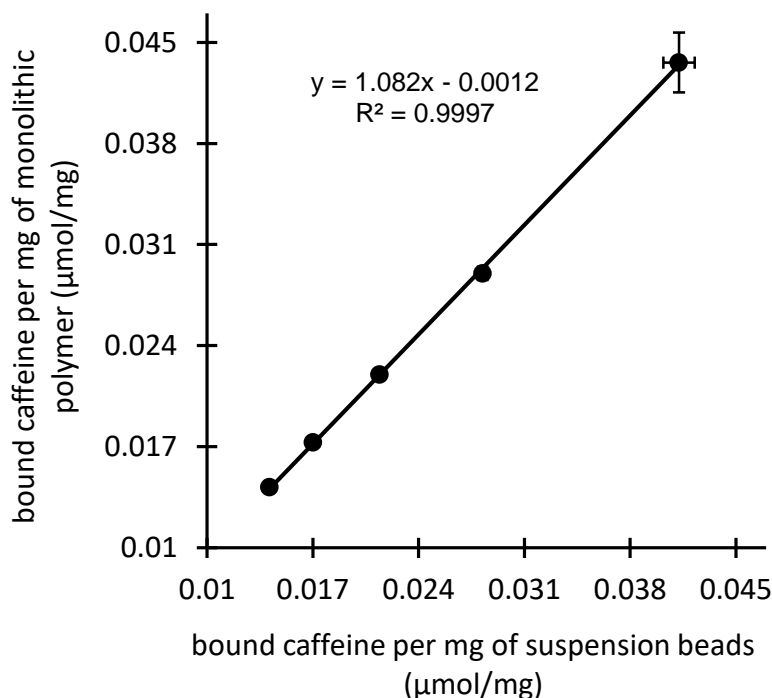


Figure 2.7 Comparison of the weight of caffeine bound from aqueous solution by DVB-*co*-NVP monolith and suspension polymers with similar NVP incorporation percentages (27 mol% and 25 mol%). The data points were collected via batch binding studies of 5 mL of 0.16 mM caffeine solutions using 10, 20, 30, 40, and 50 mg of polymers.

2.4.2 Adsorption properties of DVB-co-NVP with varying NVP mol percent.

Once the suitability of the monolith polymers to serve as models for DVB-co-NVP sorbents was established, the adsorption properties of the monolith polymers with varying NVP mol% were compared. Initial binding studies were carried out using caffeine as the analyte, which has an intermediate polarity as measured by its octanol/water partition coefficient ($\log P = -0.07$). Binding isotherms were measured for a series of monolith polymers with NVP feed mol% from 0 to 60 mol% (Figure 2.8). As expected, the binding capacities for the polar analyte, caffeine, increased as the percentages of the polar monomer NVP increased from 0 to 30 mol%. This is evident from a comparison of the binding isotherms for the polymers prepared with 0, 20, and 30 mol% NVP feed percentages. Interestingly, the binding capacities reached a maximum with the 30 mol% NVP feed percentage polymer and then steadily decreased for the 40, 50, and 60 mol% NVP polymers.

Possible explanations for the intermediate 30 mol% NVP polymer having the highest binding capacity were explored. Our initial expectations were that the binding capacities for the moderately polar analyte, caffeine, would continue to increase as the percentage of the polar NVP monomer increased. However, this was clearly not the case as the 60 mol% NVP feed ratio polymer had one of the lowest binding capacities. Only the pure DVB (0 mol% NVP) polymer had a lower binding capacity.

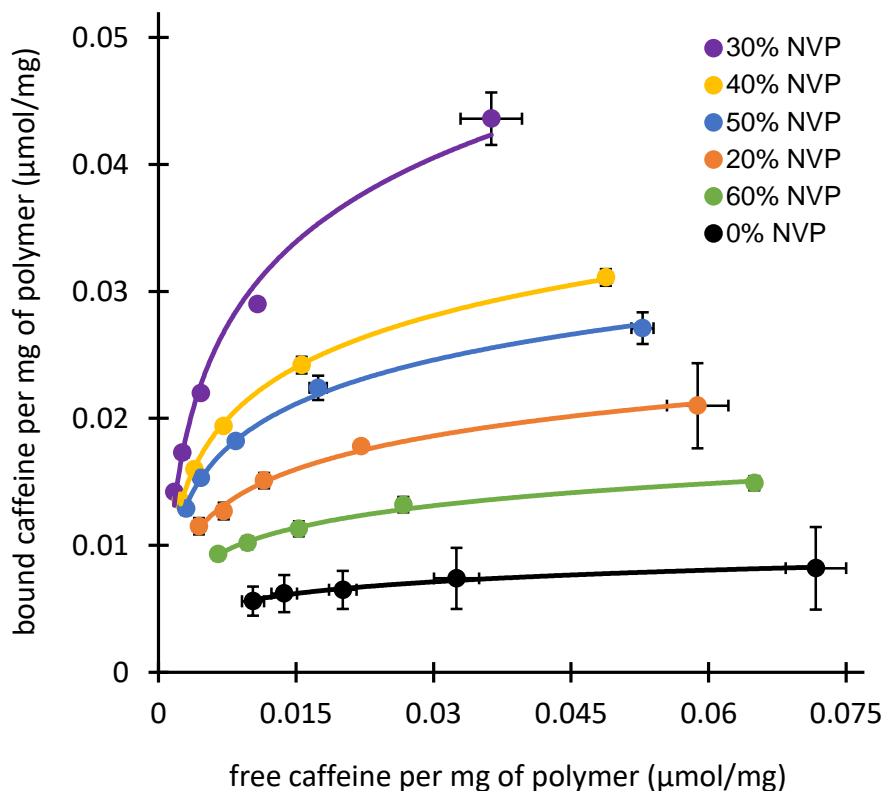


Figure 2.8 Caffeine binding isotherms for monolith polymers formed with 0, 20, 30, 40, 50, and 60 mol% NVP feed percentages. The isotherms were fit with a Freundlich isotherm, which provided the best fit.

First, the possibility that the 30 mol% feed ratio NVP polymer had the highest surface area was examined. The specific surface areas of representative monolith polymers with 0, 30, and 60 mol% NVP feed ratios were measured by BET analysis and compared (Table 2.1). The polymer surface areas did not correlate with the binding capacity trends. The monolith polymers surface areas varied from approximately 100 to 1000 m^2g^{-1} (Table 2.1). The polymer with the lowest NVP feed percentage (0 mol%) had the highest surface area of 927 m^2g^{-1} , and the surface areas rapidly decreased with increasing NVP mol%. The 60 mol% NVP feed ratio polymer had the lowest surface area of 162 m^2g^{-1} . These observations were consistent with previous polymer monolith studies, as polymers with higher percentages of the crosslinking monomer were more rigid and had higher internal

surface areas.³² Given these trends, the polymer surface areas alone could not explain the superior binding capacity of the 30 mol% feed ratio NVP polymer.

Next, the possibility that the binding capacity trends were due to a combination of two polymeric parameters was examined. Surface area and polymer polarity are opposing properties, which could lead to the intermediate NVP polymer having the highest binding capacities. The polymer surface areas favor the polymers with lowest NVP feed ratios, while polymer polarity would favor the polymers with the highest NVP feed ratios. To test this hypothesis, the adsorption properties of the monolith polymers were tested against two additional analytes that are more and less polar than caffeine. Adenosine and *p*-toluidine were selected. Adenosine has a lower log P (-1.5) and *p*-toluidine has a higher log P (1.39) than caffeine (-0.07). The less polar analyte, *p*-toluidine, provides a measure of the surface area as the primary binding mechanism would be the hydrophobic effect that correlates with the solvent accessible surface area of the sorbent. The more polar analyte, adenosine, provides a measure of the polar binding capacity of the polymers.

Table 2.1 Specific surface area measurement of representative monolith (DVB-*co*-NVP) polymers calculated from BET nitrogen adsorption isotherms.

NVP:DVB feed ratio	NVP:DVB measured ratio	Specific surface area
0:100	4:96 ^a	927 ± 3 m ² g ⁻¹
30:70	27:63	675 ± 3 m ² g ⁻¹
60:40	55:45	162 ± 0.4 m ² g ⁻¹

^a The non-zero value is due to the nitrogen from the AIBN initiator.

Single-point batch binding conditions were conducted with the three analytes using the monolith polymers with varying NVP feed ratios (Figure 2.9). The three analytes varied significantly in binding affinity for the polymers and thus a single set of batch binding conditions could not be found which would allow comparison of the binding profiles. Therefore, the concentration of the analyte solutions and weights of polymer were normalized for each analyte so that the polymer with the highest binding capacity in each series bound between 50 to 80% of the analyte from solution. The normalized conditions were: 0.5 mM *p*-toluidine with 10 mg polymer, 0.16 mM caffeine with 20 mg polymer, and 0.1 mM adenosine with 40 mg polymer. The single point binding studies with caffeine (Figure 2.9, black circles) were consistent with the binding isotherm studies. The 30 mol% NVP polymer had the highest binding capacity, and the 0 mol% and 60 mol% NVP polymers had the lowest caffeine binding capacities.

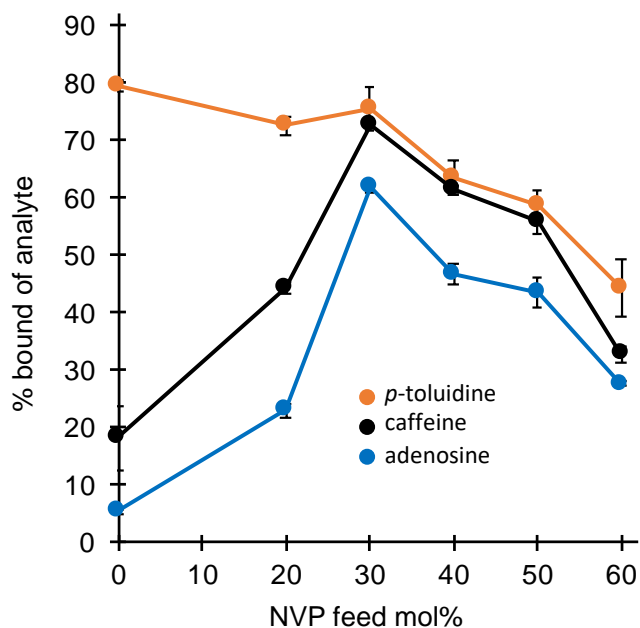


Figure 2.9 Single point binding capacities of the monolith DVB-*co*-NVP polymers with varying NVP feed ratios (0 – 60 mol%) for *p*-toluidine, caffeine, and adenosine. The batch binding conditions were: 0.5 mM *p*-toluidine with 10 mg polymer, 0.16 mM caffeine with 20 mg polymer, and 0.1 mM adenosine with 40 mg polymer in 5 mL of solvent.

The binding capacity trends provided insight into the primary adsorption mechanisms of the three analytes. Caffeine and adenosine had very similar binding profiles with a maximum binding capacity for the 30 mol% NVP polymer, which suggested that both analytes were binding to the polymer via similar mechanism. Since caffeine and adenosine are the more polar analytes, the most likely common binding mechanism are polar interactions with the amide functional groups in NVP. This is consistent with the binding capacity trends for the polymers with lower NVP mol-percentages (< 30 mol% NVP), which steadily increased with increasing percentages of NVP. The least polar analyte, *p*-toluidine, binds by a different mechanism as seen by its distinct binding profile which steadily decreases with increasing NVP mol% across the entire range from 0 to 60 mol% NVP. This is consistent with the decreasing hydrophobicity and surface area of the polymers, and thus the *p*-toluidine is binding via hydrophobic interactions.

The similarity in the binding profiles for all three analytes against the polymers containing higher NVP percentages (>30 mol% NVP) suggests a common factor that was not dependent on the binding mechanism. The most likely common factor for the higher NVP percentage polymers was polymer surface area, as the binding capacity trends mirror the measured surface area trends. Thus, the binding capacity of the high NVP percentage polymers steadily decreased with increasing NVP mol% (above 30 mol% NVP) for all three analytes, reaching a minimum with the 60 mol% NVP feed ratio polymer, which is the polymer with the lowest surface area.

Thus, the intermediate 30% NVP feed ratio polymer appears to strike an optimal balance of wettability, polarity, and surface area to provide maximal binding for polar analytes and also high affinity for less polar analytes. It is interesting to note the similarity

of the NVP incorporation percentage of the optimal monolith polymer in this study (27% incorporation percentage to the commercially available Water's Oasis HLB stationary phase (28% incorporation percentage), which we measured using the same elemental analysis.

Interestingly, the binding capacity comparisons in Figure 2.9 also suggests the 30% feed ratio NVP polymer may not be the optimal polymer for all separations, especially when separating less polar analytes from more polar analytes. This is due to the greater hydrophobicity of the polymers with lower NVP percentages. For example, the 20% NVP feed ratio polymer (Figure 2.9) shows a wider variation in the percent bound (72%, 44%, and 23%) of the three analytes: p-toluidine, caffeine, and adenosine. By comparison, the 30% NVP feed ratio polymer had a much narrower range of percent bounds values of 76%, 72%, and 62%. This demonstrates that a single DVB-*co*-NVP polymer may not be optimal for all application for the three analytes. The ability to more precisely synthesize HLB polymers with wider ranges of hydrophilic to lipophilic monomer ratios via monolith polymerization enables greater control over the tuning and optimization of their adsorption and separation properties.

2.5 Conclusions

The ability to optimize and tune the adsorption and separation properties of the HLB polymer, DVB-*co*-NVP, was examined over a wide range of monomer ratios. Using monolith polymerization, the ratio of the non-polar and polar monomers (DVB and NVP) could be effectively modulated from 0% to 55% NVP. By comparison, the traditional suspension polymerization had difficulty in preparing DVB-*co*-NVP with NVP ratios above 30 mol%. The monolith polymers had similar wettability and adsorption properties

as suspension polymers with similar NVP incorporation percentages enabling their use to systematically survey the adsorption properties of DVB-*co*-NVP with varying monomer ratios. The polymers were tested for their ability to extract analytes of varying polarity (p-toluidine, caffeine, and adenosine) from aqueous solution using batch binding studies. The intermediate 30% NVP feed ratio polymer displayed the optimal balance of polarity and wettability to extract polar analytes such as caffeine and adenosine from aqueous solution. For the separation of hydrophobic analytes such as p-toluidine from more polar analytes like caffeine or adenosine, more hydrophobic polymers containing lower percentages of the polar NVP monomer were superior. We are currently studying the separation abilities of the DVB-*co*-NVP sorbents with widely varying NVP ratios on an array of real-world SPE analytes and will report on these results in future reports.

2.6 Supplemental Information

A time-dependent binding study was done. Analyte (caffeine) was allowed to bind to 20 mg DVB-*co*-NVP polymer prepared with 50% NVP for 0 minutes (no binding case), 30 minutes, 1, 2, 4, 8, and 16 hours. Allowing the polymer to bind the caffeine for more than 30 minutes did not substantially increase the concentration of caffeine bound to the polymer. A plateau was observed in the binding curve (Figure 2.10) hence 30 minutes was selected optimal time for the batch binding experiments.

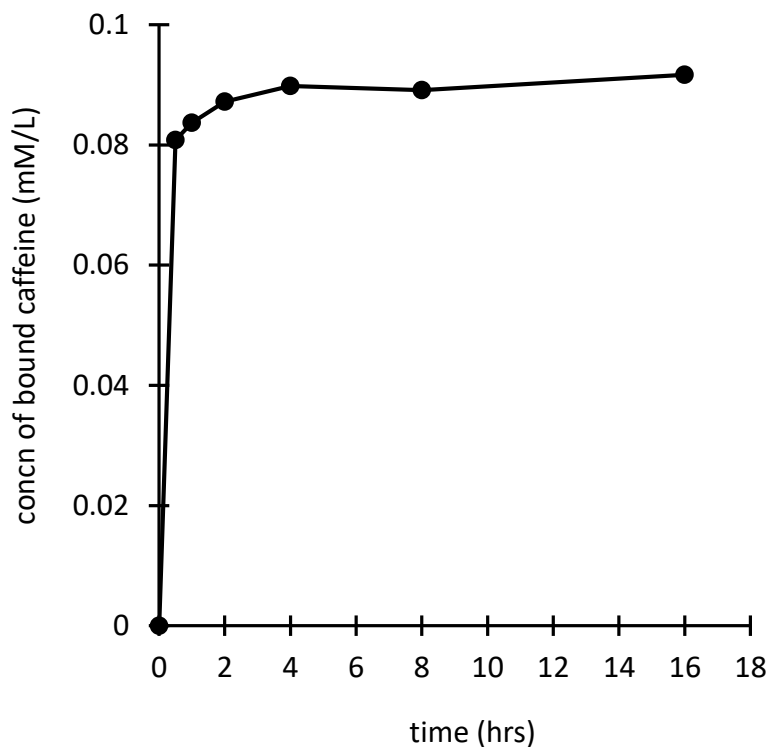


Figure 2.10 Time-dependent binding curve for 5 mL of 0.16mM caffeine solution to 20 mg DVB-*co*-NVP polymer prepared with 50% NVP.

2.7 References

- (1) Young, R. J.; Lovell, P. A. *Introduction to Polymers*, 3rd ed.; CRC Press: Boca Raton, FL, 2011.
- (2) Andrade-Eiroa, A.; Canle, M.; Leroy-Cancellieri, V.; Cerdà, V. Solid-Phase Extraction of Organic Compounds: A Critical Review (Part I). *TrAC, Trends Anal. Chem.* **2016**, *80*, 641–654. <https://doi.org/10.1016/j.trac.2015.08.015>.
- (3) Fontanals, N.; Marcé, R.M.; Borrull, F. New Materials in Sorptive Extraction Techniques for Polar Compounds. *J. Chromatogr. A* **2007**, *1152* (1–2), 14–31. <https://doi.org/10.1016/j.chroma.2006.11.077>.
- (4) Fontanals, N.; Puig, P.; Galià, M.; Marcé, R. M.; Borrull, F. New Hydrophilic Polymeric Resin Based on 4-Vinylpyridine–Divinylbenzene for Solid-Phase Extraction of Polar Compounds from Water. *J. Chromatogr. A* **2004**, *1035* (2), 281–284. <https://doi.org/10.1016/j.chroma.2004.02.049>.
- (5) Masqué, N.; Marcé, R. M.; Borrull, F. New Polymeric and Other Types of Sorbents for Solid-Phase Extraction of Polar Organic Micropollutants from Environmental Water. *TrAC, Trends Anal. Chem.* **1998**, *17* (6), 384–394. [https://doi.org/10.1016/S0165-9936\(98\)00019-3](https://doi.org/10.1016/S0165-9936(98)00019-3).

- (6) Fontanals, N.; Galià, M.; Marcé, R. M.; Borrull, F. Solid-Phase Extraction of Polar Compounds with a Hydrophilic Copolymeric Sorbent. *J. Chromatogr. A* **2004**, *1030* (1–2), 63–68. <https://doi.org/10.1016/j.chroma.2003.10.076>.
- (7) Fontanals, N.; Galià, M.; Marcé, R. M.; Borrull, F. Comparison of Hydrophilic Polymeric Sorbents for On-Line Solid-Phase Extraction of Polar Compounds from Aqueous Samples. *Chromatographia* **2004**, *60* (9), 511–515. <https://doi.org/10.1365/s10337-004-0419-1>.
- (8) Fontanals, N.; Marcé, R. M.; Borrull, F. New Hydrophilic Materials for Solid-Phase Extraction. *TrAC, Trends Anal. Chem.* **2005**, *24* (5), 394–406. <https://doi.org/10.1016/j.trac.2005.01.012>.
- (9) Murakami, H.; Tomita, H.; Aoyanagi, T.; Sugita, T.; Miki, Y.; Esaka, Y.; Inoue, Y.; Teshima, N. Effects of Pendant-like Hydrophilic Monomers on the Adsorption Properties of Reversed-Phase-Type Sorbents for Solid-Phase Extraction. *Anal. Chim. Acta* **2019**, *1075*, 106–111. <https://doi.org/10.1016/j.aca.2019.05.019>.
- (10) Peters, E. C.; Svec, F.; Fréchet, J. M. J. Rigid Macroporous Polymer Monoliths. *Adv. Mat.* **1999**, *11* (14), 1169–1181. [https://doi.org/10.1002/\(SICI\)1521-4095\(199910\)11:14<1169::AID-ADMA1169>3.0.CO;2-6](https://doi.org/10.1002/(SICI)1521-4095(199910)11:14<1169::AID-ADMA1169>3.0.CO;2-6).
- (11) Zaidi, S. A. R.; Ali, S. W.; Shah, G. B. Synthesis and Characterization of a Cation-Exchange Resin Based on Vinylpyrrolidone-Co-Divinylbenzene: Effect of Nature and Amount of Diluent on Different Resin Properties. *J. Appl. Polym. Sci.* **2004**, *92* (6), 3917–3920. <https://doi.org/10.1002/app.20421>.
- (12) Maciejewska, M. Synthesis and Characterization of Textural and Thermal Properties of Polymer Monoliths. *J. Therm. Anal. Calorim.* **2015**, *121* (3), 1333–1343. <https://doi.org/10.1007/s10973-015-4538-8>.
- (13) Vlach, E. G.; Tennikova, T. B. Preparation of Methacrylate Monoliths. *J. Sep. Sci.* **2007**, *30* (17), 2801–2813. <https://doi.org/10.1002/jssc.200700284>.
- (14) Svec, F.; Fréchet, J. M. J. Molded Rigid Monolithic Porous Polymers: An Inexpensive, Efficient, and Versatile Alternative to Beads for the Design of Materials for Numerous Applications. *Ind. Eng. Chem. Res.* **1999**, *38* (1), 34–48. <https://doi.org/10.1021/ie970598s>.
- (15) Svec, F. Porous Polymer Monoliths: Amazingly Wide Variety of Techniques Enabling Their Preparation. *J. Chromatogr. A* **2010**, *1217* (6), 902–924. <https://doi.org/10.1016/j.chroma.2009.09.073>.
- (16) Bouvier, E. S. P.; Meirowitz, R. E.; McDonald, P. D. Water-Wettable Chromatographic Media for Solid Phase Extraction. **1999**, *US5882521A*, *Google patents*, 8.
- (17) Gilart, N.; Marcé, R. M.; Cormack, P. A. G.; Fontanals, N.; Borrull, F. Development of New Polar Monolithic Coatings for Stir Bar Sorptive Extraction: Sample Preparation. *J. Sep. Sci.* **2014**, *37* (16), 2225–2232. <https://doi.org/10.1002/jssc.201400472>.
- (18) Singh, V.; Purohit, A. K.; Chinthakindi, S.; Goud D, R.; Tak, V.; Pardasani, D.; Shrivastava, A. R.; Dubey, D. K. Magnetic Hydrophilic–Lipophilic Balance Sorbent for Efficient Extraction of Chemical Warfare Agents from Water Samples. *J. Chromatogr. A* **2016**, *1434*, 39–49. <https://doi.org/10.1016/j.chroma.2016.01.028>.

- (19) Horák, D.; Beneš, M. J. Macroporous Poly(Vinylpyrrolidone–Co–Ethylene Dimethacrylate) Beads by Suspension Polymerization. *React. Funct. Polym.* **2000**, *45* (3), 189–195. [https://doi.org/10.1016/S1381-5148\(00\)00025-0](https://doi.org/10.1016/S1381-5148(00)00025-0).
- (20) Umpleby, R. J.; Baxter, S. C.; Chen, Y.; Shah, R. N.; Shimizu, K. D. Characterization of Molecularly Imprinted Polymers with the Langmuir–Freundlich Isotherm. *Anal. Chem.* **2001**, *73* (19), 4584–4591. <https://doi.org/10.1021/ac0105686>.
- (21) Umpleby, R. J.; Baxter, S. C.; Bode, M.; Berch, J. K.; Shah, R. N.; Shimizu, K. D. Application of the Freundlich Adsorption Isotherm in the Characterization of Molecularly Imprinted Polymers. *Anal. Chim. Acta* **2001**, *435* (1), 35–42. [https://doi.org/10.1016/S0003-2670\(00\)01211-3](https://doi.org/10.1016/S0003-2670(00)01211-3).
- (22) Rampey, A. M.; Umpleby, R. J.; Rushton, G. T.; Iseman, J. C.; Shah, R. N.; Shimizu, K. D. Characterization of the Imprint Effect and the Influence of Imprinting Conditions on Affinity, Capacity, and Heterogeneity in Molecularly Imprinted Polymers Using the Freundlich Isotherm-Affinity Distribution Analysis. *Anal. Chem.* **2004**, *76* (4), 1123–1133. <https://doi.org/10.1021/ac0345345>.
- (23) Rushton, G. T.; Karns, C. L.; Shimizu, K. D. A Critical Examination of the Use of the Freundlich Isotherm in Characterizing Molecularly Imprinted Polymers (MIPs). *Anal. Chim. Acta* **2005**, *528* (1), 107–113. <https://doi.org/10.1016/j.aca.2004.07.048>.
- (24) Svec, F. Less Common Applications of Monoliths: Preconcentration and Solid-Phase Extraction. *J. Chromatogr. B* **2006**, *841* (1), 52–64. <https://doi.org/10.1016/j.jchromb.2006.03.055>.
- (25) Potter, O. G.; Hilder, E. F. Porous Polymer Monoliths for Extraction: Diverse Applications and Platforms. *J. Sep. Sci.* **2008**, *31* (11), 1881–1906. <https://doi.org/10.1002/jssc.200800116>.
- (26) Saunders, K. C.; Ghanem, A.; Boon Hon, W.; Hilder, E. F.; Haddad, P. R. Separation and Sample Pre-Treatment in Bioanalysis Using Monolithic Phases: A Review. *Anal. Chim. Acta* **2009**, *652* (1), 22–31. <https://doi.org/10.1016/j.aca.2009.05.043>.
- (27) Namera, A.; Nakamoto, A.; Saito, T.; Miyazaki, S. Monolith as a New Sample Preparation Material: Recent Devices and Applications. *J. Sep. Sci.* **2011**, *34* (8), 901–924. <https://doi.org/10.1002/jssc.201000795>.
- (28) Arrua, R. D.; Causon, T. J.; Hilder, E. F. Recent Developments and Future Possibilities for Polymer Monoliths in Separation Science. *The Analyst* **2012**, *137* (22), 5179. <https://doi.org/10.1039/c2an35804b>.
- (29) Arrua, R. D.; Talebi, M.; Causon, T. J.; Hilder, E. F. Review of Recent Advances in the Preparation of Organic Polymer Monoliths for Liquid Chromatography of Large Molecules. *Anal. Chim. Acta* **2012**, *738*, 1–12. <https://doi.org/10.1016/j.aca.2012.05.052>.
- (30) Hong, T.; Yang, X.; Xu, Y.; Ji, Y. Recent Advances in the Preparation and Application of Monolithic Capillary Columns in Separation Science. *Anal. Chim. Acta* **2016**, *931*, 1–24. <https://doi.org/10.1016/j.aca.2016.05.013>.
- (31) Masini, J. C.; Svec, F. Porous Monoliths for On-Line Sample Preparation: A Review. *Anal. Chim. Acta* **2017**, *964*, 24–44. <https://doi.org/10.1016/j.aca.2017.02.002>.

- (32) Santora, B. P.; Gagné, M. R.; Moloy, K. G.; Radu, N. S. Porogen and Cross-Linking Effects on the Surface Area, Pore Volume Distribution, and Morphology of Macroporous Polymers Obtained by Bulk Polymerization. *Macromolecules* **2001**, *34* (3), 658–661. <https://doi.org/10.1021/ma0004817>.
- (33) Tu, Y.; Xu, G.; Jiang, L.; Hu, X.; Xu, J.; Xie, X.; Li, A. Amphiphilic Hyper-Crosslinked Porous Cyclodextrin Polymer with High Specific Surface Area for Rapid Removal of Organic Micropollutants. *Chem. Eng. J.* **2020**, *382*, 123015. <https://doi.org/10.1016/j.cej.2019.123015>.
- (34) Morin-Crini, N.; Winterton, P.; Fourmentin, S.; Wilson, L. D.; Fenyvesi, É.; Crini, G. Water-Insoluble β -Cyclodextrin–Epichlorohydrin Polymers for Removal of Pollutants from Aqueous Solutions by Sorption Processes Using Batch Studies: A Review of Inclusion Mechanisms. *Prog. Polym. Sci.* **2018**, *78*, 1–23. <https://doi.org/10.1016/j.progpolymsci.2017.07.004>.

CHAPTER 3

SOLID-PHASE EXTRACTION OF REGULATED ANALYTES WITH DIFFERENT
LOG P VALUES FROM HUMAN URINE SAMPLES BY POLY (DIVINYLCO-N-
VINYLPIRROLIDONE) WITH A WIDE RANGE OF MONOMER RATIOS

3.1 Abstract

Hydrophilic-lipophilic balance (HLB) polymers due to their unique capacity for extracting polar and non-polar analytes from the aqueous sample have the potential to absorb regulated drugs from the human urine sample. HLB polymers are widely used as sample preparation sorbents for SPE applications. In this study, a series of HLB polymers based on divinylbenzene (DVB) (hydrophobic) and N-vinylpyrrolidone (NVP) (hydrophilic) prepared by robust monolith polymerization were used as SPE sorbent materials to extract 37 different regulated drugs (analytes) spiked in human urine matrices. Log P values of the analytes ranged from -1.78 to 4.98. The study showed that the least polar SPE sorbent (0 mol% NVP) did not perform well in adsorbing any of the analytes in comparison to medium and more polar SPE sorbents while the more hydrophilic sorbent performed relatively well.

3.2 Introduction

Abuse of different regulated drugs has long been a socio-economic problem.¹ Drug abuse has also been a serious problem in sports activities as some participants knowingly or unknowingly take regulated drugs to enhance their performance.²⁻⁴ Hence the proper detection of drugs is very important in forensic science. The presence of regulated drugs is commonly tested by blood and urine samples analysis.^{2,5-7} One problem is the low concentrations of the drugs in the urine or blood samples. Therefore, sample pre-concentration is vital, prior to analysis using standard analytical techniques such as HPLC, GC, and LC. SPE has been a fast, cost-effective, and efficient sample pre-concentration method. SPE can be easily integrated into standard analytical workflows improving accuracy and detection limits.⁸ SPE also helps purify the sample and remove the matrix

materials. Hence SPE methods are generally preferred over liquid-liquid extraction (LLE) methods for pre-concentrating the dilute and sensitive samples due to ease of application and lower volumes of hazardous solvents.⁵ A wide range of sorbents has been developed for SPE applications. Some examples are styrene-divinylbenzene (St-DVB), methacrylate-divinylbenzene (MA-DVB), N-vinylimidazole-divinylbenzene (NVIIm-DVB), poly(vinylpyrrolidone-*co*-ethylene dimethacrylate) poly(VP-EDMA), and divinylbenzene-*co*-N-vinylpyrrolidone (DVB-*co*-NVP). Most of these sorbents are made of two monomers. However commercial sorbents are available with a narrow range of monomer ratios. Therefore, the preparation of SPE sorbents with different ratios of monomers and examining their extraction properties can be very helpful in identifying the optimal sorbent for the separation of different types of analytes.

In our previous study, we reported the preparation and study of absorption properties of DVB-*co*-NVP polymers that span a wide range of NVP monomer ratios from 0 mol% to 60 mol%.⁹ The absorption efficiencies for the monolith particles were performed by batch binding studies. This study examines the utility of DVB-*co*-NVP polymers with varying NVP/DVB ratios in real-world analytical SPE applications. Hence, this study focuses on the SPE of 37 different regulated analytes with different chemical properties. These include stimulants, opiates, anticonvulsants, amphetamines, analgesics, fentanyl, cocaine analogs, skeletal muscle relaxants (non-benzodiazepine), benzodiazepines, and antidepressants. The regulated analytes were extracted from human urine using DVB-*co*-NVP based SPE sorbents and analyzed using LC-MS.

3.3 Experimental section

3.3.1 Reagents

The analytes were purchased from Cerilliant Corporation.

3.3.2 Synthesis and characterization of DVB-*co*-NVP polymers

The monolith DVB-*co*-NVP polymers in this study were synthesized as described in our previous study.⁹ The series of DVB-*co*-NVP polymer monolith particles, 75-125 μm size range from the previous study were used without any modifications. Hence the polymer series had the same properties and no further characterization was performed.

3.3.3 Recovery of the analytes via SPE

Five milligrams of the dry mass of each sorbent were measured and filled in the DPX pipette tips fitted with the polypropylene frits at the end and a barrier at the top. Microplates containing 200 microliters of human urine spiked with 10 microliters aliquots of 1.0 mgL^{-1} of each analyte forming a mixture of 37 regulated analytes were loaded onto the Hamilton Microlab NIMBUS96 robot for sample preparation. Each sample was then aspirated and dispensed five times to allow the analytes to bind to the sorbent filled in the DPX pipette tips. The elimination of the conditioning step aided in making sample preparation faster which is an advantage of HLB sorbents over other reverse-phase sorbents. The sorbent was then aspirated and dispensed two times with water to remove the salts and other common matrix interferences. Lastly, the target compounds are eluted by aspirating and dispensing an elution solvent (300 μL of 80:20 dichloromethane/isopropanol). The concentrated sample was then heated to 60 $^{\circ}\text{C}$ for 30 minutes to evaporate the elution solvent and reconstituted with 10% 100 μL methanol/water. LC-MS/MS analysis was performed on 5

μ L samples using a SCIEX 6500+ triple stage quadrupole mass spectrometer coupled to an Agilent 1260 HPLC system with a Phenomenex biphenyl (2.6 μ m; 50 \times 30 mm) column to measure the recovery percentages of analytes. The recovery percentages of analytes were calculated based on the total analytes in the neat sample.

3.4 Results and discussion

3.4.1 Recovery efficiencies of series of HLB DVB-*co*-NVP

We previously described the adsorption efficiencies of a series of DVB-*co*-NVP monolith polymers by batch binding studies.⁹ The successful extraction of the analytes with different log P values from aqueous samples demonstrated the practicality of copolymers with varying NVP percentages for real-world analytical separations. With the ability to make sorbents with varying hydrophilicities by monolith polymerization, we were able to recover a wide range of regulated analytes from a human urine sample with different QSAR properties. Differences in the recovery percentages were observed for the DVB-*co*-NVP polymers with different NVP percentages. DVB-*co*-NVP monolith polymer is a HLB polymer so the conditioning step could be omitted making the sample preparation process faster. The more hydrophobic polymers (0% and 20% NVP feed ratio) did not perform well for all the analytes. Whereas the more hydrophilic sorbents (30%, 40%, 50%, and 60% NVP) had the highest recoveries for all the analytes (green highlights in Table 3.1).

The SPE recovery percentages survey demonstrates that no single polymer has the optimal retention properties for all the analytes. Therefore, this study demonstrates that the enhancements in analyte retention and extraction efficiencies can be achieved by the

selection of the polymer sorbent with the optimal balance of hydrophobic and hydrophilic co-monomers.

Table 3.1 Recovery percentages of different analytes for series of DVB-co-NVP monolith polymer series.

Analyte	Log P	0% NVP	20% NVP	30% NVP	40% NVP	50% NVP	60% NVP
pregabalin	-1.78	0.9 ± 0.1	2.9 ± 0.1	3.7 ± 0.2	1.4 ± 0.6	1.9 ± 1.1	0.7 ± 0.1
gabapentin	-1.1	0.3 ± 0.1	1.7 ± 0.2	5.1 ± 1.7	2.8 ± 1.6	2.6 ± 0.4	1.4 ± 0.8
benzoylecgonine	-0.3	0.8 ± 0.2	8.3 ± 0.5	24.4 ± 1.4	15.2 ± 0.1	19.3 ± 0.8	4.7 ± 0.1
cotinine	0.07	0.6 ± 0.1	12.3 ± 0.7	42.6 ± 1.1	44.8 ± 2.6	35.0 ± 3.1	22.5 ± 1.8
hydromorphone	0.11	1.0 ± 0.4	16.0 ± 0.7	52.2 ± 0.1	48.2 ± 3.6	51.4 ± 0.4	24.1 ± 2.8
methylphenidate	0.2	11.8 ± 3.0	40.3 ± 0.2	56.1 ± 0.1	58.1 ± 4.5	60.2 ± 0.5	66.7 ± 2.1
oxycodone	0.66	2.3 ± 0.5	17.0 ± 0.4	32.5 ± 1.1	32.4 ± 3.9	36.0 ± 2.5	26.6 ± 0.5
meprobamate	0.7	3.2 ± 0.3	24.4 ± 3.1	35.0 ± 0.6	37.0 ± 0.4	41.6 ± 3.0	42.8 ± 0.8
oxymorphone	0.83	0.8 ± 0.3	13.4 ± 0.8	62.0 ± 0.6	52.5 ± 1.0	48.9 ± 0.6	21.9 ± 0.2
morphine	0.89	0.8 ± 0.2	13.8 ± 0.9	57.8 ± 0.1	47.2 ± 2.3	41.1 ± 1.2	21.7 ± 1.1
codeine	1.19	2.0 ± 0.8	20.8 ± 1.5	44.1 ± 1.0	45.9 ± 2.8	49.0 ± 2.3	31.3 ± 3.6
hydrocodone	1.2	3.1 ± 1.0	22.3 ± 0.3	38.8 ± 0.1	39.6 ± 2.2	42.7 ± 1.7	35.4 ± 1.6
α-hydroxy alprazolam	1.53	6.4 ± 1.7	27.5 ± 1.1	40.5 ± 4.2	40.9 ± 5.1	26.0 ± 1.1	34.5 ± 0.9
6-MAM	1.55	2.8 ± 1.0	25.1 ± 1.2	44.2 ± 0.1	45.2 ± 2.8	44.7 ± 3.1	49.1 ± 2.6
norfentanyl	1.6	2.8 ± 0.8	24.7 ± 0.2	45.5 ± 0.1	44.3 ± 4.0	46.5 ± 0.5	30.8 ± 1.9
amphetamine	1.76	2.3 ± 0.8	20.7 ± 0.7	52.8 ± 6.3	53.4 ± 2.6	58.7 ± 1.3	37.5 ± 3.0
7-aminoclonazepam	1.8	1.5 ± 0.2	12.8 ± 1.4	14.1 ± 1.9	16.2 ± 0.7	15.5 ± 0.4	19.9 ± 1.2
methamphetamine	2.07	3.3 ± 1.0	24.2 ± 0.5	51.2 ± 3.6	51.7 ± 4.3	59.1 ± 1.3	40.3 ± 3.3
carisoprodol	2.1	27.0 ± 3.2	42.8 ± 2.5	69.2 ± 7.4	50.7 ± 1.0	54.5 ± 3.4	43.0 ± 1.9
alprazolam	2.12	10.3 ± 2.7	31.5 ± 2.1	41.7 ± 3.2	43.4 ± 3.9	26.9 ± 0.5	33.4 ± 3.8
MDMA	2.14	3.4 ± 1.1	30.2 ± 0.8	51.4 ± 0.3	53.9 ± 1.7	55.4 ± 0.5	58.7 ± 1.5
temazepam	2.19	16.6 ± 3.5	37.6 ± 0.9	46.0 ± 2.3	56.2 ± 2.8	35.9 ± 0.1	40.7 ± 4.8
oxazepam	2.24	8.6 ± 1.5	29.9 ± 3.0	40.8 ± 1.0	40.9 ± 4.7	38.8 ± 0.9	38.5 ± 2.1
o-dsmethyltramadol	2.3	1.6 ± 0.7	20.9 ± 0.1	46.3 ± 0.5	48.2 ± 5.5	53.9 ± 1.0	35.5 ± 3.6
lorazepam	2.39	9.3 ± 0.5	29.3 ± 3.5	39.0 ± 0.1	39.8 ± 4.7	38.3 ± 1.5	38.1 ± 4.6
clonazepam	2.41	12.8 ± 0.5	26.9 ± 4.6	35.1 ± 1.2	31.3 ± 5.7	26.6 ± 1.7	28.3 ± 2.1
mepiridine	2.72	14.5 ± 2.8	35.9 ± 0.9	42.1 ± 0.6	44.9 ± 3.2	45.6 ± 0.1	57.9 ± 0.9
diazepam	2.82	15.9 ± 4.7	33.8 ± 8.8	40.3 ± 1.5	45.5 ± 3.8	34.6 ± 1.1	38.3 ± 5.3
nordiazepam	2.93	13.5 ± 2.5	28.3 ± 5.2	35.6 ± 0.8	34.9 ± 2.5	32.8 ± 1.6	31.8 ± 3.1
tramadol	3.01	5.9 ± 1.7	31.8 ± 0.6	55.3 ± 0.3	55.5 ± 2.5	56.4 ± 0.3	59.7 ± 1.6
zolpidem	3.02	15.8 ± 3.7	40.6 ± 0.6	54.0 ± 2.0	53.5 ± 3.3	58.0 ± 1.4	67.2 ± 3.9
methadone	3.93	8.6 ± 0.9	31.9 ± 13.5	54.9 ± 6.0	55.0 ± 5.2	60.5 ± 1.7	68.2 ± 1.2
fentanyl	4.05	18.6 ± 3.4	37.6 ± 5.3	43.3 ± 2.1	46.2 ± 3.4	45.7 ± 1.2	57.7 ± 1.0
nortriptyline	4.51	5.9 ± 0.3	22.7 ± 13.7	31.8 ± 0.1	32.9 ± 3.8	46.0 ± 2.7	41.0 ± 1.8
cyclobenzaprine	4.79	6.4 ± 0.1	23.8 ± 15.7	35.1 ± 0.3	36.6 ± 5.3	51.2 ± 3.3	46.7 ± 1.4
amitriptyline	4.92	7.9 ± 0.3	29.4 ± 17.9	42.0 ± 0.7	44.4 ± 6.4	59.2 ± 3.4	57.5 ± 2.0
buprenorphine	4.98	15.6 ± 1.6	34.2 ± 7.4	36.6 ± 4.2	41.2 ± 3.0	44.7 ± 1.4	53.6 ± 1.6

3.4.2 Selectivity pattern for analytes

The binding affinity patterns for the 37 different analytes against the series of DVB-*co*-NVP polymers varied widely. For example, the polymer with maximum recovery varied depending on the analyte. However, the binding affinity patterns were similar for analytes with similar structures or QSAR properties. An example is shown in Figure 3.1 for the analytes, amitriptyline, cyclobenzaprine, and nortriptyline that, have similar molecular structures (Figure 3.2) and also similar selectivity patterns. Therefore, the 50% NVP sorbent has optimal recovery for amitriptyline, cyclobenzaprine, and nortriptyline followed by the 60% NVP and then 40% \approx 30% NVP polymers.

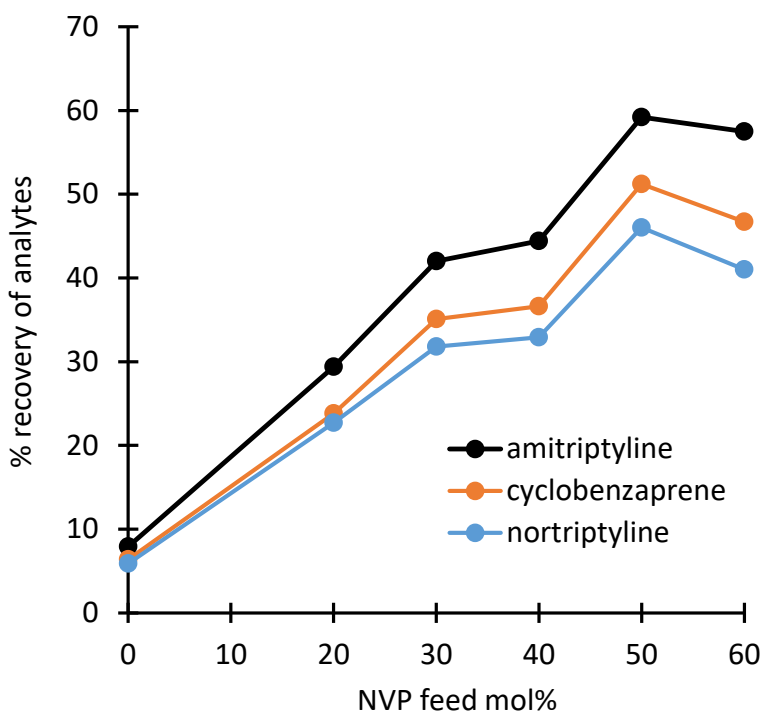


Figure 3.1 Binding capacities of monolith DVB-*co*-NVP polymers with varying NVP feed ratios (0 – 60 mol%) for structurally similar analytes (amitriptyline, cyclobenzaprine, and nortriptyline) showing similar binding patterns.

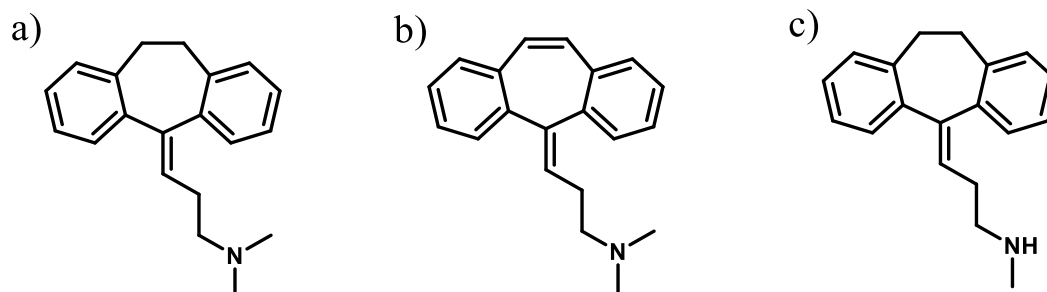


Figure 3.2 Examples of structurally similar analytes a) amitriptyline, b) cyclobenzaprine, and c) nortriptyline.

Similar binding patterns were also correlated to similarities in other QSAR properties such as physiological charge, log P, and pKa (base) despite the difference in molecular structure. Analytes MDMA, 6-MAM, tramadol, and methylphenidate have similar binding patterns (Figure 3.3) but different molecular structures (Figure 3.4) which can be attributed to the similarity in their charges under physiological conditions which is evident from their similar pKa (base) values (MDMA = 10.14, 6-MAM = 9.08, tramadol = 9.23, methylphenidate = 9.09).

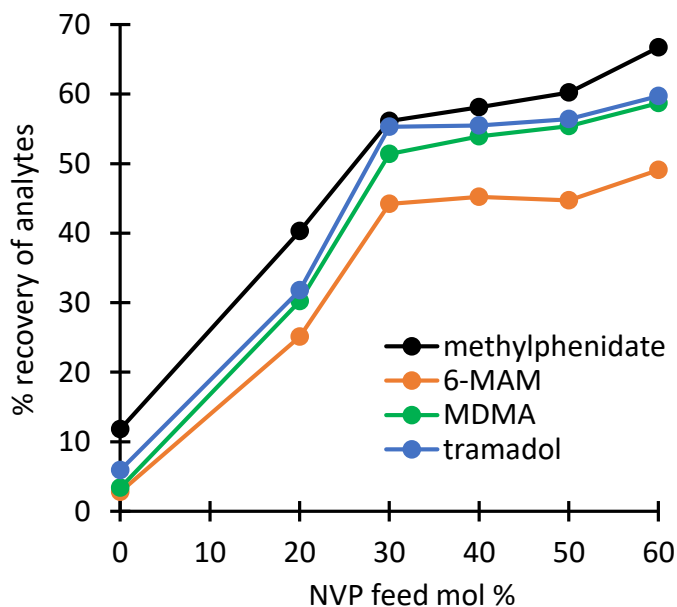


Figure 3.3 Binding capacities of monolith DVB-*co*-NVP polymers with varying NVP feed ratios (0 – 60 mol%) for methylphenidate, 6-mam, MDMA, and tramadol showing similar binding patterns.

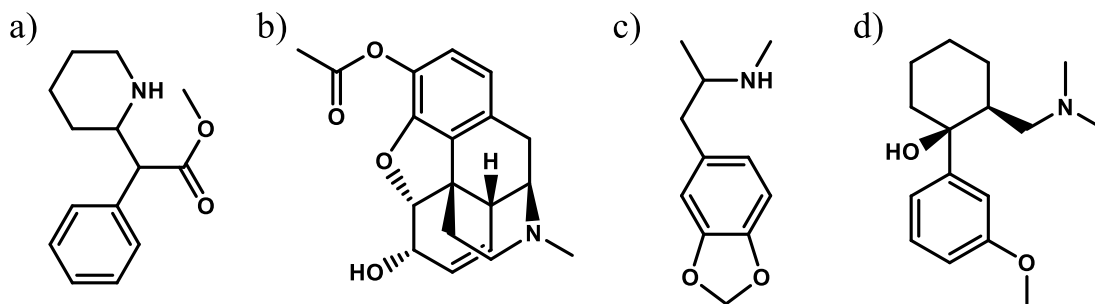


Figure 3.4 Structure of analytes a) MDMA, b) 6-MAM, c) tramadol, and d) methyphenidate with similar pK_a (base) values.

Comparison of selectivity patterns for different analytes provides insight into the recovery performance of the series of DVB-*co*-NVP polymers. The selection of the polymer with optimal recovery performance depends on the analyte and the selectivity patterns of the other analytes in the sample mixture. An example, for the analytes oxymorphone, methamphetamine, and fentanyl (Figure 3.5) is shown in Figure 3.6 that have different $\log P$ values and different selectivity patterns. Oxymorphone had a maximum recovery with the 30% NVP polymer, while methamphetamine and fentanyl had the highest recovery percentages with the 50% NVP and 60% NVP polymers respectively.

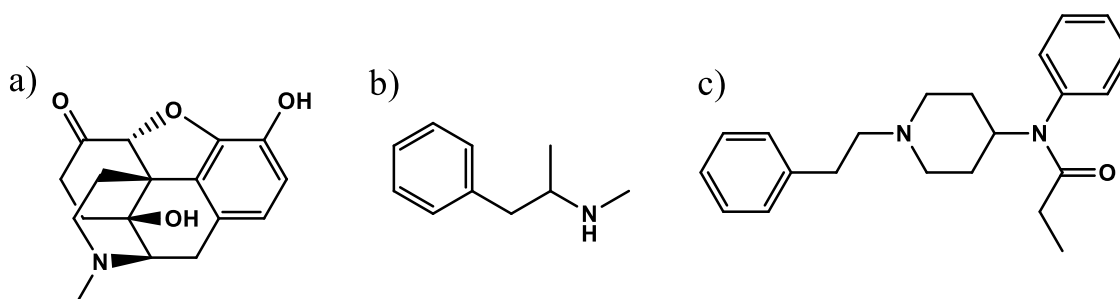


Figure 3.5 Structure of analytes a) oxymorphone ($\log P = 0.83$), b) methamphetamine ($\log P = 2.07$), and c) fentanyl ($\log P = 4.05$).

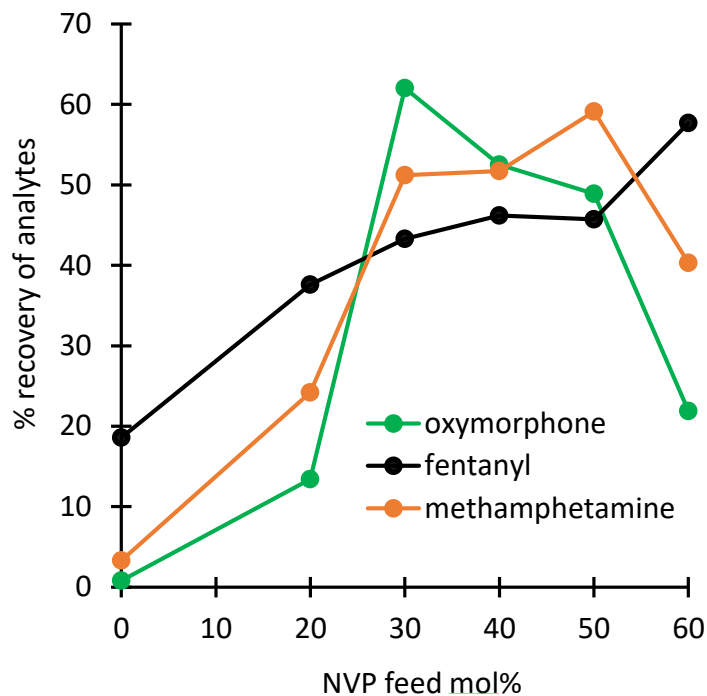


Figure 3.6 Binding capacities of monolith DVB-*co*-NVP polymers with varying NVP feed ratios (0 – 60 mol%) for oxymorphone, fentanyl, and methamphetamine.

The correlation of the selectivity patterns of the analytes with QSAR properties was investigated. Principal component analysis (PCA) assessed the similarities and differences in the normalized binding patterns for the 37 analytes against the series of DVB-*co*-NVP polymers (Figure 3.7). Analytes having similar binding patterns are grouped together. The analytes with similar binding patterns showed some similarities in properties such as molar volume and log P. For example, in Figure 3.7 analytes with similar molar volumes were plotted with the same color. Likewise, analytes with similar log P values were coded with the same shapes. The PCA study revealed the binding patterns were correlated with multiple QSAR properties as no single property was able to accurately predict the binding patterns.

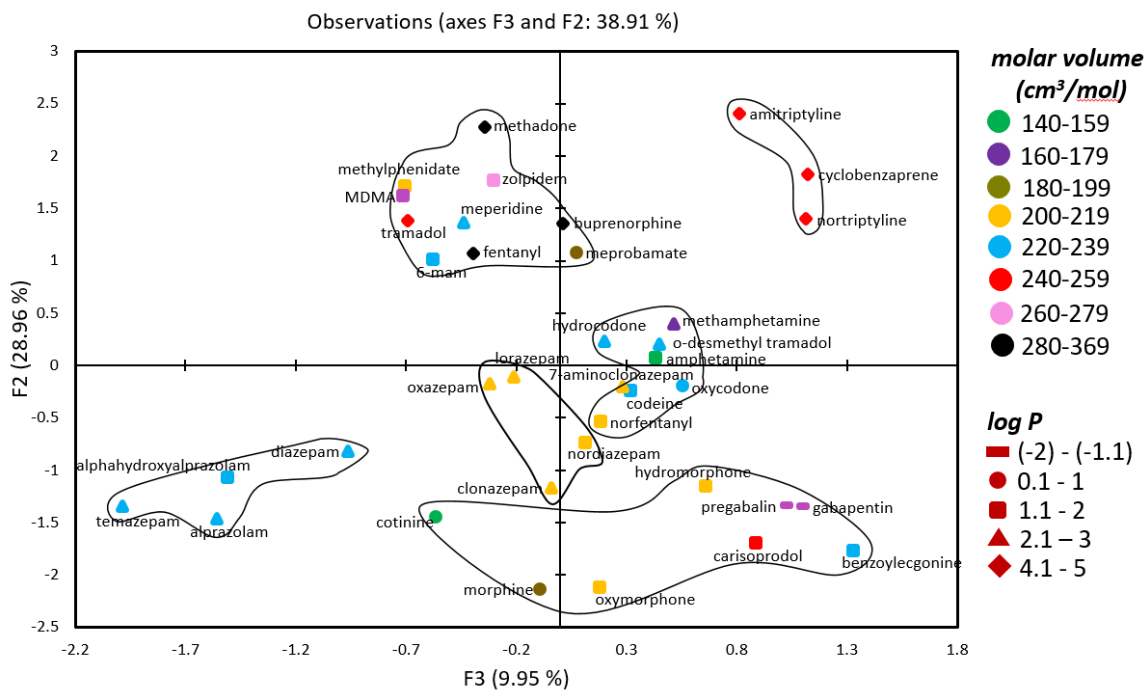


Figure 3.7 Principal component analysis (PCA) plot for different analytes in response to binding patterns.

In our previous study, we reported that the optimal DVB-*co*-NVP composition varied depending on the analyte or analytes. A DVB-*co*-NVP polymer with a particular composition could be ideal for the extraction of individual analytes but might not perform well while separating the mixture of analytes. A similar trend was observed in the recovery study of the 37 analytes. The recovery studies demonstrate the utility of testing the series of DVB-*co*-NVP polymers to identify optimal conditions for the separation of the mixture of analytes. For example, oxycodone, methamphetamine, and fentanyl have maximum recovery with 30%, 50%, and 60% NVP polymer but the separation of fentanyl from oxycodone and methamphetamine could be more efficient with 0% NVP polymer (Figure 3.6).

3.5 Conclusions

A series of DVB-*co*-NVP polymers with a wide range of NVP monomer ratios (0 mol% to 60 mol%) were tested for their extraction and separation capacities of 37 different regulated analytes. These HLB polymers were more efficient in extracting the analytes directly from the human urine without the need for pre-wetting the polymer sorbents. Most of the analytes were recovered successfully with widely varying recovery percentages. For example, analytes such as amitriptyline, cyclobenzaprine, and nortriptyline were recovered best by 50% NVP polymer. Whereas, methylphenidate, 6-MAM, MDMA, and tramadol had the maximum recovery with 60% NVP polymer. Therefore, an optimal performing polymer composition could be selected for the recovery and separation of analytes depending on the selectivity patterns.

3.6 References

- (1) Feng, J.; Wang, L.; Dai, I.; Harmon, T.; Bernert, J. T. Simultaneous Determination of Multiple Drugs of Abuse and Relevant Metabolites in Urine by LC-MS-MS*. *J. Anal. Toxicol.* **2007**, *31* (7), 359–368. <https://doi.org/10.1093/jat/31.7.359>.
- (2) Thevis, M.; Geyer, H.; Tretzel, L.; Schänzer, W. Sports Drug Testing Using Complementary Matrices: Advantages and Limitations. *J. Pharmaceut. Biomed. Anal.* **2016**, *130*, 220–230. <https://doi.org/10.1016/j.jpba.2016.03.055>.
- (3) Thevis, M.; Kuuranne, T.; Geyer, H.; Schänzer, W. Annual Banned-Substance Review: Analytical Approaches in Human Sports Drug Testing. *Drug Test. Anal.* **2017**, *9* (1), 6–29. <https://doi.org/10.1002/dta.2139>.
- (4) Görgens, C.; Guddat, S.; Thomas, A.; Thevis, M. Recent Improvements in Sports Drug Testing Concerning the Initial Testing for Peptidic Drugs (< 2 KDa) – Sample Preparation, Mass Spectrometric Detection, and Data Review. *Drug Test. Anal.* **2018**, *10* (11–12), 1755–1760. <https://doi.org/10.1002/dta.2503>.
- (5) Josefsson, M.; Sabanovic, A. Sample Preparation on Polymeric Solid Phase Extraction Sorbents for Liquid Chromatographic-Tandem Mass Spectrometric Analysis of Human Whole Blood—A Study on a Number of Beta-Agonists and Beta-Antagonists. *J. Chromatogr. A* **2006**, *1120* (1), 1–12. <https://doi.org/10.1016/j.chroma.2006.03.013>.
- (6) Persona, K.; Madej, K.; Knihnicki, P.; Piekoszewski, W. Analytical Methodologies for the Determination of Benzodiazepines in Biological Samples. *J. Pharmaceut. Biomed. Anal.* **2015**, *113*, 239–264. <https://doi.org/10.1016/j.jpba.2015.02.017>.

- (7) Domínguez-Romero, J. C.; García-Reyes, J. F.; Lara-Ortega, F. J.; Molina-Díaz, A. Screening and Confirmation Capabilities of Liquid Chromatography-Time-of-Flight Mass Spectrometry for the Determination of 200 Multiclass Sport Drugs in Urine. *Talanta* **2015**, *134*, 74–88. <https://doi.org/10.1016/j.talanta.2014.10.050>.
- (8) Rossi, D. T.; Zhang, N. Automating Solid-Phase Extraction: Current Aspects and Future Prospects. *J. Chromatogr. A* **2000**, *17*.
- (9) Karki, I.; Li, P.; Vik, E. C.; Manzewitsch, A.; Divirgilio, E.; Brewer, W. E.; Shimizu, K. D. Absorption Properties of Monolithic Poly (Divinylbenzene-*co*-*N*-Vinylpyrrolidone) over a Wide Range of Monomer Ratios. *React. Funct. Polym.* **2021**, *163*, 104888. <https://doi.org/10.1016/j.reactfunctpolym.2021.104888>.

CHAPTER 4

MOLECULARLY IMPRINTED POLYMERS (MIPs) FOR CO₂ CAPTURE

4.1 Abstract

Molecularly imprinted polymers (MIPs) are the synthetic polymers with tailored molecular recognition properties from a template species that was introduced during the synthesis of the polymer. MIPs are inexpensive and easy to prepare, thus, have a wide range of applications in different fields. MIPs with enhanced adsorption and desorption properties could be good CO₂ capture materials. This chapter is focused on the development of MIPs with higher capacities and adsorption efficiencies for CO₂ capture. One strategy to optimize the CO₂ adsorption is by increasing the specific surface area of MIPs. Hence this chapter focuses on the development of higher specific surface area MIPs by selecting suitable monomers for polymerization.

4.2 Introduction

MIPs are materials having enhanced affinity towards a template molecule.¹⁻⁴ MIPs are more widely used in separation applications like SPE. The history of molecular imprinting started in 1940s⁵ and 1950s⁶ with Dickey's experiment to create affinity for a dye molecule in silica gel.⁷ Molecular imprinting has been a powerful technique to prepare cost-efficient polymeric materials having tailored molecular recognition properties. The molecular recognition properties can be tailored by choice of the template. The template molecule pre-organizes the recognition groups in the monomers to form a template-monomer assembly in the pre-polymerization mixture. The pre-organized functional monomers are covalently fixed in the cross-linked polymer matrix formed during the polymerization step (Figure 4.1). Removal of the template molecule reveals the recognition sites. MIPs are the synthetic alternatives to natural antibodies and are easy to prepare in large quantities by polymerizing the functional monomers and cross-linker in the presence

of a template molecule of choice. Thus these synthetic materials with molecular memory have found applications in chromatography, solid-phase extraction (SPE), and gas adsorption.

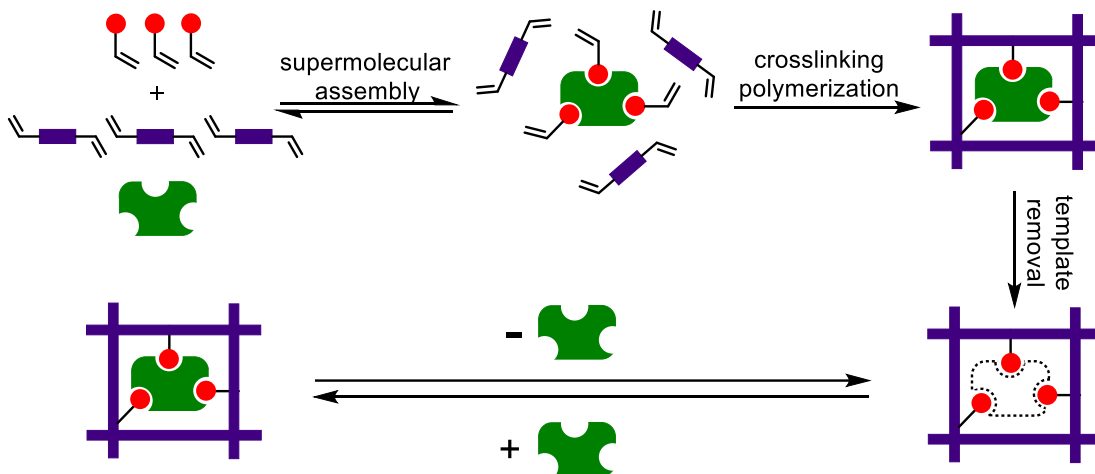
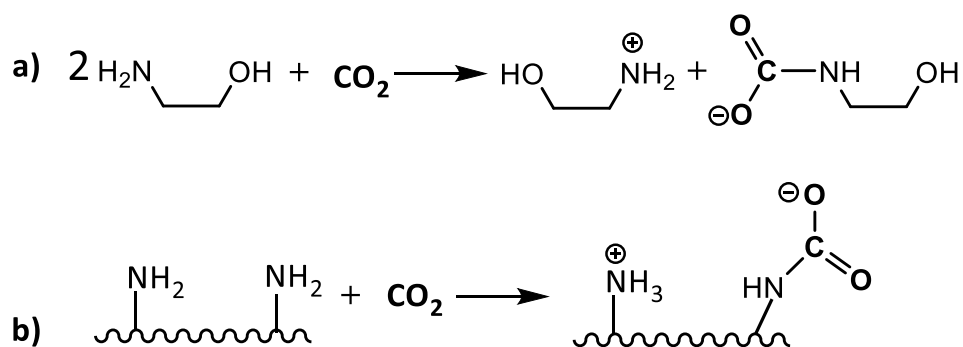


Figure 4.1 Schematic representation of molecular imprinting process to make MIPs.

Increasing atmospheric CO₂ level has been strongly linked to global warming and climate change. To address this problem, an array of technological solutions are being developed to reduce or slow the rate of CO₂ emissions.⁷⁻¹¹ One of the most widely explored solutions is CO₂ capture and sequestration. While a number of advanced materials have been developed that are more efficient than current technologies, their high costs, short lifetimes, and inability to scale to industrial processes have limited their applicability. Thus, one of the most established methods simply uses solutions of ethanolamine (EA) that chemically react with CO₂ (Scheme 4.1a).^{12,13} EA is inexpensive and aqueous solutions have very high capacities for CO₂ (1 mol CO₂ per 2 mol EA). EA forms a stable chemical adduct with CO₂ (either carbamic acid or carbonic acid/ester). The EA-bound CO₂ can be released simply by heating (further lowering costs). However, EA has limitations. The solutions have large heat capacities requiring very high energy consumption to release CO₂.

Therefore, ‘dry’ versions of the reactive-amine strategy are being examined (Scheme 4.1b).¹⁴ Amine groups have been incorporated into high surface area and porous materials with some success.¹⁵ The problem has been that higher-capacity amine-based materials are too expensive, have low to moderate capacities, and have slow reactivities.

Our strategy will be to use the molecular imprinting process to address these limitations. CO₂ will be used as templating agents to create binding sites with the shape of the template and lined with complementary binding or recognition groups. The primary advantage is that materials with tailored recognition and binding properties can be quickly and inexpensively prepared using commercial or readily accessible polymer precursors. Previous CO₂ MIPs suffered from low surface areas (< 60 m²g⁻¹) that limited adsorption capacities.¹⁶⁻¹⁹ The cross-linker divinylbenzene, consistently yields polymers with significantly higher surface areas.²⁰ Therefore, the use of divinylbenzene as the cross-linker could yield polymers with high surface areas.

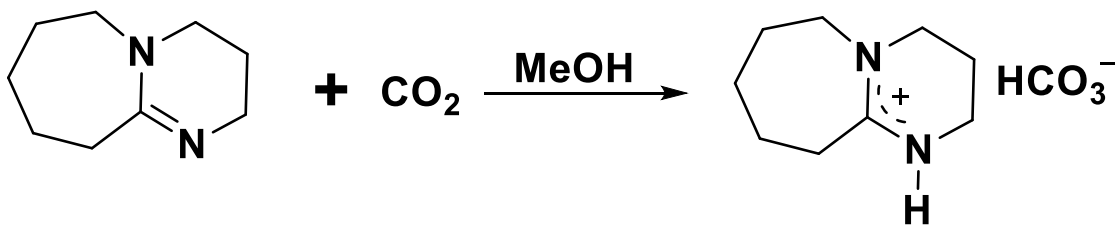


Scheme 4.1 a) reaction of ethanolamine (EA) with carbon dioxide to form a stable carbamic acid salt b) chemisorption polymers based on polyamine materials.

4.3 Experimental section

4.3.1 Modeling of the functional monomer

First, a reactive functional monomer with an amine or amidine functional group was designed which will act as a nucleophilic monomer. The amine or amidine monomer can then be polymerized with a commercially available cross-linker monomer such as divinylbenzene and a nucleophile monomer (4-vinylphenyl methanol) to form a cross-linked polymer. The CO₂ absorption property of the amine or amidine monomer was tested using a model system. CO₂ absorption modeling was done on DBU (1, 8-diazabicyclo[5.4.0]undec-7-ene) which is an amidine,^{21,22} that is analogous to the amidine functional monomer used in this study. CO₂ was bubbled into DBU in presence of methanol solvent which formed white precipitate, (Figure 4.2) indicated the absorption of CO₂ by DBU forming [DBUH⁺][HCO₃⁻] (Scheme 4.2).



Scheme 4.2 Reaction of CO₂ with DBU in methanol solvent to form [DBUH⁺][HCO₃⁻].



Figure 4.2 (left) DBU in methanol before bubbling CO₂ (right) [DBUH⁺][HCO₃⁻] formed after bubbling in CO₂ for 10 minutes.

IR spectra of DBU in methanol before and after bubbling CO₂ also showed the absorption of CO₂ by DBU methanol mixture. The presence of a broad peak at 1640 cm⁻¹ and a new peak at 880 cm⁻¹ suggests the presence of the DBU carbonate salt (Figure 4.3).^{18,21,23,24}

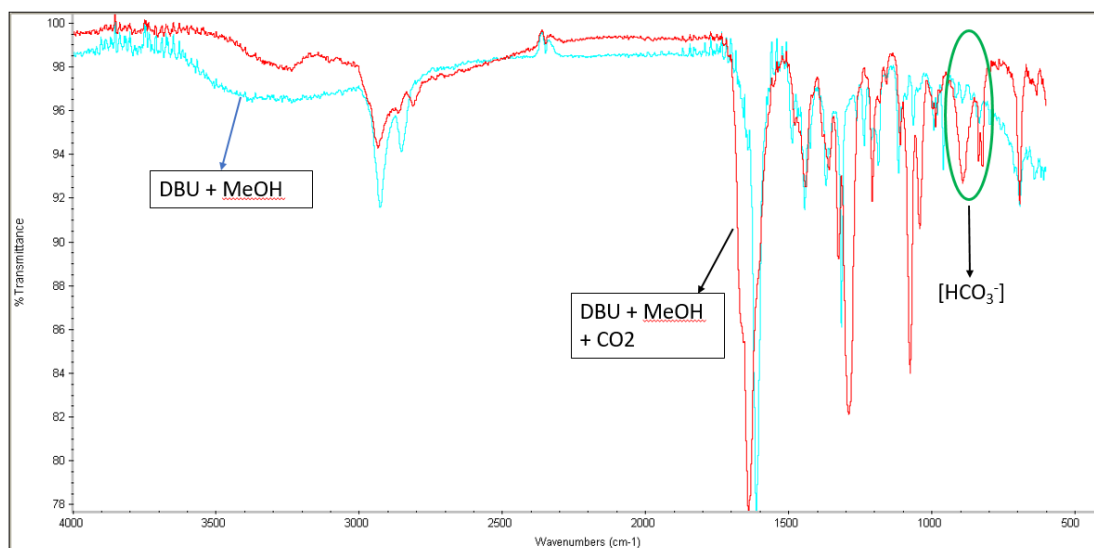
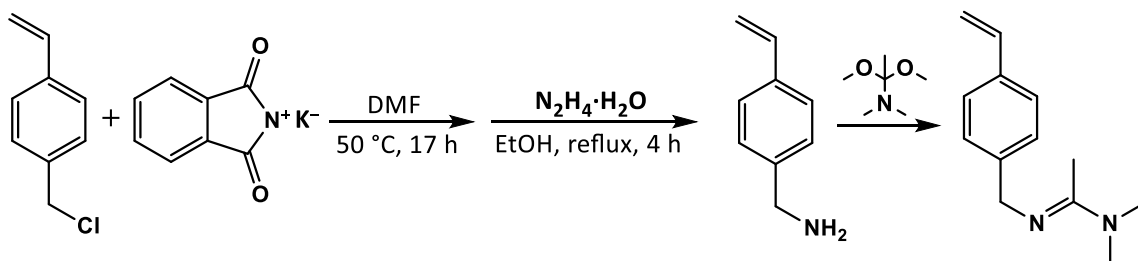


Figure 4.3 IR spectrum of DBU in methanol before and after CO₂ bubbling.

4.3.2 Synthesis of reactive monomer

The 4-vinylbenzyl amidine monomer was prepared following the procedure from the literature with some modifications (Scheme 4.3).²⁵⁻²⁷



Scheme 4.3 Synthesis route of 4-vinylbenzyl amidine monomer.

In a 100 mL round bottom flask, 9.74 g 4-vinylbenzyl chloride (63.81 mmol) and 11.82 g phthalimide potassium salt (63.78 mmol) were dissolved into 40 mL dimethylformamide (DMF) and was heated at 50 °C for 17 hours with stirring. The resulting mixture was diluted with chloroform (CHCl₃). DMF was removed by washing with water. The mixture in CHCl₃ was finally washed with aqueous sodium hydroxide (0.2 mol L⁻¹) and water successively. Chloroform was removed using a rotary evaporator and the white raw product was recrystallized from methanol (12.1 g, 71%).

Next, 8 g of 4-vinylbenzylphthalimide (30.38 mmol) was dissolved in ethanol with heating and 2.55 g hydrazine monohydrate (N₂H₄·H₂O) (50.99 mmol) was slowly added. The white solid mass was formed after heating the mixture for 2 hours which was filtered off and washed with ethanol. The filtrate was dried using a rotary evaporator leaving colorless oily mass (4-vinylbenzyl amine) (2.1 g, 51%). ¹H NMR (300 MHz, CDCl₃): δ 7.33 (d, *J* = 7.98 Hz, 2H), 7.19 (d, *J* = 7.98 Hz, 2H), 6.66 (dd, *J* = 10.83, 10.70 Hz, 1 H), 5.69 (d, *J* = 17.51 Hz, 1H), 5.18 (d, *J* = 10.77 Hz, 1H), 3.75 (s, 2H), 2.55 (s, 3H).

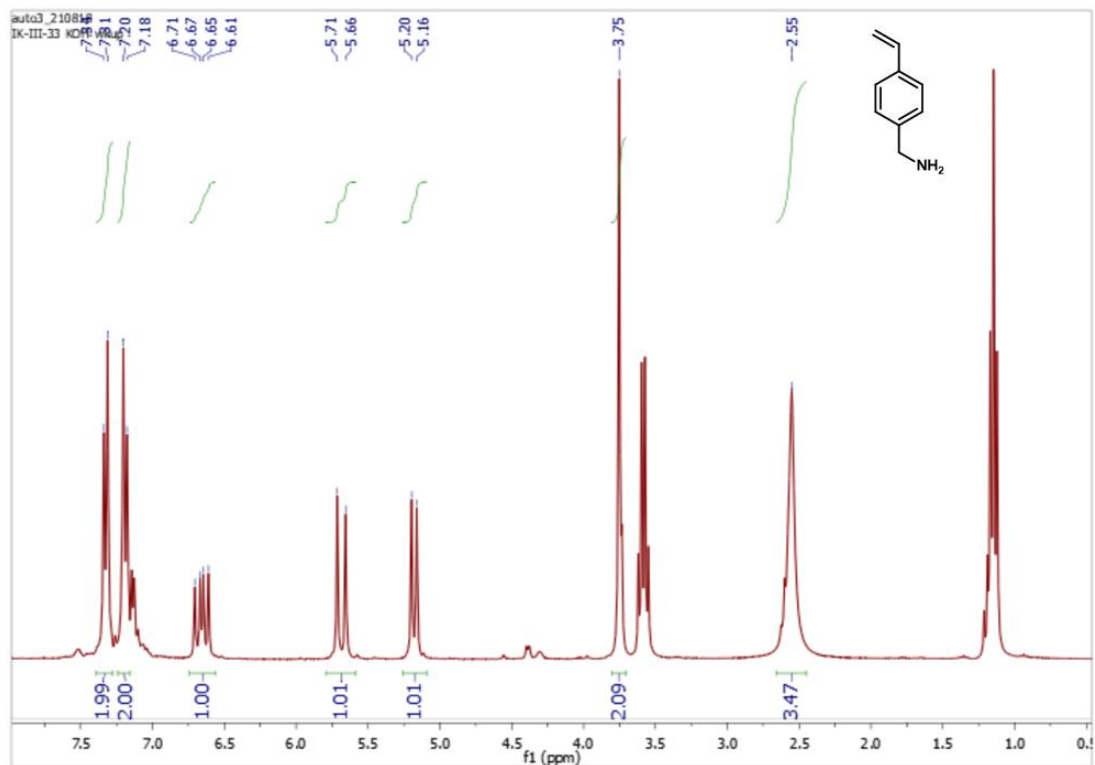


Figure 4.4 ¹H NMR spectra of vinylbenzyl amine monomer.

To a 50 mL round bottom flask 1 g of 4-vinylbenzyl amine (7.5 mmol) was added followed by 1.2 g of *N,N*-dimethylacetamide dimethylacetal (9.0 mmol). The mixture was stirred at room temperature for 15 minutes followed by heating at 65 °C for 2 hours. Excess *N,N*-dimethylacetamide dimethylacetal, and the side product methanol were removed with a rotary evaporator to give yellow oily mass (7.3 g, 97%). ¹H NMR (300 MHz, CDCl₃): δ 7.37 (d, *J* = 8.15 Hz, 2H), 7.30 (d, *J* = 8.15 Hz, 2H), 6.72 (dd, *J* = 10.81, 10.81 Hz, 1 H), 5.72 (d, *J* = 18.19 Hz, 1H), 5.19 (d, *J* = 11.41 Hz, 1H), 4.50 (s, 2H), 2.96 (s, 6H), 1.91 (s, 3H).

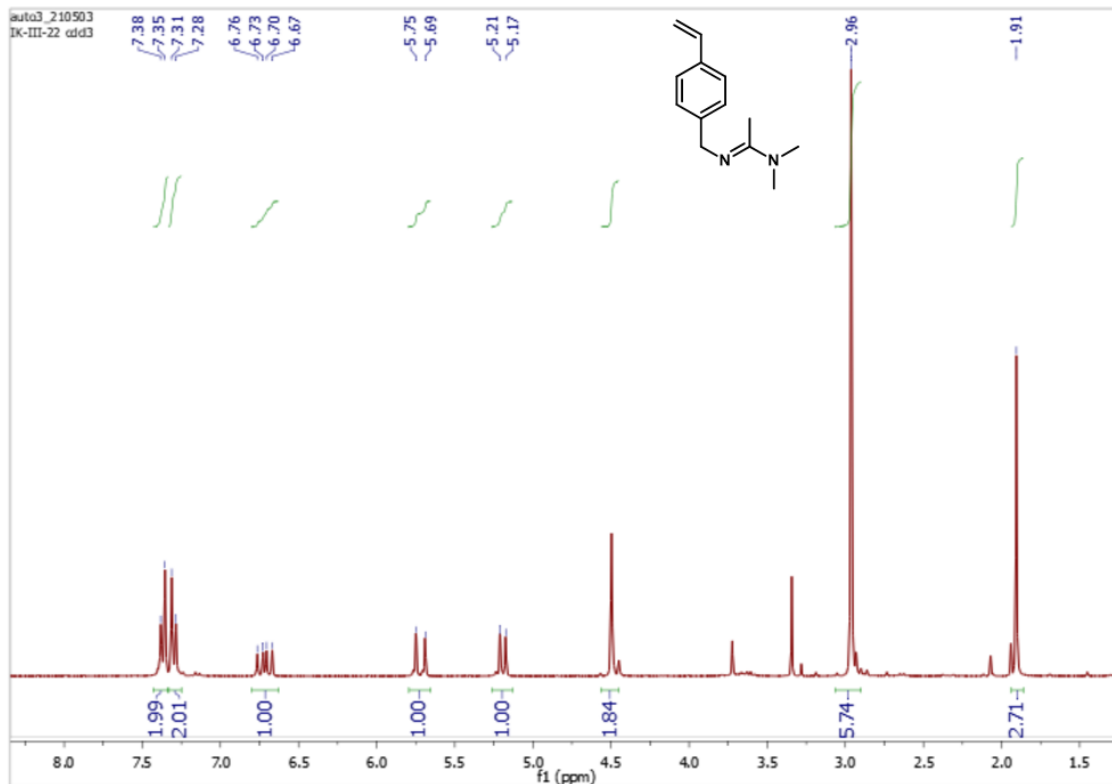


Figure 4.5 ¹H NMR spectra of vinylbenzyl amidine monomer.

4.3.3 Synthesis of DVB-*co*-VBA polymer

DVB-*co*-VBA polymers were prepared by free radical polymerization. Polymers were prepared with 10:90, 15:85, VBA/DVB mol/mol feed ratios using toluene as porogen. An example of a monolith polymerization procedure is provided below for the preparation of DVB-*co*-VBA with a 10 mol% VBA feed ratio. Divinylbenzene (1.09 mL, 7.68 mmol), 4-vinylbenzyl amidine (0.14 mL, 0.77 mmol), and 10 mol% AIBN (0.138 g, 0.844 mmol) were dissolved in 1.5 mL toluene in a 2 dram vial. The mixture was sonicated and then degassed under nitrogen for 5 min. The vials were sealed and heated at 70 °C for 8 hours. The resulting monoliths were ground into small particles using a mortar and pestle. The ground polymer was washed three times with 5 mL of methanol, which was decanted to

remove the smallest particles. The remaining particles were washed using Soxhlet extraction with water for 24 hours. The washed polymer particles were dried under vacuum and used for further characterization.

4.3.4 Confirmation of 4-vinylbenzyl amidine incorporation

Preliminary confirmation of the incorporation of VBA was done by IR spectrum of the polymer prepared with 10 mol% and 15 mol% VBA feed in. IR spectra of DVB-*co*-VBA polymers were compared against the polymer made with only divinylbenzene crosslinker. Peaks at 1369 cm^{-1} are assigned to C-N^{28-30} stretching and at 1683 cm^{-1} to $\text{C=N}^{31,32}$ (green ovals, Figure 4.6 and Figure 4.7), which were absent in the IR spectrum of the polymer prepared with only divinylbenzene cross-linker (Figure 4.8).

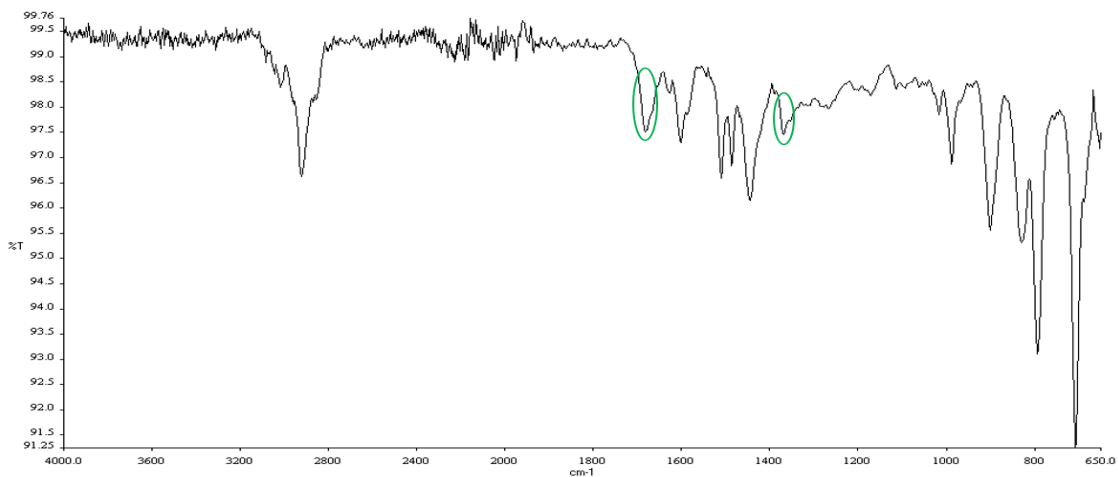


Figure 4.6 IR spectrum of DVB-*co*-VBA polymer made with 10 mol% VBA.

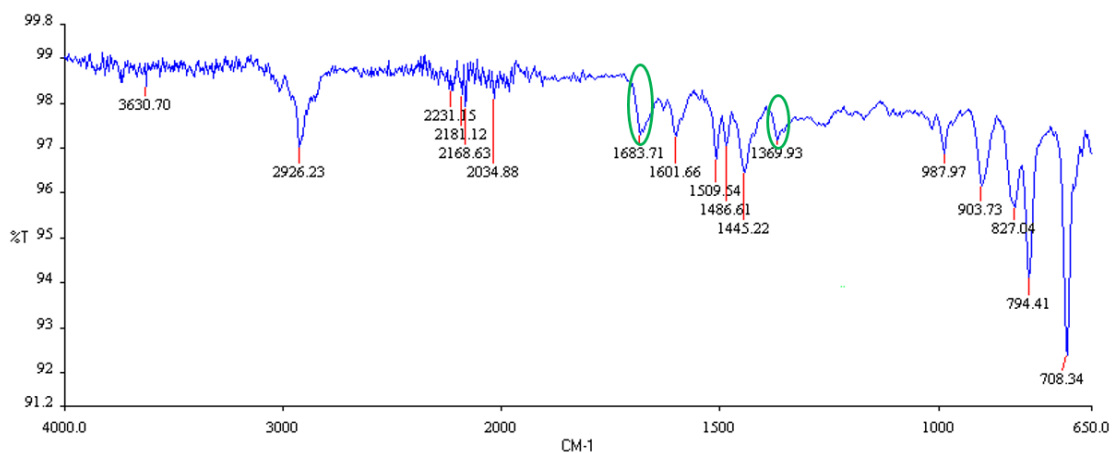


Figure 4.7 IR spectrum of DVB-*co*-VBA polymer made with 15 mol% VBA.

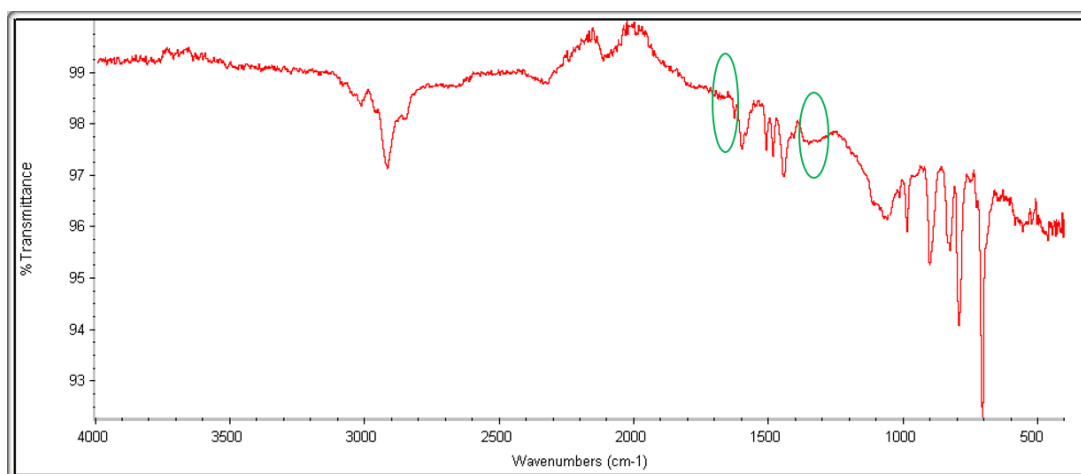


Figure 4.8 IR spectrum of DVB only polymer.

4.3.5 CO₂ adsorption test by the non-imprinted version of DVB-*co*-VBA polymer

Once the incorporation of 4-vinylbenzyl amidine in the polymer was confirmed by the IR spectra comparison, the CO₂ adsorption by the non-imprinted polymer was tested. For the test, 30 mg of DVB-*co*-VBA prepared with 10 mol% VBA was soaked in dichloromethane, chloroform, and methanol overnight. The overnight soaked polymer sample was bubbled with CO₂ for 10 minutes, filtered and the CO₂ adsorption was investigated with the IR spectra. The strong IR absorption of the free amidine at around

1683 cm^{-1} disappeared forming a merged peak at around 1655 cm^{-1} indicating the formation of resonance stabilized amidinium structure, ($-\text{N}-\text{C}=\text{N}^+- \leftrightarrow -\text{N}^+=\text{CH}-\text{N}-$) upon CO_2 absorption (Figure 4.9). By comparison, a similar absorption band was not observed for polymer soaked in dichloromethane, chloroform (Figure 4.9 and Figure 4.10), and bubbled with CO_2 . One possible reason could be the polymer was not readily wetted by dichloromethane and chloroform as with methanol.

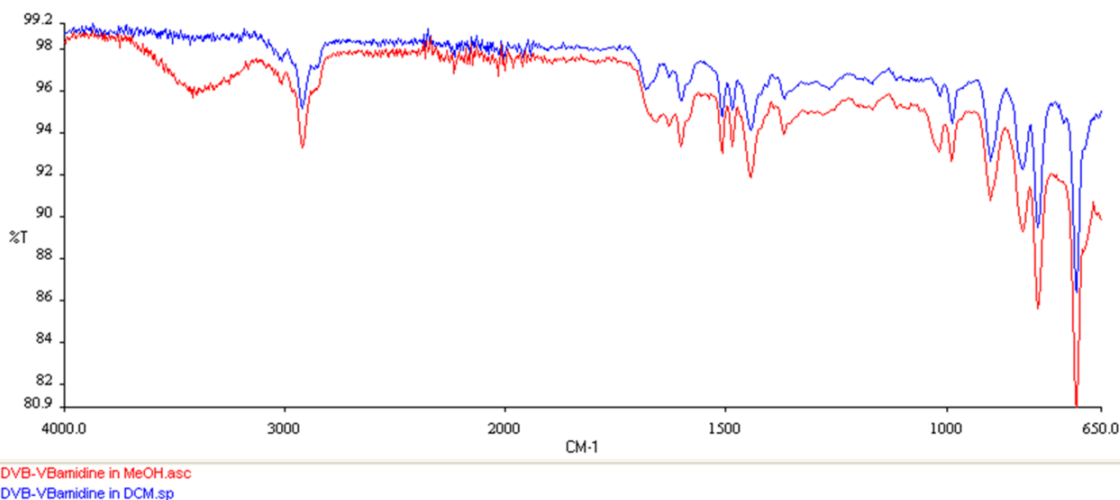


Figure 4.9 IR absorption for DVB-*co*-VBA polymer soaked in solvents and CO_2 bubbled (red spectrum soaked in methanol, blue spectrum soaked in dichloromethane)

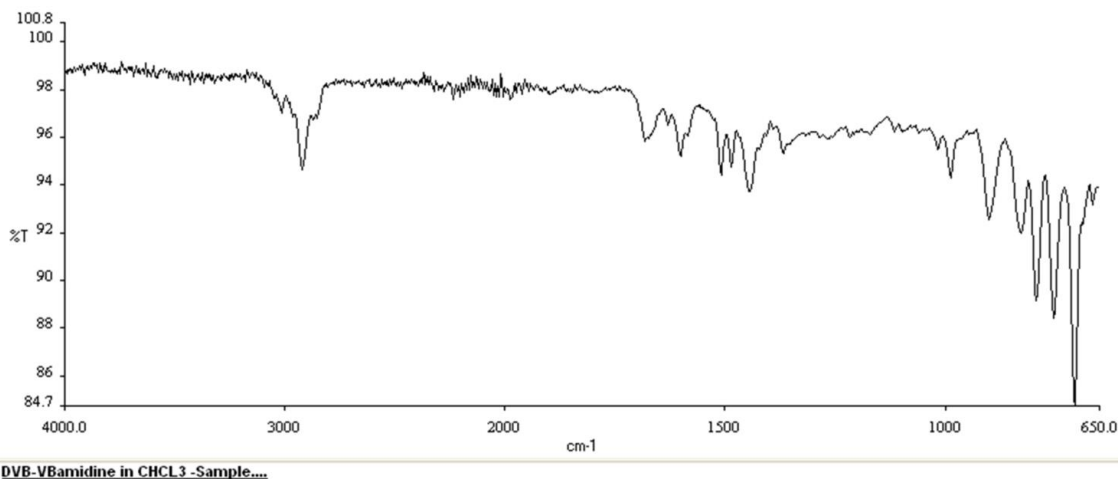


Figure 4.10 IR absorption for DVB-*co*-VBA polymer soaked in chloroform and CO_2 bubbled.

4.4 Conclusions

In conclusion, a functional monomer capable of CO₂ capture was modeled and synthesized which was copolymerized with a commercially available cross-linker that forms a polymer framework with a higher specific area to form a non-imprinted DVB-*co*-VBA monolithic polymer resin. The monolith polymer particles were able to absorb CO₂ after wetting with a suitable solvent. Among the three solvents tested for wetting and CO₂ absorption, methanol was more suitable. Preparation of the CO₂ imprinted version of the DVB-*co*-VBA polymer monolith and its efficiency for CO₂ capture and sequestration is subject to future studies.

4.5 References

- (1) Mayes, A. G.; Whitcombe, M. J. Synthetic Strategies for the Generation of Molecularly Imprinted Organic Polymers. *Adv. Drug Delivery Rev.* **2005**, *57* (12), 1742–1778. <https://doi.org/10.1016/j.addr.2005.07.011>.
- (2) Whitcombe, M. J.; Kirsch, N.; Nicholls, I. A. Molecular Imprinting Science and Technology: A Survey of the Literature for the Years 2004–2011. *J. Mol. Recognit.* **2014**, *27* (6), 297–401. <https://doi.org/10.1002/jmr.2347>.
- (3) Andersson, L. I. Molecular Imprinting for Drug Bioanalysis: A Review on the Application of Imprinted Polymers to Solid-Phase Extraction and Binding Assay. *J. Chromatogr. B: Biomed. Sci. Appl.* **2000**, *739* (1), 163–173. [https://doi.org/10.1016/S0378-4347\(99\)00432-6](https://doi.org/10.1016/S0378-4347(99)00432-6).
- (4) Chen, L.; Wang, X.; Lu, W.; Wu, X.; Li, J. Molecular Imprinting: Perspectives and Applications. *Chem. Soc. Rev.* **2016**, *45* (8), 2137–2211. <https://doi.org/10.1039/C6CS00061D>.
- (5) Dickey, F. H. The Preparation of Specific Adsorbents. *Proc. Natl. Acad. Sci. U S A* **1949**, *35* (5), 227–229.
- (6) Dickey, F. H. Specific Adsorption. *J. Phys. Chem.* **1955**, *59*, 695–707.
- (7) Figueroa, J. D.; Fout, T.; Plasynski, S.; McIlvried, H.; Srivastava, R. D. Advances in CO₂ Capture Technology—The U.S. Department of Energy’s Carbon Sequestration Program. *Int. J. Greenhouse Gas Control* **2008**, *2* (1), 9–20. [https://doi.org/10.1016/S1750-5836\(07\)00094-1](https://doi.org/10.1016/S1750-5836(07)00094-1).
- (8) MacDowell, N.; Florin, N.; Buchard, A.; Hallett, J.; Galindo, A.; Jackson, G.; S. Adjiman, C.; K. Williams, C.; Shah, N.; Fennell, P. An Overview of CO₂ Capture Technologies. *Energy Environ. Sci.* **2010**, *3* (11), 1645–1669. <https://doi.org/10.1039/C004106H>.

- (9) Yu, C.-H.; Huang, C.-H.; Tan, C.-S. A Review of CO₂ Capture by Absorption and Adsorption. *Aerosol Air Qual. Res.* **2012**, *12* (5), 745–769. <https://doi.org/10.4209/aaqr.2012.05.0132>.
- (10) Li, B.; Duan, Y.; Luebke, D.; Morreale, B. Advances in CO₂ Capture Technology: A Patent Review. *Appl. Energy* **2013**, *102*, 1439–1447. <https://doi.org/10.1016/j.apenergy.2012.09.009>.
- (11) Wang, M.; Lawal, A.; Stephenson, P.; Sidders, J.; Ramshaw, C. Post-Combustion CO₂ Capture with Chemical Absorption: A State-of-the-Art Review. *Chem. Eng. Res. Des.* **2011**, *89* (9), 1609–1624. <https://doi.org/10.1016/j.cherd.2010.11.005>.
- (12) Luis, P. Use of Monoethanolamine (MEA) for CO₂ Capture in a Global Scenario: Consequences and Alternatives. *Desalination* **2016**, *380*, 93–99. <https://doi.org/10.1016/j.desal.2015.08.004>.
- (13) Li, K.; Cousins, A.; Yu, H.; Feron, P.; Tade, M.; Luo, W.; Chen, J. Systematic Study of Aqueous Monoethanolamine-Based CO₂ Capture Process: Model Development and Process Improvement. *Energy Sci. Eng.* **2016**, *4* (1), 23–39. <https://doi.org/10.1002/ese3.101>.
- (14) Park, Y.; Lin, K.-Y. A.; Park, A.-H. A.; Petit, C. Recent Advances in Anhydrous Solvents for CO₂ Capture: Ionic Liquids, Switchable Solvents, and Nanoparticle Organic Hybrid Materials. *Front. Energy Res.* **2015**, *3*. <https://doi.org/10.3389/fenrg.2015.00042>.
- (15) Guo, H.; Li, C.; Shi, X.; Li, H.; Shen, S. Nonaqueous Amine-Based Absorbents for Energy Efficient CO₂ Capture. *Appl. Energy* **2019**, *239*, 725–734. <https://doi.org/10.1016/j.apenergy.2019.02.019>.
- (16) Nabavi, S. A.; Vladisavljević, G. T.; Eguagie, E. M.; Li, B.; Georgiadou, S.; Manović, V. Production of Spherical Mesoporous Molecularly Imprinted Polymer Particles Containing Tunable Amine Decorated Nanocavities with CO₂ Molecule Recognition Properties. *Chem. Eng. J.* **2016**, *306*, 214–225. <https://doi.org/10.1016/j.cej.2016.07.054>.
- (17) He, H.; Zhuang, L.; Chen, S.; Liu, H. Solid Amine Adsorbent Prepared by Molecular Imprinting and Its Carbon Dioxide Adsorption Properties. *Chem – Asian J.* **2016**, *11* (21), 3055–3061. <https://doi.org/10.1002/asia.201601031>.
- (18) Liu, F.; Kuang, Y.; Wang, S.; Chen, S.; Fu, W. Preparation and Characterization of Molecularly Imprinted Solid Amine Adsorbent for CO₂ Adsorption. *New J. Chem.* **2018**, *42* (12), 10016–10023. <https://doi.org/10.1039/C8NJ00686E>.
- (19) Zhao, Y.; Shen, Y.; Ma, G.; Hao, R. Adsorption Separation of Carbon Dioxide from Flue Gas by a Molecularly Imprinted Adsorbent. *Environ. Sci. Technol.* **2014**, *48* (3), 1601–1608. <https://doi.org/10.1021/es403871w>.
- (20) Santora, B. P.; Gagné, M. R.; Moloy, K. G.; Radu, N. S. Porogen and Cross-Linking Effects on the Surface Area, Pore Volume Distribution, and Morphology of Macroporous Polymers Obtained by Bulk Polymerization. *Macromolecules* **2001**, *34* (3), 658–661. <https://doi.org/10.1021/ma0004817>.
- (21) Heldebrant, D. J.; Jessop, P. G.; Thomas, C. A.; Eckert, C. A.; Liotta, C. L. The Reaction of 1,8-Diazabicyclo[5.4.0]Undec-7-Ene (DBU) with Carbon Dioxide. *J. Org. Chem.* **2005**, *70* (13), 5335–5338. <https://doi.org/10.1021/jo0503759>.

- (22) J. Heldebrant, D.; R. Yonker, C.; G. Jessop, P.; Phan, L. Organic Liquid CO₂ Capture Agents with High Gravimetric CO₂ Capacity. *Energy Environ. Sci.* **2008**, *1* (4), 487–493. <https://doi.org/10.1039/B809533G>.
- (23) J. Beckman, E.; Munshi, P. Ambient Carboxylation on a Supported Reversible CO₂ Carrier: Ketone to β -Keto Ester. *Green Chem.* **2011**, *13* (2), 376–383. <https://doi.org/10.1039/C0GC00704H>.
- (24) Gao, F.; Wang, Z.; Ji, P.; Cheng, J.-P. CO₂ Absorption by DBU-Based Protic Ionic Liquids: Basicity of Anion Dictates the Absorption Capacity and Mechanism. *Front. Chem.* **2019**, *6*, 658. <https://doi.org/10.3389/fchem.2018.00658>.
- (25) Doherty, S.; Knight, J. G.; Backhouse, T.; Abood, E.; Al-shaikh, H.; Clemmet, A. R.; Ellison, J. R.; Bourne, R. A.; Chamberlain, T. W.; Stones, R.; Warren, N. J.; Fairlamb, I. J. S.; Lovelock, K. R. J. Heteroatom Donor-Decorated Polymer-Immobilized Ionic Liquid Stabilized Palladium Nanoparticles: Efficient Catalysts for Room-Temperature Suzuki-Miyaura Cross-Coupling in Aqueous Media. *Adv. Synth. Catal.* **2018**, *360* (19), 3716–3731. <https://doi.org/10.1002/adsc.201800561>.
- (26) Liu, H.; Yin, H.; Feng, Y. A CO₂-Switchable Amidine Monomer: Synthesis and Characterization. *Des. Monomers Polym.* **2017**, *20* (1), 363–367. <https://doi.org/10.1080/15685551.2016.1270027>.
- (27) Zhang, L.; Zhang, J.; Wei, S.; Li, S.; Ma, X. Amine-Functionalized Hollow Mesoporous Nano-Bowl with Bulky Acid-Imprinted Free Space around Base Sites and DMF-Annealed Mesoporous Channels as an Efficient Solid Base Catalyst. *Appl. Catal. A: General* **2020**, *600*, 117560. <https://doi.org/10.1016/j.apcata.2020.117560>.
- (28) Chaterjee, S.; Krupadam, R. J. Amino Acid-Imprinted Polymers as Highly Selective CO₂ Capture Materials. *Environ. Chem. Lett.* **2019**, *17* (1), 465–472. <https://doi.org/10.1007/s10311-018-0774-z>.
- (29) Patil, Y. S.; Mahindrakar, J. N.; Salunkhe, P. H.; Ubale, V. P.; Ghanwat, A. A. Synthesis, Characterization and Structure–Property Relationships of Processable Poly(Amide-Imide)s Containing Novel Tetraphenylthiophene-Thiazole Diimide-Diacid (TPTPThDIDA) Moiety. *J. Macromol. Sci. Part A* **2018**, *55* (7), 572–581. <https://doi.org/10.1080/10601325.2018.1483201>.
- (30) Zhao, Y.; Shen, Y.; Bai, L.; Hao, R.; Dong, L. Synthesis and CO₂ Adsorption Properties of Molecularly Imprinted Adsorbents. *Environ. Sci. Technol.* **2012**, *46* (3), 1789–1795. <https://doi.org/10.1021/es203580b>.
- (31) Akbarzadeh, E.; Shockravi, A.; Vatanpour, V. Efficient Thiazole-Based Polyimines as Selective and Reversible Chemical Absorbents for CO₂ Capture and Separation: Synthesis, Characterization and Application. *Polymer* **2019**, *182*, 121840. <https://doi.org/10.1016/j.polymer.2019.121840>.
- (32) Li, Y.-N.; He, L.-N.; Lang, X.-D.; Liu, X.-F.; Zhang, S. An Integrated Process of CO₂ Capture and in Situ Hydrogenation to Formate Using a Tunable Ethoxyl-Functionalized Amidine and Rh/Bisphosphine System. *RSC Adv.* **2014**, *4* (91), 49995–50002. <https://doi.org/10.1039/C4RA08740B>.

CHAPTER 5

A TUTORIAL ON PERFORMING SAPT AND I-SAPT CALCULATIONS

5.1 Abstract

Symmetry adapted perturbation theory (SAPT) is a well-established computational method to calculate intermolecular and intramolecular interaction energies. These interactions are computed from the component electrostatics, exchange (repulsion), induction (polarization), and dispersion energies. This chapter aims to train new users in our group in applying SAPT calculations for the study of intermolecular interactions, and I-SAPT for intramolecular interactions.

5.2 Introduction

Non-covalent interactions (NCIs) play a very important role in many physical, biochemical, and chemical phenomena.^{1,2} Due to their ubiquity and wide impact, the study and understanding of NCIs is important for many biological and synthetic systems relying on self-assembly or molecular recognition. The challenge is that most individual NCIs are very weak (0.1 to 5 kcal/mol) which until recently was within the margin for error in DFT calculations. NCIs can be calculated with two main methodologies in quantum chemistry: the supermolecular and the perturbative approach. The supermolecular approach treats the total interaction energy as the difference between the energy of the whole complex and the sum of energies of each isolated fragment or unit. A major drawback of such an approach is basis set superposition error (BSSE).³ This error reduces with the use of larger basis sets and thus, more accurate results can be very computationally costly. The perturbative approach computes the interaction energy as a perturbation to the Hamiltonian operator of the individual fragments or monomers.² SAPT is a widely adopted perturbation theory based method to calculate the total interaction energy.⁴ The SAPT approach to investigate the interaction energies, was first introduced by Eisenchitz and London in the 1930s.³ Later

in the 1970s and 1980s, generally applicable versions of SAPT were developed.^{5,6} SAPT avoids the problem of basis set error and includes treatment of correlated interactions such as dispersion and polarization, and thus can be more accurate at lower basis sets and lower computational costs. In addition, SAPT provides the physically meaningful components of the interaction energy such as electrostatics, exchange (repulsion), induction (polarization), and dispersion. I-SAPT is a type of SAPT method to calculate the intramolecular interaction energy and is currently available in Psi4. More exhaustive descriptions of SAPT theory and application can be found in the review articles.^{4,7,8} SAPT0 is the simplest many-body symmetry adapted perturbative approximation method that gives reasonable total interaction energies. SAPT0 treats the monomers at the Hartree-Fock level and adds induction terms inherited from a HF dimer treatment, dispersion terms that emerge from second-order perturbation theory to the electrostatics, and exchange terms.² The equation for SAPT0 is shown below.

$$E_{int}^{SAPT0} = E_{elst}^{(10)} + E_{exch}^{(10)} + E_{ind}^{(20)} + E_{exch-ind}^{(20)} + E_{disp}^{(20)} + E_{exch-disp}^{(20)} + \delta E_{HF}^{(2)}$$

SAPT decomposes the intermolecular interaction energy into four fundamental components: electrostatics, exchange, induction, and dispersion.

Electrostatics: Electrostatics is the Coulomb interaction between the charge densities of isolated molecules or monomers. The charge densities are a combination of the electron charges in the molecule. The electrostatic component is the sum of the long-range electrostatic interactions between permanent multipole moments (charge, dipole, quadrupole, etc.) as well as the short-range electrostatic interactions arising from charge penetration.⁹

Exchange: The exchange component is the short-range repulsive forces due to the Pauli exclusion principle which diminishes exponentially with the distance.⁹

Induction: The induction component encompasses the interaction involving mutual polarization between the molecules and the charge transfer component. The electric field from molecule A can polarize molecule B and vice versa which gives rise to a leading-order (i.e. second or third-order) induction term.⁹ The charge transfer component is the interaction due to the charge transfer from the occupied molecular orbitals (MOs) of one monomer to the virtual MOs of the other and vice versa.

Dispersion: The dispersion component is an attractive interaction due to intermonomer electron correlation. The correlated fluctuation of electron density on both molecules generates an attractive effect. Dispersion interactions are weak binding interactions formed by all molecular surfaces including non-polar molecules and noble gas atoms. Dispersion interactions are stronger for larger, more polarizable molecules.⁹

5.2.1 How to do a SAPT calculation?

Q-Chem¹⁰ is a commercial general quantum chemistry application which can do many general computational analyses such as conformation analyses, geometry optimization, transition state optimization, and SAPT calculations. Q-Chem is commonly installed on a server where individual jobs are submitted from the network computers. Psi4¹¹ is an open-source quantum chemical computing platform which also can perform SAPT and I-SAPT calculations.

To install Psi4 on a windows PC, anaconda or conda must be installed first following the instructions in the link: https://psicode.org/posts/psi4education_setup/. For

Mac and Linux, Psi4 can be directly installed without anaconda or conda. Next, install the Psi4 program package in the conda or anaconda terminal following the installation steps in the link given above. Once installed, Psi4 jobs are run in the anaconda or conda terminal.

5.2.2 Creating a SAPT input file

Running a Q-Chem or Psi4 SAPT calculation requires a text input file that contains the atomic coordinates, basis sets, type of SAPT calculation, and fragment assignments or molecular coordinates. A correct input file is very important for successful SAPT or any other quantum chemical calculation.

First, the atomic coordinates molecule or the complex of interest is built in Spartan with the proper geometry and conformation. The SAPT calculation does not optimize or change the input coordinates. In Spartan, molecular mechanics (MM) was used to get initial starting structures. For bimolecular complexes, geometric constraints may be necessary to position atoms or molecules at the proper distances and orientations. The geometry optimization can then be done using higher methods (B3LYP/B3LYP-D3 functional and 6-31G* or 6-311G* basis sets). While viewing the final structure in Spartan, atom labels are turned on to identify each atom type and number, after which the structure is saved as a Spartan input file to generate the cartesian (XYZ) coordinates. The atom labels make it easier to separate the cartesian coordinates of the atoms in the interacting fragments or molecules. An example of a molecule in Spartan with the atom labels turned on is shown in Figure 5.1.

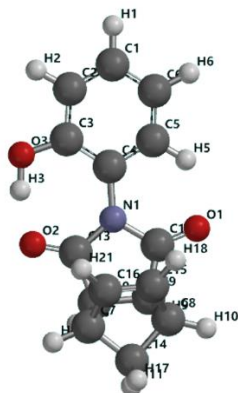


Figure 5.1. Optimized transition state (TS) structure of phenol rotor with labels turned on.

Table 5.1 XYZ coordinates of optimized phenol rotor (TS) that will be used for an I-SAPT calculation in Psi4.

H1	1.443934581	-0.386690497	-4.542491334
C1	1.408867904	-0.248489425	3.465278131
C4	1.274847435	0.091532576	-0.640079695
C2	0.338863317	-0.733363589	-2.738502488
C6	2.430699581	0.415188669	-2.788658619
C5	2.354754240	0.574477748	-1.412234428
C3	0.228841951	-0.586563178	-1.341188965
H2	-0.482850770	-1.255619271	-3.218351566
H6	3.290053934	0.812295591	-3.320226824
H5	3.160126617	1.086936174	-0.917876611
N1	1.313207762	0.347107306	0.810974165
C12	2.389213981	1.050599037	1.471092895
C9	2.042888611	1.260700559	2.923826518
C10	0.705507880	0.559520415	3.122572572
C13	0.353231742	0.000364261	1.771776972
H9	2.859636201	0.878127749	3.541111343
O1	3.421905709	1.442327241	0.977424246
O2	-0.671362846	-0.653322406	1.611259200
C7	-0.256698456	1.723313200	3.601746272
H8	-1.172850368	1.360782007	4.068239095
H16	0.712644150	-0.254172774	3.852378665
C8	1.727020908	2.765305180	3.300128449
H10	2.621244076	3.359164285	3.490111372
C14	0.749631857	2.512629737	4.474858369
H11	1.183598908	1.917889739	5.288001037
H17	0.326138420	3.436417564	4.879763019
C15	0.761613919	3.297972457	2.251136705
H18	1.039262140	3.963782359	1.441540884
C16	-0.415259305	2.681435905	2.431645529
H21	-1.295566279	2.741245014	1.801067490
O3	-0.903201801	-1.126850345	-0.854590492
H3	-0.939945948	-1.034043286	0.128824514

The input file is generated as a text file on a desktop PC or server. The XYZ coordinates from the Spartan input file are copied to the text file and the atomic coordinates are grouped into the interacting and non-interacting fragments of a molecule or grouped into the two interacting molecules in the complex. An example is shown of a molecule for an I-SAPT calculation in Figure 5.1. The norbornene-PhOH rotor is shown in Spartan with the atomic labels and the corresponding XYZ coordinates in Table 5.1. The element labels in the Psi4 SAPT or I-SAPT input file can be letters (H, C, O) or numbers (1, 6, 8). The interacting fragments of interest are the phenolic OH group (O3 and H3) and the carbonyl group (C13 and O2). The atomic coordinates of the fragments are separated from each other and the remaining atoms in the molecules by “- -” marks in the input file. The molecule and fragment coordinates are each preceded by the multiplicity (0 1 for no unpaired electrons, or 0 2 for an unpaired electron). If the fragment is attached by 1 bond, then the fragment will be a doublet (0 2). If the fragment is connected by 2 bonds, then it is a singlet (0 1). The remaining framework will be 0 2 or 0 1 if the number of “broken” bonds to the fragments are odd or even, respectively. The job submission codes for the I-SAPT calculations are then inserted in the text document and the input file is then ready for submission. These can be copied from the example input file shown in Table 5.2 which is a fi-SAPT(0) job with a jun-cc-pVDZ basis set. The input file is saved as a text document into the desktop folder of the computer with the Psi4 program.

Different types of SAPTs are available in Psi4, including the traditional bimolecular SAPT and the intramolecular I-SAPT. Psi4 can also run these using the simplest SAPT0 and also higher-order SAPT (SAPT2+, SAPT2+(3), and SAPT2+3). The current version of Q-Chem cannot run I-SAPT.

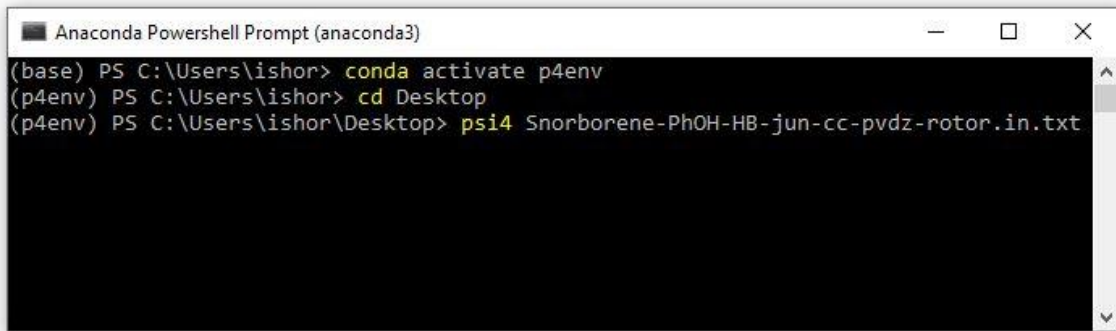
Table 5.2 I-SAPT Psi4 input file for the norbornene-PhOH hydrogen bonding rotor for the I-SAPT0 calculation between the phenol OH fragment and the imide C=O fragment.

```

molecule mol {
0 1
--
0 2
O -0.903201801 -1.126850345 -0.854590492
H -0.939945948 -1.034043286 0.128824514
--
0 1
C 0.353231742 0.000364261 1.771776972
O -0.671362846 -0.653322406 1.611259200
--
0 2
H 1.443934581 -0.386690497 -4.542491334
C 1.408867904 -0.248489425 -3.465278131
C 1.274847435 0.091532576 -0.640079695
C 0.338863317 -0.733363589 -2.738502488
C 2.430699581 0.415188669 -2.788658619
C 2.354754240 0.574477748 -1.412234428
C 0.228841951 -0.586563178 -1.341188965
H -0.482850770 -1.255619271 -3.218351566
H 3.290053934 0.812295591 -3.320226824
H 3.160126617 1.086936174 -0.917876611
N 1.313207762 0.347107306 0.810974165
C 2.389213981 1.050599037 1.471092895
C 2.042888611 1.260700559 2.923826518
C 0.705507880 0.559520415 3.122572572
H 2.859636201 0.878127749 3.541111343
O 3.421905709 1.442327241 0.977424246
C -0.256698456 1.723313200 3.601746272
H -1.172850368 1.360782007 4.068239095
H 0.712644150 -0.254172774 3.852378665
C 1.727020908 2.765305180 3.300128449
H 2.621244076 3.359164285 3.490111372
C 0.749631857 2.512629737 4.474858369
H 1.183598908 1.917889739 5.288001037
H 0.326138420 3.436417564 4.879763019
C 0.761613919 3.297972457 2.251136705
H 1.039262140 3.963782359 1.441540884
C -0.415259305 2.681435905 2.431645529
H -1.295566279 2.741245014 1.801067490
symmetry c1
no_reorient
no_com
}
set {
basis jun-cc-pvdz
scf_type df
guess sad
freeze_core true
}
energy('fisapt0')

```

The SAPT calculation is performed by running Psi4 with the input file. First, open the anaconda terminal in the PC (Figure 5.2). Second, activate the preinstalled Psi4 environment with the command: `conda activate p4env`. The Psi4 environment should be activated every time after opening the new anaconda terminal to get it ready for job submission. Save the input text file on the desktop and change the directory to desktop with the command: `cd Desktop`. Finally, the job submission can be completed with the command: `psi4 [input file name]`.



```
Anaconda Powershell Prompt (anaconda3)
(base) PS C:\Users\ishor> conda activate p4env
(p4env) PS C:\Users\ishor> cd Desktop
(p4env) PS C:\Users\ishor\Desktop> psi4 Snorborene-PhOH-HB-jun-cc-pvdz-rotor.in.txt
```

Figure 5.2. Commands in anaconda terminal for activating Psi4 environment and job submission

SAPT calculations are relatively fast but computation times will depend upon the size of the molecule and the basis set chosen for calculation. For example, the calculation of a smaller molecule is faster than a larger one and will also be faster with a smaller basis set. The generally recommended basis set for most SAPT and I-SAPT calculations in Psi4 is the truncated Dunning's basis set (jun-cc-pVDZ). After the completion of the calculation, the output file is saved on the desktop as a text document: [input file name].dat. The decomposed interaction energies are at the end of the output file; an example of the SAPT decomposed energies from the output file are shown in Table 5.3.

Table 5.3 SAPT decomposed energies for the OH•••O=C interaction in the norbornene-PhOH rotor TS.

SAPT Results			
Electrostatics	-39.08110811 [mEh]	-24.52376558 [kcal/mol]	-102.60743521 [kJ/mol]
Elst10,r	-39.08110811 [mEh]	-24.52376558 [kcal/mol]	-102.60743521 [kJ/mol]
Exchange	50.51421947 [mEh]	31.69815128 [kcal/mol]	132.62506495 [kJ/mol]
Exch10	50.51421947 [mEh]	31.69815128 [kcal/mol]	132.62506495 [kJ/mol]
Exch10(S^2)	49.17585875 [mEh]	30.85831725 [kcal/mol]	129.11119937 [kJ/mol]
Induction	-17.24476189 [mEh]	-10.82125146 [kcal/mol]	-45.27611610 [kJ/mol]
Ind20,r	-26.59262502 [mEh]	-16.68712413 [kcal/mol]	-69.81892737 [kJ/mol]
Exch-Ind20,r	16.93176555 [mEh]	10.62484329 [kcal/mol]	44.45434434 [kJ/mol]
delta HF,r (2)	-7.58390242 [mEh]	-4.75897062 [kcal/mol]	-19.91153306 [kJ/mol]
Induction (A<-B)	-5.47928688 [mEh]	-3.43830443 [kcal/mol]	-14.38586572 [kJ/mol]
Induction (B<-A)	-11.76547501 [mEh]	-7.38294703 [kcal/mol]	-30.89025037 [kJ/mol]
Dispersion	-5.78786778 [mEh]	-3.63194186 [kcal/mol]	-15.19604476 [kJ/mol]
Disp20	-8.17479394 [mEh]	-5.12976064 [kcal/mol]	-21.46291853 [kJ/mol]
Exch-Disp20	2.38692616 [mEh]	1.49781878 [kcal/mol]	6.26687377 [kJ/mol]
Total HF	-5.81165052 [mEh]	-3.64686576 [kcal/mol]	-15.25848635 [kJ/mol]
Total SAPT0	-11.59951830 [mEh]	-7.27880763 [kcal/mol]	-30.45453111 [kJ/mol]

5.2.3 Analysis of SAPT results

The I-SAPT calculation allows the computation of intramolecular interaction energies between the interacting fragments. An example of results from SAPT calculations and how they can be used in the study of NCIs is shown below. The I-SAPT calculation was performed for hydrogen bonding (HB) and non-hydrogen bonding (nHB) norbornene-PhOH rotors and the norbornene-PhOCH₃ control rotor (Figure 5.3). The SAPT0 decomposed energies of the rotors were calculated using the jun-cc-pVDZ basis set and are tabulated in Table 5.4. The decomposed energies provide useful information about which energy component has the most dominant role in stabilizing the rotors in the transition state and raises or lowers the rotational barrier.

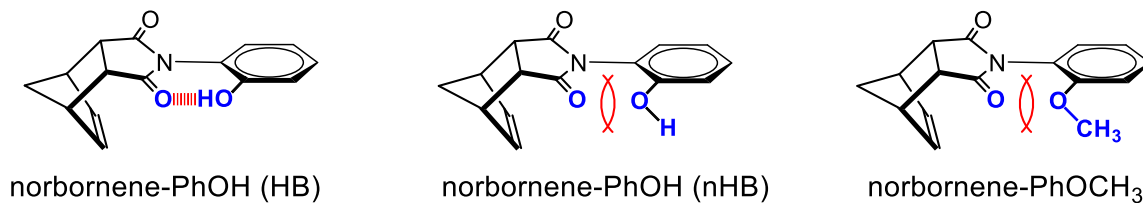


Figure 5.3 Transition state structure of norbornene-PhOH (HB), norbornene-PhOH (nHB), and norbornene-PhOCH₃ rotors with the interacting fragments highlighted in blue.

Table 5.4 Calculated decomposed SAPT0 energies for different rotors.

Rotor	Interacting groups	E_{exch}	E_{elst}	E_{ind}	E_{disp}	E_{total}
Norbornene-PhOH (HB)	OH•••O=C	31.69	-24.52	-10.82	-3.63	-7.28
Norbornene-PhOH (nHB)	HO•••O=C	10.47	8.29	-1.97	-1.31	15.48
Norbornene-PhOCH ₃ (nHB)	CH ₃ O•••O=C	12.14	7.63	-2.22	-1.62	15.93

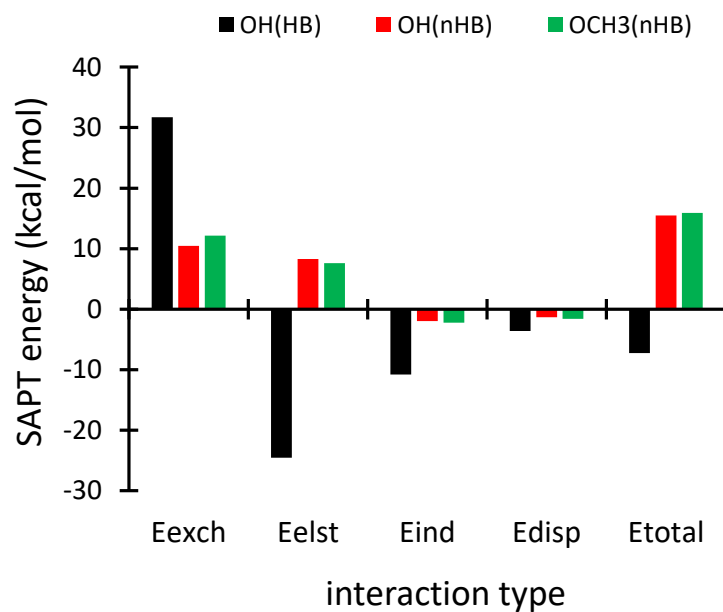


Figure 5.4 I-SAPT decomposed energies for the intramolecular interaction for different rotors calculated with jun-cc-pVDZ basis set.

The I-SAPT analysis of the rotors gives insight into the contribution of different interaction terms for the hydrogen bond stabilization of the transition state (TS) rotors in Figure 5.4. The analysis was consistent with previous energy decomposition analyses of hydrogen bond interactions.¹² A linear correlation plot with a slope of 2.31 (Figure 5.5) was obtained by plotting total SAPT interaction energies (E_{total}) against the experimental (ΔG^\ddagger) rotational barriers for norbornene-PhOH, norbornene-PhOCH₃, norbornene-PhNH₂, norbornene-PhN(CH₃)₂ and norbornene-PhNHCOCF₃ rotors. This also confirms that the total SAPT interaction energies of the hydrogen bonding, and non-hydrogen bonding rotors, transition states follow the experimental rotational barrier trends for the molecular rotors.

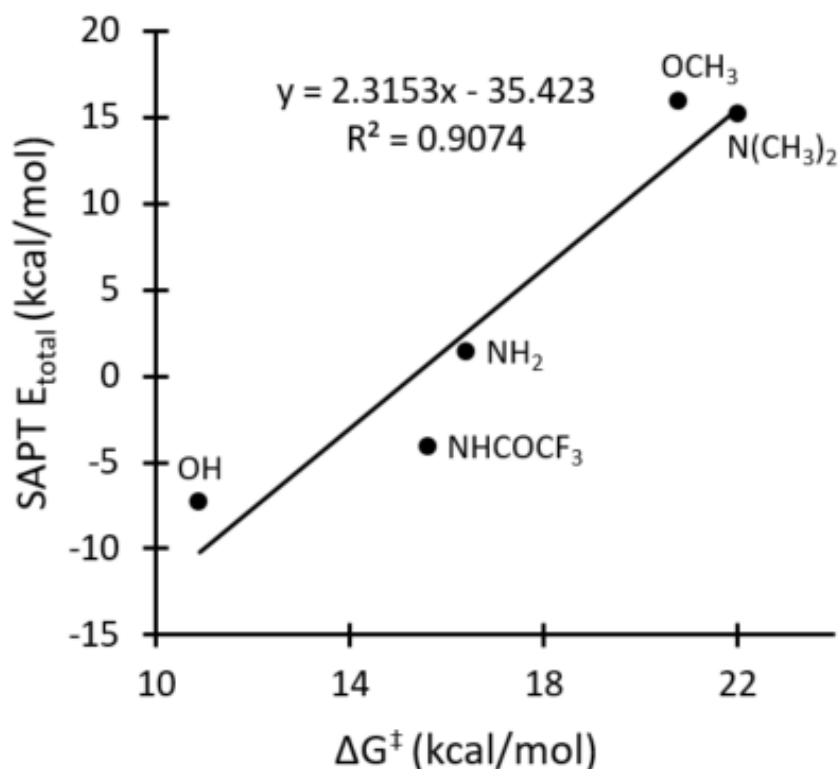


Figure 5.5 Correlation of total SAPT energies (SAPT E_{total}) and experimental (ΔG^\ddagger) rotational barriers for norbornene-PhOH, norbornene-PhOCH₃, norbornene-PhNH₂, norbornene-PhN(CH₃)₂, and norbornene-PhNHCOCF₃ rotors.

In the hydrogen bonding transition state (TS) of the phenol rotor (Figure 5.4, black bars), the large attractive term (-38.97 kcal/mol) is mainly made up of the electrostatic component with lesser contributions from the induction, and dispersion components. The attractive interactions are balanced out by an almost equally large repulsive exchange term (+31.69 kcal/mol). Thus the overall hydrogen bonding interaction is smaller but still attractive (-7.28 kcal/mol). Comparison of the exchange components of the hydrogen bonding and the non-hydrogen bonding structures of the phenol rotor show that the exchange (repulsion) in the hydrogen bonded phenol rotor is a combination of the repulsion from the two oxygen atoms (O•••O) (33%) and the proton with the carbonyl oxygen (O•••H--O) (67%). This is confirmed by the similarity of the exchange terms of the non-hydrogen bonded OH rotor and the control OCH₃ which cannot form an intramolecular hydrogen bond. The significant repulsive interactions in the hydrogen bonding rotor are due to the fact the hydrogen bonds position the heavy atoms and the hydrogen bonding proton within their van der Waals (vdw) radii.¹² The repulsive interactions of the control non-hydrogen bonding rotor played a significant role in the large TS stabilization of the hydrogen bonds by canceling approximately one-third of the destabilizing repulsive interactions of the hydrogen bonding interactions.¹²

The I-SAPT interaction energy analysis revealed the total interaction energy in the hydrogen bonded phenol rotor is small but still attractive, while, the total interaction energy in the non-hydrogen bonded control rotor is destabilizing as the non-hydrogen bonded rotor lacks the attractive components (E_{elst} , E_{ind} , and E_{disp}) but still has one-third of the repulsive interactions. Thus the overall difference energy tends to be highly attractive ($\Delta E = -22.76$ kcal/mol) which is almost three times the total interaction energy of the hydrogen bonding

rotor. The large TS stabilization by the relatively weak hydrogen bond was attributed to the significant repulsive exchange component of the non-hydrogen bonding rotor. The large repulsive exchange component of the hydrogen bonding TS was ‘prepaid’ or partially balanced by the repulsive interactions in the control rotor. Therefore, difference energy (ΔE) contains all the attractive terms of the hydrogen bonding interaction, but only two-thirds of the large repulsive exchange component. A detailed explanation for the stability of the transition state hydrogen bonding rotors can be found in our recent article.¹²

5.3 Conclusions

This chapter provides the background and instructions to perform SAPT/I-SAPT calculations to obtain decomposed interaction energies. The I-SAPT calculation was performed for the hydrogen bonding and non-hydrogen bonding norbornene-PhOH rotors, and the norbornene-PhOCH₃ control rotor. The calculated I-SAPT interaction energies demonstrated that the weak hydrogen bond can stabilize the transition state with a surprisingly high magnitude due to the large exchange repulsion prepaid by the positioning of a phenolic proton between the two heavy oxygen atoms while forming the hydrogen bond. This study hence revealed the importance of the exchange (repulsive) interaction term in the stability of the hydrogen bonding norbornene-PhOH rotor.

5.4 Supplemental Information

Spartan structure and the XYZ coordinates for the non-hydrogen bonded norbornene-PhOH, and norbornene-PhOCH₃ rotor are given in Table 5.5.

Table 5.5 XYZ coordinates of the TS structures of the norbornene-PhOH, and norbornene-PhOCH₃ rotors.

H1	1.699097429	-0.781976623	-4.483925394	H1	1.964229780	-0.479872970	-4.304662040
C1	1.598657119	-0.524720899	-3.435204324	C1	1.864862736	-0.240873073	-3.249373088
C4	1.269642426	0.152617039	-0.690080277	C4	1.539109921	0.402934026	-0.488882656
C2	0.490404167	-0.933565299	-2.722084255	C2	0.734198346	-0.646520579	-2.550569635
C6	2.569786094	0.203903238	-2.772996413	C6	2.854589861	0.453503268	-2.570007754
C5	2.398948218	0.524807645	-1.436614552	C5	2.686656846	0.760215168	-1.221631924
C3	0.307331710	-0.634516735	-1.367711071	C3	0.557609918	-0.366243234	-1.186786412
H2	-0.275980709	-1.527121851	-3.216110818	H2	-0.031001727	-1.211640648	-3.067494679
H6	3.466110109	0.536538681	-3.283653390	H6	3.762724912	0.772021532	-3.072937230
H5	3.165557577	1.110910075	-0.964144800	H5	3.463695741	1.319990938	-0.732123731
N1	1.221450007	0.545119131	0.709871301	N1	1.479555254	0.789642821	0.921237513
C12	2.155041465	1.453498571	1.276691961	C12	2.433887264	1.688832608	1.497123546
C9	2.008276808	1.465816259	2.775695828	C9	2.286020365	1.708663608	3.001668192
C10	0.765957792	0.637922991	3.061141747	C10	1.022479126	0.900434566	3.288946855
C13	0.243386950	0.210560076	1.709127342	C13	0.489529610	0.473966988	1.933248035
H9	2.926282839	1.062109608	3.209206520	H9	3.198521532	1.288674426	3.438778769
O1	2.951638210	2.141958456	0.693828108	O1	3.254259511	2.365648230	0.910618731
O2	-0.835266293	-0.270394798	1.549978496	O2	-0.609767495	0.003956875	1.790522873
C7	-0.169127502	1.633762593	3.825258470	C7	0.102185433	1.921705773	4.060067661
H8	-0.982734782	1.150458117	4.361714061	H8	-0.721081238	1.451915616	4.599534151
O3	-0.782806803	-1.137928277	-0.755044803	O3	-0.517508246	-0.841396947	-0.519817529
H16	0.952777202	-0.257889794	3.657470846	H16	1.192136118	0.002084910	3.891923407
C8	1.669942072	2.862155393	3.396603158	C8	1.973579625	3.119447621	3.631849526
H10	2.538022853	3.501422256	3.541931095	H10	2.857821103	3.740768020	3.778956892
C14	0.896170655	2.390344920	4.645358367	C14	1.191071421	2.653608845	4.886578212
H11	1.483350114	1.741133172	5.302978545	H11	1.766818381	1.987410622	5.541505076
H17	0.478308140	3.217640894	5.221557257	H17	0.790662654	3.488464812	5.469294782
C15	0.530529003	3.439299597	2.576360277	C15	0.839763945	3.729594240	2.819299934
H18	0.640346264	4.222480189	1.837139390	H18	0.963702353	4.523277843	2.090553662
C16	-0.558397365	2.712654693	2.830803588	C16	-0.269070235	3.020310448	3.074053440
H21	-1.521598751	2.779259696	2.341629467	H21	-1.237584067	3.114091432	2.595185263
H3	-1.301103120	-1.628259120	-1.396775727	C17	-1.515937550	-1.578309089	-1.198483152
				H4	-1.989408406	-0.988650122	-1.995150014
				H7	-2.259692680	-1.818606812	-0.436751024
				H12	-1.118620167	-2.509051971	-1.626275599

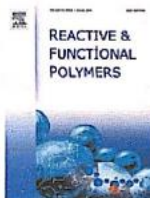
5.5 References

- (1) Salonen, L. M.; Ellermann, M.; Diederich, F. Aromatic Rings In Chemical And Biological Recognition: Energetics And Structures. *Angew. Chem. Int. Ed.* **2011**, *50* (21), 4808–4842. <https://doi.org/10.1002/anie.201007560>.
- (2) Parker, T. M.; Burns, L. A.; Parrish, R. M.; Ryno, A. G.; Sherrill, C. D. Levels Of Symmetry Adapted Perturbation Theory (SAPT). I. Efficiency And Performance For Interaction Energies. *J. Chem. Phys.* **2014**, *140* (9), 094106. <https://doi.org/10.1063/1.4867135>.
- (3) Szalewicz, K. Symmetry-Adapted Perturbation Theory Of Intermolecular Forces. *Wiley Interdiscip. Rev.: Comput. Mol. Sci.* **2012**, *2* (2), 254–272. <https://doi.org/10.1002/wcms.86>.
- (4) Jeziorski, B.; Moszynski, R.; Szalewicz, K. Perturbation Theory Approach To Intermolecular Potential Energy Surfaces Of Van Der Waals Complexes. *Chem. Rev.* **1994**, *94* (7), 1887–1930. <https://doi.org/10.1021/cr00031a008>.
- (5) Szalewicz, K.; Jeziorski, B. Symmetry-Adapted Double-Perturbation Analysis Of Intramolecular Correlation Effects In Weak Intermolecular Interactions. *Mol. Phys.* **1979**, *38* (1), 191–208. <https://doi.org/10.1080/00268977900101601>.
- (6) Rybak, S.; Jeziorski, B.; Szalewicz, K. Many-Body Symmetry-Adapted Perturbation Theory Of Intermolecular Interactions. H₂O And HF Dimers. *J. Chem. Phys.* **1991**, *95* (9), 6576–6601. <https://doi.org/10.1063/1.461528>.
- (7) Szalewicz, K.; Patkowski, K.; Jeziorski, B. Intermolecular Interactions Via Perturbation Theory: From Diatoms To Biomolecules. In *Intermolecular Forces And Clusters II*; Wales, D. J., Ed.; Structure And Bonding; Springer: Berlin, Heidelberg, **2005**; Pp 43–117. https://doi.org/10.1007/430_004.
- (8) Cársky, P.; Paldus, J.; Pittner, J. *Recent Progress In Coupled Cluster Methods: Theory And Applications*; Springer Science & Business Media, **2010**.
- (9) Patkowski, K. Recent Developments in Symmetry-Adapted Perturbation Theory. *Wiley Interdiscip. Rev.: Comput. Mol. Sci.* **2020**, *10* (3), e1452. <https://doi.org/10.1002/wcms.1452>.
- (10) Shao, Y.; Gan, Z.; Epifanovsky, E.; Gilbert, A. T. B.; Wormit, M.; Kussmann, J.; Lange, A. W.; Behn, A.; Deng, J.; Feng, X.; Ghosh, D.; Goldey, M.; Horn, P. R.; Jacobson, L. D.; Kaliman, I.; Khaliullin, R. Z.; Kuś, T.; Landau, A.; Liu, J.; Proynov, E. I.; Rhee, Y. M.; Richard, R. M.; Rohrdanz, M. A.; Steele, R. P.; Sundstrom, E. J.; Woodcock, H. L.; Zimmerman, P. M.; Zuev, D.; Albrecht, B.; Alguire, E.; Austin, B.; Beran, G. J. O.; Bernard, Y. A.; Berquist, E.; Brandhorst, K.; Bravaya, K. B.; Brown, S. T.; Casanova, D.; Chang, C.-M.; Chen, Y.; Chien, S. H.; Closser, K. D.; Crittenden, D. L.; Diedenhofen, M.; Distasio, R. A.; Do, H.; Dutoi, A. D.; Edgar, R. G.; Fatehi, S.; Fusti-Molnar, L.; Ghysels, A.; Golubeva-Zadorozhnaya, A.; Gomes, J.; Hanson-Heine, M. W. D.; Harbach, P. H. P.; Hauser, A. W.; Hohenstein, E. G.; Holden, Z. C.; Jagau, T.-C.; Ji, H.; Kaduk, B.; Khistyayev, K.; Kim, J.; Kim, J.; King, R. A.; Klunzinger, P.; Kosenkov, D.; Kowalczyk, T.; Krauter, C. M.; Lao, K. U.; Laurent, A. D.; Lawler, K. V.; Levchenko, S. V.; Lin, C. Y.; Liu, F.; Livshits, E.; Lochan, R. C.; Luenser, A.; Manohar, P.; Manzer, S. F.; Mao, S.-P.; Mardirossian, N.; Marenich, A. V.; Maurer, S. A.; Mayhall, N. J.; Neuscamman, E.; Oana, C. M.; Olivares-Amaya, R.; O'Neill, D. P.; Parkhill, J. A.; Perrine, T. M.; Peverati, R.;

- Prociuk, A.; Rehn, D. R.; Rosta, E.; Russ, N. J.; Sharada, S. M.; Sharma, S.; Small, D. W.; Sodt, A.; Stein, T.; Stück, D.; Su, Y.-C.; Thom, A. J. W.; Tsuchimochi, T.; Vanovschi, V.; Vogt, L.; Vydrov, O.; Wang, T.; Watson, M. A.; Wenzel, J.; White, A.; Williams, C. F.; Yang, J.; Yeganeh, S.; Yost, S. R.; You, Z.-Q.; Zhang, I. Y.; Zhang, X.; Zhao, Y.; Brooks, B. R.; Chan, G. K. L.; Chipman, D. M.; Cramer, C. J.; Goddard, W. A.; Gordon, M. S.; Hehre, W. J.; Klamt, A.; Schaefer, H. F.; Schmidt, M. W.; Sherrill, C. D.; Truhlar, D. G.; Warshel, A.; Xu, X.; Aspuru-Guzik, A.; Baer, R.; Bell, A. T.; Besley, N. A.; Chai, J.-D.; Dreuw, A.; Dunietz, B. D.; Furlani, T. R.; Gwaltney, S. R.; Hsu, C.-P.; Jung, Y.; Kong, J.; Lambrecht, D. S.; Liang, W.; Ochsenfeld, C.; Rassolov, V. A.; Slipchenko, L. V.; Subotnik, J. E.; Van Voorhis, T.; Herbert, J. M.; Krylov, A. I.; Gill, P. M. W.; Head-Gordon, M. Advances In Molecular Quantum Chemistry Contained In The Q-Chem 4 Program Package. *Mol. Phys.* **2015**, *113* (2), 184–215. <https://doi.org/10.1080/00268976.2014.952696>.
- (11) Smith, D. G. A.; Burns, L. A.; Simmonett, A. C.; Parrish, R. M.; Schieber, M. C.; Galvelis, R.; Kraus, P.; Kruse, H.; Di Remigio, R.; Alenaizan, A.; James, A. M.; Lehtola, S.; Misiewicz, J. P.; Scheurer, M.; Shaw, R. A.; Schriber, J. B.; Xie, Y.; Glick, Z. L.; Sirianni, D. A.; O'Brien, J. S.; Waldrop, J. M.; Kumar, A.; Hohenstein, E. G.; Pritchard, B. P.; Brooks, B. R.; Schaefer, H. F.; Sokolov, A. Yu.; Patkowski, K.; Deprince, A. E.; Bozkaya, U.; King, R. A.; Evangelista, F. A.; Turney, J. M.; Crawford, T. D.; Sherrill, C. D. P Si4 1.4: Open-Source Software For High-Throughput Quantum Chemistry. *J. Chem. Phys.* **2020**, *152* (18), 184108. <https://doi.org/10.1063/5.0006002>.
- (12) C. Vik, E.; Li, P.; M. Maier, J.; O. Madukwe, D.; A. Rassolov, V.; J. Pellechia, P.; Masson, E.; D. Shimizu, K. Large Transition State Stabilization From A Weak Hydrogen Bond. *Chem. Sci.* **2020**, *11* (28), 7487–7494. <https://doi.org/10.1039/D0SC02806A>.

APPENDIX A COPYRIGHT CLEARANCE

Copyright Clearance for Chapter 2



Absorption properties of monolithic poly (divinylbenzene-co-N-vinylpyrrolidone) over a wide range of monomer ratios

Author:

Ishwor Karki, Ping Li, Erik C. Vik, Alexander Manzewitsch, Evan Divirgilio, William E. Brewer, Ken D. Shimizu

Publication: Reactive and Functional Polymers

Publisher: Elsevier

Date: June 2021

© 2021 Elsevier B.V. All rights reserved.

Journal Author Rights

Please note that, as the author of this Elsevier article, you retain the right to include it in a thesis or dissertation, provided it is not published commercially. Permission is not required, but please ensure that you reference the journal as the original source. For more information on this and on your other retained rights, please visit: <https://www.elsevier.com/about/our-business/policies/copyright#Author-rights>

BACK

CLOSE WINDOW